8-2018

Final Causality in the Thought of Thomas Aquinas

Joel Johnson
Purdue University

AGENT-BASED APPROACH FOR SYSTEM IDENTIFICATION AND OPTIMAL CONTROL OF HIGH PERFORMANCE BUILDINGS

by

Jaewan Joe

A Dissertation

Submitted to the Faculty of Purdue University

In Partial Fulfillment of the Requirements for the degree of

Doctor of Philosophy

Lyles School of Civil Engineering

West Lafayette, Indiana

August 2018

THE PURDUE UNIVERSITY GRADUATE SCHOOL
STATEMENT OF COMMITTEE APPROVAL

Dr. Panagiota Karava, Chair
School of Civil Engineering
Dr. Athanasios Tzempelikos
School of Civil Engineering
Dr. James E. Braun
School of Mechanical Engineering
Dr. Jianghai Hu
School of Electrical and Computer Engineering

Approved by:
Dr. Dulcy M. Abraham
Head of the Graduate Program

TABLE OF CONTENTS

LIST OF TABLES

LIST OF FIGURES

ABSTRACT

Author: Joe, Jaewan. PhD
Institution: Purdue University
Degree Received: May 2018
Title: Agent-based Approach for System Identification and Optimal Control of High Performance Buildings.
Major Professor: Panagiota Karava

Commercial buildings have strong impacts on humans and the environment. They not only affect occupants' comfort, health, and well-being but also consume more than 19% of the total energy consumption in the US. High performance building designs can achieve significant energy savings, with new building technologies such as advanced building envelopes, thermally activated building systems, on-site power production and thermal storage; dynamic effects related to variability in occupancy and environmental conditions; diversity in occupant thermal preferences; and the integration of these diverse technologies into an overall control system design. Model-based predictive control (MPC) is a promising approach for the realization of high performance buildings as operations can be optimized for the specific building and climate through an estimated process model that predicts the future evolution of the system, while incorporating the most up-to-date information on weather forecast and system dynamics.

Despite of the advantages, there are still significant obstacles associated with the realization of MPC implementation in actual buildings. First of all, the process of generating a control-oriented building model, which is referred as system identification, can be complex and not easily reproduced, due to the customized design of buildings and HVAC systems. Also, MPC computation could become intractable due to the large decision dimension for large-scale systems. To date, the formulation, solution, and integration of optimal controls into existing building management systems (BMS), may not be easily scalable to other buildings on account of the design customization and control intractability. It is envisioned that in the future, with new technology for sensing, information processing and communication, distributed intelligence would be embedded into devices and would be widely deployed into actual buildings. Towards the realization of this plug-and-play intelligent building operation, the research objective of this thesis is to develop a multi-agent system approach to optimal control of high performance buildings, based on new algorithms for distributed system identification and distributed model predictive

control (DMPC). From the application perspective, the focus is thermal environment control of open-plan office spaces. Radiant floor systems are evaluated as high performance features and used as test-beds to demonstrate the proposed agent-based framework for zone and local environment control.

As a first step, a multi-agent systems approach for data-driven grey-box building models is introduced. Each zone is divided into sub-systems (agents), and a parameter set for each sub-system is first estimated individually, and then integrated into an inverse model for the zone using the dual decomposition algorithm. Two case-studies are designed and conducted using the Living Laboratories at Purdue's Herrick Building as test-beds to validate the estimated control-oriented models under realistic operation conditions. The results show that the model prediction accuracy of the new approach is fairly good for implementation in predictive control while models can be developed and integrated with improved efficiency, flexibility and scalability, compared to centralized approaches.

In the next step, a centralized MPC strategy is developed for zone thermal environment control in an occupied office space with radiant comfort delivery along with a chiller and boiler as HVAC sources. The MPC controller deploys an optimization algorithm based on constraint quadratic programming with hard comfort bounds, which yields an exact numerical solution, and it is straight forward and robust for this application. Results from the MPC implementation during the cooling season show that more than 34% cost savings are achieved by load shifting to utilize higher chiller efficiency with lower outdoor air temperature, and lower electricity prices. In the heating application, the energy use reduction from the optimized control is around 16% compared to conventional control.

In the final step, a distributed optimization algorithm, inspired by the Proximal Jacobian Alternating Direction Method of Multipliers (PJ-ADMM), is introduced. It includes multiple MPCs run iteratively while exchanging control input information until they converge. With this tractable approach, agents solve individual optimization problems in parallel, through information exchange and broadcasting, with a smaller scale of the input and constraints, facilitating optimal solutions with improved efficiency. The developed algorithm is tested using field data from an occupied open-plan office space with localized comfort delivery along with distributed sensing, control, and data communication capabilities. The radiant comfort delivery system with predictive control is capable of providing localized thermal environments, thereby improving occupant

satisfaction, while achieving more than 27% reduction in electricity consumption compared to baseline feedback control.

In summary, this thesis introduces a new agent-based approach for system identification and MPC, which is implemented and tested using an actual building as test-bed. The results show significantly improved performance compared to conventional systems and controls. The overall methodology could be packaged into a toolbox integrated into open-source building control platforms, existing building management systems, or embedded into new smart devices. It is a scalable solution that can be extended to other smart and connected environments, e.g., multiple building systems, multi-zone buildings, building clusters integrated with power grids and automobiles.

CHAPTER 1. INTRODUCTION

1.1 Motivation

The boundary conditions for building control of modern buildings are becoming increasingly dynamic, as evidenced by deployment of new building technologies for energy and comfort delivery, increasing use of intermittent, low carbon energy sources, the view of occupants as service users who participate, decide, provide feedback, and communicate with building systems, and the advent of dynamic electricity pricing and smart electric grids. Advanced supervisory control strategies, such as model predictive control (MPC), have the potential to address the growing complexity of control requirements of modern buildings, considering their specific energy and comfort delivery features and the local climate. Also, MPC can leverage information from the deployment of low-cost sensing, and other smart and connected devices to optimize the operation of a building over a prediction horizon while incorporating the most up-to-date information on weather forecast and system dynamics.

For example, in recent years, following the development of low-cost sensing, smart devices and the Internet of Things (IoT) technology, the potential for spatial control granularity is extended and conventional zone control with a single set-point is evolving to occupancy prediction-based (Jia and Spanos 2016, Liao and Barooah 2010, Yang et al. 2014, Zhang et al. 2010, Zhao et al. 2014) or personalized control (Zhang, Arens, and Zhai 2015, Bauman et al. 2015, Pasut et al. 2015, Xu et al. 2017). Space conditioning is provided when zones are occupied (Weng and Agarwal 2012) to achieve energy savings and satisfy occupants with diverse thermal preferences (Jazizadeh, Ghahramani, and Becerik-Gerber 2013; Jazizadeh et al. 2014; Konis and Annavaram 2017; Lee et al. 2017; Lee et al. 2018; Ryu, Kim, and Yun 2015). Building systems and devices are beginning to embed analytical software for communications and enhanced control functions. To provide thermal environments with higher resolution, new smart devices can be deployed in building systems, and eventually transform the configuration of Building Management Systems (BMS) fundamentally (Stluka et al. 2017). At the same time, the connectivity between building occupants and such devices is extended with sensing and computing abilities of cell phones or single board computers (e.g., Raspberry Pi) and wireless communication methods (e.g., ZigBee or Bluetooth), and it is geared towards a new BMS configuration (Zhao et al. 2016).

To accommodate this trend for high performance buildings, the multi-agent approach proposed in this thesis provides an ideal framework as agents and their network can be easily configured and dynamically re-configured and are amenable for designing scalable sensing, data processing, optimization, and control algorithms in adaption to the changing conditions. For buildings with complex systems for better performance, it is possible to utilize their modularity to deploy plug-and-play approaches that improve efficiency, flexibility and scalability.

In this thesis, from the application perspective, the focus is thermal environment control of open-plan office spaces. Open-plan spaces have become a new trend in office buildings, and with the availability of data from sensors, smart devices and occupants, smart comfort delivery can provide significant opportunities for energy savings (Bauman et al. 2015; Pasut et al. 2015) as conditioning can be deployed where it is actually needed. Radiant floor systems are evaluated as high performance features and used as test-bed to demonstrate the proposed agent-based framework. Specific advantages of the radiant floor system are (Fabrizio et al. 2012; Kim and Olesen 2015a; Kim and Olesen 2015b; Nall 2013a; Nall 2013b; Nall 2013c; Olesen 2008; Rhee and Kim 2015; Sastry and Rumsey 2014): (a) The room air temperature can be maintained at lower and higher setpoint for the heating and cooling season respectively due to the radiative heat exchange with the large floor surface, thereby less energy is consumed while maintaining equivalent comfort. (b) The large slab surface area yields uniform heat transfer to the room so occupant thermal comfort is improved. (c) The system is operated with moderate chilled or hot water temperature so the efficiency of the plant is higher. Therefore, radiant floor systems provide improved thermal comfort, and reduced energy use when advanced control strategies are used (Gayeski et al. 2012; May-Ostendorp et al. 2013). From a localized thermal management perspective, radiant systems with distributed sensing and control loops, are capable of providing different thermal environments by selectively conditioning a slab section as opposed to air systems in which the air is mixed easily in an open space. This leads to better occupant comfort as different thermal preferences can be simultaneously met.

1.2 Control-oriented building models

To date, research on MPC of buildings has been mainly carried out in simulation environments (Braun, Montgomery, and Chaturvedi 2001; Cigler et al. 2012; Corbin et al. 2012; Feng et al. 2015; Hu and Karava 2014; Lehmann et al. 2013; Li et al. 2015; Oldewurtel et al. 2012; Sourbron,

Verhelst, and Helsen 2013; Sun et al. 2010). Experimental and field studies, despite being the exemption rather than the rule, show promising results (Bengea et al. 2013; De Coninck and Helsen 2016; Ma, Borrelli, and Hencey 2012; Ma et al. 2012; Široký et al. 2011; Matuško, and Borrelli 2014; West, Ward, and Wall 2014). In previous studies has been concluded that the pathway of obtaining a suitable model that can be implemented in a predictive controller is time-consuming, corresponding to around 70% of the project engineering cost (Henze 2013), and not easily repeatable. Developing control-oriented models through a system identification approach, based on actual experiments, can be a long process particularly for high performance buildings due to the large number of sub-systems for energy and comfort delivery and the increased complexity of the integrated building system and its dynamic behavior. In such cases, the model structure typically includes a large number of estimate parameters, increasing the computational time and impeding finding a global minimum. Also, various sub-systems form a multiple input and multiple output (MIMO) system entailing different characteristics of dynamics in each sub-system; thereby, a centralized parameter estimation approach is hardly feasible for this case. Agent-based methods, i.e. a special class of distributed approaches enables parallel estimation of each sub-system. This includes identifying agents, their function and network structure, and estimating model parameters for both individual agents in the system, using information locally known or observable by each agent, and their connections. Decomposition methods are used to solve a large-scale optimization problem by breaking it up into smaller sub-problems with lower dimension of variables, and solving the sub-problems independently.

1.3 Multi-agent distributed MPC

It is believed that smart building features would be widely adopted if intelligence is embedded into physical devices (Cai et al. 2016a). Distributed optimization methods enable this realization for the control of coupled but separable sub-systems that are jointly optimized. In order to coordinate the solution of the sub-problems, a network of intelligent agents is formed. In multi-agent networks, agents are equipped with the capability of sensing, information processing and communication (Jennings and Bussmann 2003; Necoara, Nedelcu, and Dumitrache 2011; Negenborn and Maestre 2014; Samar, Boyd, and Gorinevsky 2007). This approach, known as multi-agent DMPC, is a tractable solution for large-scale problems due to the reduced computation cost with less decision variables for each local optimization problem, the feasibility to find an optimal solution by

focusing on one objective, the possibility to easily adapt model parameters with respect to the varying environments, and the robustness in terms of whole system operation in the case of fault or failure of subsystems (Figure 1.1).

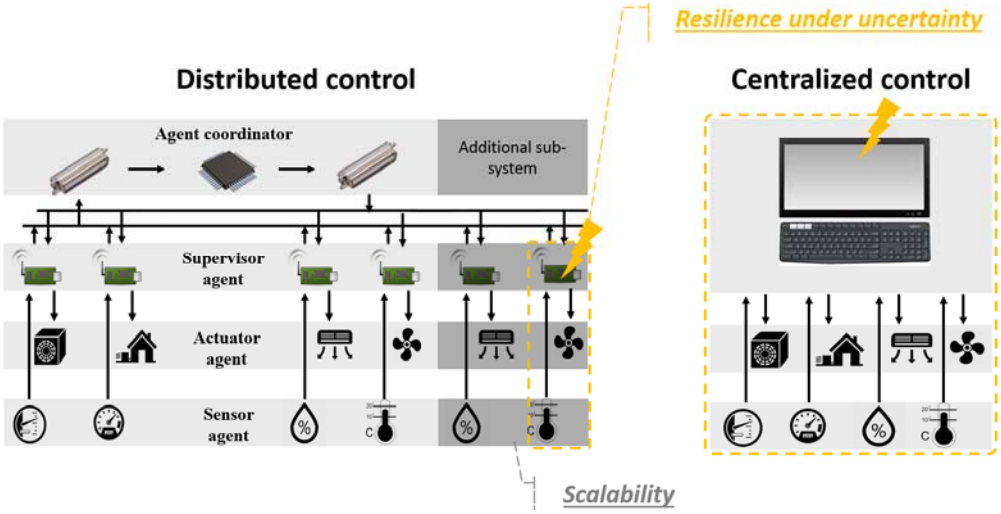

Figure 1.1 Multi-agent distributed MPC compared with centralized MPC

1.4 Objectives

This thesis presents an agent-based approach for system identification and MPC with the following distinct advantages: (a) scalability: sub-system models can be developed and integrated in a plug-and-play manner, reducing the expertise and engineering cost that is required for control-oriented models of high performance buildings, such as those with complex energy and comfort delivery systems; (b) efficiency: each agent faces a smaller-scale problem compared to centralized identification schemes; (c) flexibility: agents form agent-networks that can be easily configured and dynamically re-configured in adaptation to system upgrades and retrofits. These advantages are demonstrated with experimental and simulation studies and implementation to an actual test-bed. The specific objectives of this thesis are:

1. Develop a distributed system identification approach for data-driven building models.
    a. Identify building sub-system agents, their function and network structure.
    b. Design and conduct an experimental approach to estimate the sub-system (agent) model parameters and formulate the dual decomposition method for developing the integrated model for the zone.
    c. Demonstrate the approach with different case studies.

2. Evaluate the performance of radiant floor systems with MPC in office environments.
    a. Formulate a robust optimization algorithm for MPC.
    b. Implement the MPC controller during the cooling and heating seasons.
    c. Analyze the energy performance of the system through comparison with baseline air delivery systems and conventional controls.
3. Develop a DMPC algorithm for intelligent control of office buildings with high resolution thermal environments.
    a. Formulate a distributed optimization problem for MPC.
    b. Implement the DMPC algorithm in an actual test-bed with radiant comfort delivery.
    c. Investigate the performance of the algorithm and localized comfort delivery system.

1.5 Outline

Figure 1.2 shows the outline of this study. Chapter 2 presents a state-of-art literature review on studies related to the multi-agent systems, distributed optimization for building control applications, and advanced technology for thermal environment control including radiant and localized comfort delivery systems. The agent-based framework for control-oriented building models is discussed in Chapter 3. Chapter 4 evaluates the energy performance of radiant floor cooling and heating systems with MPC through implementation in an actual test-bed and comparison with baseline air delivery systems and conventional controls. In Chapter 5, a distributed optimization algorithm is deployed into MPC formulation and the developed DMPC controller is implemented to optimize the operation of a localized radiant cooling system.

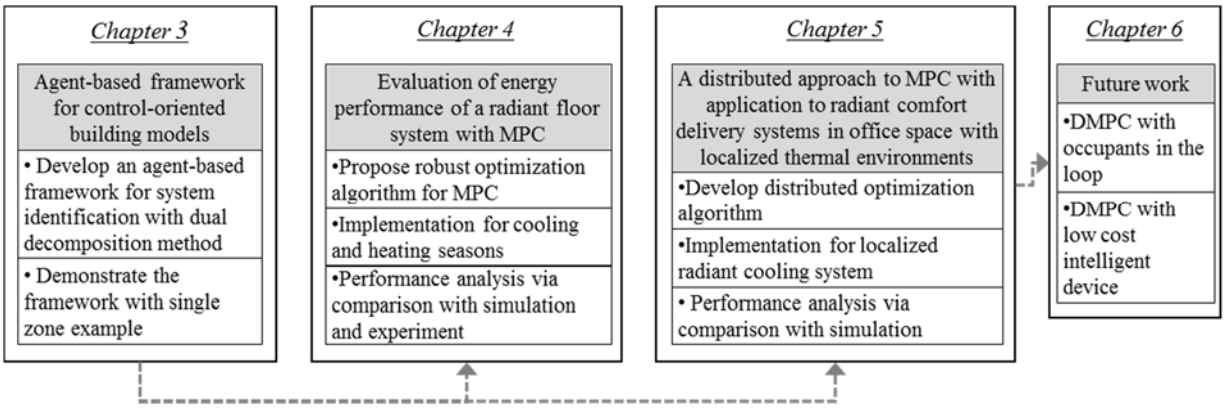

Figure 1.2 Research outline

CHAPTER 2. LITERATURE REVIEW

2.1 Agent-based approach

Agent-based methods have been applied to building control problems. Several studies are concept-based, focused on defining the agents and their functions (Davidsson and Boman 2005; Duan and Lin 2008; Kelly and Bushby 2012; Sharples, Callaghan, and Clarke 1999; Simoes and Bhattarai 2011; Treado 2010; Treado and Delgoshaei 2010; Zhao, Suryanarayanan, and Simões 2013; Mo 2003). Other studies considered actual buildings to demonstrate the application of decomposition methods (Cai et al. 2015; Ma, Anderson, and Borrelli 2011; Moroşan et al. 2010), manage the needs and resources (Lacroix, Ines, and Mercier 2012; Mokhtar et al. 2013; Yang and Wang 2013), and exchange information of room air temperature trajectory between adjacent zones (Moroşan et al. 2010; Putta et al. 2014). Our literature review shows that very few studies have developed estimation frameworks in sensor networks of complex systems, based on distributed optimization (Necoara, Nedelcu, and Dumitrache 2011; Samar, Boyd, and Gorinevsky 2007). Also, this approach has not been exploited previously as a potential solution for control-oriented models of building systems that can be easier to develop and integrate. This distributed formulation is distinct from the control application in the sense that is a static problem in terms of the estimate parameters and could be easily generalized to other cases where the controller type is identical.

In previous studies that utilize the multi-agent approach for building control applications, agents are defined in many different ways. For example, in some cases definitions are made according to the HVAC source, namely electrical, heating and cooling agents (Zhao, Suryanarayanan, and Simões 2013; Simoes and Bhattarai 2011). Other definitions are based on the control hierarchy such as central, local (Wang, Yang, and Wang 2010), or producer, distributor, consumer (Lacroix, Ines, and Mercier. 2012). Finally, agents may also represent building occupants (Davidsson and Boman 2005; Duan and Lin 2008; Mo and Mahdavi 2003). Although theoretical approaches for agent definitions exist (Jennings and Bussmann 2003), previous research mainly focuses on specific examples or case studies.

2.2 System identification

Grey-box models are considered as robust controllers and have been adopted for many building applications (Bacher and Madsen 2011; Berthou et al. 2014; Braun and Chaturvedi 2002; Cai and Braun 2015; De Coninck and Helsen 2016; Hazyuk, Ghiaus, and Penhouet 2012; Jiménez, Madsen, and Andersen 2008; Kramer, Schijndel, and Schellen 2013; Prívara et al. 2012; Prívara et al. 2013; Reynders, Diriken, and Saelens 2014; Široký et al. 2011; Žáčeková, Váňa, and Cigler 2014). Their structure is fairly simple compared to white-box models implemented in building energy simulation tools, and thereby are suitable for implementation in MPC. Compared to black-box models, grey-box models require a shorter period of data for training (Braun and Chaturvedi 2002; Reynders, Diriken, and Saelens 2014) and preserve the physical meaning and insight of each parameter (Hazyuk, Ghiaus, and Penhouet 2012; Reynders, Diriken, and Saelens 2014). Also, grey-box models do not require training data for different control schemes unlike black-box models, whose prediction is hardly matched with the experimental data unless all control schemes and output ranges are reflected in the training period (Braun and Chaturvedi 2002; Hazyuk, Ghiaus, and Penhouet 2012). In some cases, a grey-box model has been utilized as an initial model and then transferred to a final ARMAX (Jiménez, Madsen, and Andersen 2008), transfer function (Braun and Chaturvedi 2002; Hazyuk, Ghiaus, and Penhouet 2012), or Model Predictive Control Relevant Identification (MRI) model (Prívara et al. 2012; Prívara et al. 2013; Žáčeková, Váňa, and Cigler. 2014). Overall, complexities in the estimation problem are associated with the non-linearity between the estimate parameter and output trajectory, and non-convexity of the objective function. As a result, falling in many local minima is quite common and reaching a global minimum is a difficult and time-consuming task.

Several studies emphasize the advantages of grey-box models and show good agreement with results from building simulation programs such as EnergyPlus (Prívara et al. 2013) and TRNSYS (Berthou et al. 2014; Braun and Chaturvedi 2002; Li et al. 2015; Prívara et al. 2012; Sourbron, Verhelst, and Helsen 2013), Modelica (De Coninck et al. 2015; De Coninck and Helsen 2016; Reynders, Diriken, and Saelens 2014), and white-box models developed in Matlab environment (Hazyuk, Ghiaus, and Penhouet 2012; Hu and Karava 2014). However, simulation studies have limitations with regards to their applicability to the actual building estimation problem. Features of building simulation that differentiate it from the actual building operation are: (a) Information of occupancy schedule and internal heat gain is available. (b) Sensing reflects the true value

without consideration of sensor uncertainty and sensor error range. (c) All temperature points of the building envelope and equipment heat gain are available, which are unlikely to be measured in actual buildings. (d) Rich input excitation is feasible by triggering set-point variations to unrealistic bounds. (e) Heat transfer coefficients and material properties are perfectly known so initial estimate parameters are decided based on those. Other studies were based on experiments in test-cells with well-controlled environments that allow rich input excitation without occupant interruptions (Bacher and Madsen 2011). Also, good agreement with experimental data from an actual multi-zone building has been achieved allowing a rough approximation of the state by averaging the room air temperature from 8 different zones (Braun and Chaturvedi 2002), and treating the internal heat gain as an additional estimate parameter (Braun and Chaturvedi 2002; Cai and Braun 2015).

Identifiability is an important consideration in data-driven modelling indicating if the identified set of estimated parameters represents unique values so it is considered as a true system (Ljung 1999). Local (or output) identifiability represents the sensitivity of the estimate parameter variation to the output trajectory for given training data, thus, it is dependent on the data and model structure simultaneously. It is quantitatively expressed by the information matrix and represents the degree of the parameter influence to the output trajectory:

$$\frac{\partial \hat{Y}(\theta)}{\partial \theta}^{T} \frac{\partial \hat{Y}(\theta)}{\partial \theta} \in \mathbb{R}^{m \times m}$$

$\hat{Y}$, θ, and m represent the output trajectory, estimate parameter, and number of estimate parameters. Local identifiability is guaranteed by the full rank of information matrix, which means all parameters affect the output trajectory. Structure identifiability is not related to the training data but the model structure. It represents the parameter variation to output trajectory given zero initial state and zero input except initial input of one; each element of output trajectory is expressed with Markov parameter sequence:

$$\frac{\partial M(\theta)}{\partial \theta} \in \mathbb{R}^{n \times 1}$$

where:

$$M(\theta) = \begin{bmatrix} C(\theta)B(\theta) & C(\theta)A(\theta)B(\theta) & \dots & C(\theta)A(\theta)^{n-1}B(\theta) \end{bmatrix}$$

M and n represent Markov parameter sequence and number of iteration. A, B, and C represent matrices of state space formulation. A model is structural identifiable when the structure

identifiability matrix is full rank. Local identifiability and structure identifiability have been studied theoretically (Doren et al. 2009) and a systematic experiment design for the building estimation problem has been proposed to increase the identifiability (Agbi, Song, and Krogh 2012). A recent study for a building estimation problem used the identifiability to reduce the number of estimate parameters by fixing less identifiable parameters with defined thresholds (Jie and Braun 2015).

Correlation is another important consideration in estimation problems, and it is defined differently according to the associated variables such as the estimate parameter, input signal, and residual. Parameter correlation refers to the correlated effects from two different parameters to the output trajectory; in case that two parameters give similar effects, the variation of one parameter is dependent on that of the other during the optimization process. A potential solution is transforming the parameter set to a less correlated that is a linear combination of the initial set, through Principal Component Analysis (PCA). A theoretical discussion of the PCA method was presented in Del Barrio and Guyon 2003, followed by a building application example in Del Barrio and Guyon 2004. Similar studies were carried out to decorrelate the parameters by transforming their coordinates (Jiménez, Madsen, and Andersen 2008) or fixing the most correlated parameters one at a time with defined thresholds (Jie and Braun 2015). An implementable solution is providing sufficient input excitation during the experiment. Pseudo random binary sequence (PRBS) is a typical method, which has been widely used for building applications. It has been applied for grey-box models by exciting the heat input directly (Bacher and Madsen 2011; Hazyuk, Ghiaus, and Penhouet 2012) and black-box models by manipulating the set-point temperature (Li and Wen 2014; Royer et al. 2012). Rich excitation is feasible in simulation (Hazyuk, Ghiaus, and Penhouet 2012; Li and Wen 2014; Royer et al. 2014) and experimental studies in test-cells without actual occupants (Bacher and Madsen 2011), but sometimes it reaches unrealistic bounds (Bacher and Madsen 2011; Hazyuk, Ghiaus, and Penhouet 2012; Li and Wen 2014). A recent case-study found an optimal experiment design for the input signal, which is turned out to be a bang-bang type, and reduced the data set size for estimation (Cai et al. 2016). Regarding the correlation originated from the inputs, signals of exogenous inputs such as the outdoor air temperature and solar radiation can be easily correlated. Including several days in the training data set with different weather conditions such as cloudy and sunny days resolves this issue. Finally, correlation analysis of the residual typically entails the auto-correlation and the cross-correlation between the input signal

and residual, referred as whiteness and independence test respectively (Kramer, Schijndel, and Schellen 2013). The auto-correlation function of the residual in simulation studies reveals that the residual is a white noise type (Jiménez, Madsen, and Andersen 2008; Reynders, Diriken, and Saelens 2014), which means that there is no missing input and the model structure is not too simple (Kramer, Schijndel, and Schellen 2013). Strong cross-correlation between the input and the residual represents an incorrect model structure (Kramer, Schijndel, and Schellen 2013). Previous studies have shown less cross-correlation in a simulation study where the uncertainty is not significant (Jiménez, Madsen, and Andersen 2008) and an experimental study of an actual building with free floating conditions (Kramer, Schijndel, and Schellen 2013).

Based on this background information, several days with different weather conditions were used for the experiments conducted in this study to collect training data, in order to decorrelate the exogenous input signal. Also, an air temperature setpoint was randomly selected from the comfort bound and implemented for a given time interval, to provide sufficient input excitation and to decorrelate the estimate parameters and increase their identifiability. For the grey-box model estimation, an approach using a sensitivity-based parameter range selection and range shift was implemented to avoid falling into a local minimum in the resulting non-linear and non-convex optimization problem. The local identifiability of each estimate parameter was quantified with the significance index for a given training data set, and utilized for the sub-system model comparison along with the correlation index based on the correlation coefficient of each two pairs of estimate parameters. The auto-correlation and cross-correlation functions were used to test the final estimated models as a post process technique.

2.3 Radiant floor system

Radiant floor heating and cooling systems, also known as Thermally Activated Building Systems (TABS), has been investigated for a long time and their superior performance in terms of energy savings and improved comfort, have been revealed in many studies (Fabrizio et al. 2012; Kim and Olesen 2015a; Kim and Olesen 2015b; Nall 2013a; Nall 2013b; Nall 2013c; Olesen 2008; Rhee and Kim 2015; Sastry and Rumsey 2014). Specific advantages are: (a) The room air temperature can be maintained at lower and higher setpoint for the heating and cooling season respectively due to the radiative heat exchange with the large floor surface, thereby less energy is consumed while maintaining equivalent comfort. (b) The large slab surface area yields uniform heat transfer to the

room so occupant thermal comfort is improved. (c) The system is operated with moderate chilled or hot water temperature so the efficiency of the plant is higher. However, control of this system is challenging due to the large thermal mass.

Many previous studies for the radiant floor system focused on the temperature regulation during the heating season. Conventional feedback control was implemented to control the valve and maintain the room air temperature (Ahn and Song 2010; Cho and Zaheer-uddin 1999; Haddad, Purdy, and Laouadi 2007; Rhee, Yeo, and Kim 2011) and Predicted Mean Vote (PMV) (Batista et al. 2013). Also, the outdoor air temperature was utilized to control the supply water temperature (Arteconi et al. 2014; Gwerder et al. 2008; Gwerder et al. 2009; Lehmann et al. 2011; Olesen, Sommer, and Duchting 2002; Park et al. 2014; Schmelas et al. 2015) and heat flux (Athienitis, 1997) provided to the concrete slab. Nevertheless, the conditioned rooms are mostly overheated during the daytime, even in an experiment with a test-cell (Schmelas et al. 2015). This results in waste of heating energy attributed to the naïve control strategy that requires cooling for the daytime. This overheating issue might become more severe in office environments where a significant amount of internal heat gain is generated during the occupied hours.

A distinct feature of the radiant floor system is the potential for load shifting in the cooling season. Many studies have focused on the energy and cost saving potential of air system due to pre-cooling (Turner, Walker, and Roux 2015; Braun et al. 2001; Braun 2003; Braun and Lee 2006; Cai et al. 2016; Lee and Braun 2006), which in some cases included a thermal storage system in plant side (Henze, Felsmann, and Knabe 2004). In those studies, pre-cooling strategies have clearly shown the energy and cost saving potential even with rule-based controls applied to building energy simulation tools (Turner et al. 2015), control-oriented building models (Braun et al. 2001; Braun 2003; Braun and Lee 2006; Lee and Braun 2006; Lee and Braun 2008), and field tests (Braun 2003; Lee and Braun 2006). The radiant floor system due to its large thermal capacity with concrete structure provides an opportunity to use pre-cooling. This was shown in a recent study with a heuristic control strategy (Park et al. 2014).

Feedback and heuristic strategies are deficient for radiant floor systems in terms of preventing the overheating and maximizing the pre-cooling potential in the heating and cooling season, respectively. Advanced control methods such as MPC have the ability to incorporate exogenous inputs and predict the thermal dynamics, in order to optimize the system performance over a prediction horizon (Oldewurtel et al. 2012). For the heating season, a simulation study (Candanedo

et al. 2010) and experimental implementations were carried out using fuzzy logic (Kang, Hyun, and Park 2015) and artificial neural networks (Lee, Yeo, and Kim 2002) in residential buildings. Also, the radiant floor heating system has been investigated in office environments, with actual occupants (Váňa et al. 2014) and integrated with a storage tanks and a solar-assisted air-to-water heat pump to optimize the utilization of renewable energy sources (Li et al. 2015). In cooling applications, various optimization methods were applied to solve the non-linear problem such as pattern search and particle swarm optimizer (Gayeski et al. 2012; May-Ostendorp et al. 2013) or the CPLEX (CPLEX Optimization Software) was used (Feng at al. 2015). Some of them attempted to utilize the pre-cooling potential of a hybrid system of radiant ceiling (concrete) and mixed mode cooling with natural ventilation (May-Ostendorp et al. 2013), or with a low lift chiller taking advantage of the higher efficiency at night (Gayeski et al. 2012). In other simulation studies, the yearly performance of the radiant floor system with MPC was investigated (Sourbron, Verhelst, and Helsen 2013; Lehmann et al. 2013).

Although, the radiant floor heating and cooling system has been investigated in many building applications including advanced control strategies with MPC, its potential has not been fully explored. In heating season, overheating is still seen in most cases (Candanedo et al. 2010; Kang, Hyun, and Park 2015; Lee, Yeo, and Kim 2002; Váňa et al. 2014) as it is difficult to prevent especially for buildings with large glazing area (Dermardiros et al. 2017) that might require sophisticated predictive control strategies. Very few studies examined the performance of radiant systems for cooling applications and pre-cooling is only observed in experiments with confined test-cells (Gayeski et al. 2012; May-Ostendorp et al. 2013). Moreover, for most MPC studies, the objective function formulation includes several terms (e.g., energy consumption and comfort), and thereby heuristic weights are multiplied to each term that might affect the controller performance. For non-linear optimization, an initial guess for the control input trajectory is required for every MPC calculation (Gayeski et al. 2012; Li et al. 2015), which might affect the controller performance and computation time. When it comes to the generalization of the MPC formulation to other configurations, such as localized comfort delivery, multi-zones or building clusters, using heuristics complicates the optimization problem. Also, in some studies, the evaluation of the MPC performance might not be realistic as the estimated model may have not been sufficiently accurate for implementation due to the system complexity (Feng et al. 2015) or it is not based on data that

are collected in an actual building (Candanedo et al. 2010; Henze, Felsmann, and Knabe 2004; Lehmann et al. 2013; Li et al. 2015; Sourbron, Verhelst, and Helsen 2013).

2.4 Local conditioning system

Despite the advent of new technology for distributed sensing, data communication, and information processing, advantages are confined to typical HVAC systems enhanced with new control functions (Baker and Hoyt 2016; Erickson and Cerpa 2012). Additional benefits could be leveraged using systems that facilitate the delivery of personalized or localized thermal environments (Gao and Keshav 2013a; Gao and Keshav 2013b). Various types of HVAC systems that provide different thermal conditions for an individual occupant (known as Task-ambient Conditioning (TAC) or Personal Environmental Control (PEC)) have been studied up to date (Heidarinejad et al. 2018; Vesely and Zeiler 2014; Zhang et al. 2010). These include a chair (Zhang, Arens, and Zhai 2015; Pasut et al. 2015) and desk diffusers (Amai et al. 2017; Kong et al. 2017) or heating panels (Amai et al. 2017, Vissers 2012) for conditioning body parts. However, heating is much easier to implement than cooling, primarily due to the problem of dealing with rejected heat while infrared heaters may create discomfort due to thermal asymmetry. Also, with only few exemptions (Lee et al. 2018; Andersen et al. 2016) TAC or PEC systems have operated independently from the building's environmental control. At the same time, different approaches with building-integrated HVAC such as under-plenum air distribution (UFAD) (Schiavon et al. 2011) and thermally-activated building systems (TABS), such as radiant floor heating system (Foda and Sirén 2012), have been explored focusing on sizing the cooling capacity. Although, it is challenging for building-integrated HVAC such as VAV diffusers, UFAD, and radiant systems to reach the resolution of an individual occupant, localized thermal zones can be used to facilitate different occupancy schedules and occupants preferring warm, cool or accepting a wider range of thermal conditions (Lee et al. 2017, Lee et al. 2018).

Open-plan spaces have become a new trend in office buildings, and with the availability of data from sensors, smart devices and occupants, smart comfort delivery can provide significant opportunities for energy savings (Bauman et al. 2015; Pasut et al. 2015) as conditioning is deployed where it is actually needed. When implemented in a building, it is expected to enable an expansion of the temperature set-points in unoccupied spaces, resulting in energy savings that can

be over 20% compared to baseline approaches depending on the building and climate (Hoyt, Arens, and Zhang 2014).

From a localized thermal management perspective, radiant systems with distributed sensing and control loops, are capable of providing different thermal environments by selectively conditioning a slab section as opposed to air systems in which the air is mixed easily in an open space. This leads to better occupant comfort as different thermal preferences can be simultaneously met.

However, conventional feedback strategies for radiant floor systems are limited in terms of providing the anticipated benefits for building climate control, due to the large thermal capacity. Model predictive control (MPC) is considered as a promising solution for this system as shown in literature (Bengea et al. 2014; Sourbron, Verhelst and Helsen 2013; Váňa et al. 2014; Feng et al. 2015). In this approach, operation is optimized using information for the specific building and climate through an estimated process model to predict the future evolution of the system, while incorporating the most up-to-date information on weather forecast and system dynamics (Braun 1990; Oldewurtel et al. 2012). The benefits of such systems can be augmented by incorporating in sensing and control frameworks the building occupants, i.e. their schedule and thermal preferences, to facilitate localized comfort delivery in open-plan office spaces.

On the other hand, MPC requires high engineering cost for developing control-oriented building models which is referred to as system identification. In the case of high performance buildings, in which the requirements for thermal environments with higher resolution and energy savings are increased, complex building designs bring additional challenges for developing building models and typical parameter estimation techniques may become infeasible (Joe and Karava 2016). Moreover, as the building scale becomes large or finer control granularity is needed, the dimension of control variables is increased; thereby the computation cost to find optimal solutions is also higher, which makes the MPC problem intractable (Cai et al. 2016; Ma 2012). In this regard, scalable distributed algorithms need to be developed that are applicable to building applications for smart thermal environment control and flexible to different scales of the system for the generalization.

2.5 Distributed algorithm for MPC

In controls community, the concept of DMPC was developed to simplify complex control problems and has been investigated for a long time. As a result, several theoretical DMPC

approaches exist. An extensive overview and classification is presented in (Negenborn and Maestre 2014). Other comprehensive reviews exist with application to power (Camponogara et al. 2002) and chemical system (Christofides et al. 2013) applications. In these studies, the general DMPC structure is discussed and compared to centralized or decentralized MPC approaches, by presenting the goal of decomposition (Camponogara et al. 2002) and reviewing the evolution of theoretical approaches (Christofides et al. 2013). With regards to the details of the optimization problem and its decomposition, a well-organized and comprehensive classification based on the couplings in cost function and constraints between the sub-systems is discussed in (Necoara, Nedelcu, and Dumitrache 2011) along with various decomposition algorithms.

In building applications, Bender's decomposition, one of the initial decomposition methods, was used for a multi-zone heating case with central radiant floor and individual convectors (Moroşan et al. 2010). A classical but more recent decomposition method, the primal decomposition, was utilized for solving a resource allocation problem using a coordinator between the grid and a multi-zone building (Lamoudi, Alamir and Béguery 2011) and a building cluster (Pflaum, Alamir, and Lamoudi 2014). The dual decomposition method has been implemented on a multi-zone building application with an Air Handling Unit (AHU) and multiple Variable Air Volume (VAV) boxes (Koehler and Borrelli 2013; Ma, Anderson, and Borrelli 2011; Ma, Richer, and Borrelli 2012). This approach was also applied to a distributed estimation problem (Joe and Karava 2016) as a negotiation strategy and was demonstrated using a case study with an open-plan office space with a radiant floor system. However, dual decomposition is not guaranteed to converge for certain problems whose objective functions are not strictly convex, and requires a fine tuning of step-size parameters. On the other hand, the alternating directions of multipliers (ADMM) is another primal-dual based method that utilizes an extra quadratic penalty term when formulating the Lagrangian function, which has much better convergence behavior compared to dual decomposition. ADMM has been used for several case studies of multi-zone buildings including HVAC component coordination (Cai et al. 2016a) and demand response (Cai et al. 2016c) and monthly optimization to reduce demand charge (Cai et al. 2016b) Nevertheless, the conventional ADMM method is based on a sequential update that requires the order and priority of the agents. Very recently a Proximal Jacobian ADMM (PJ ADMM) method that facilitates parallel computation was developed and implemented for a simulation case study with a single zone served with several roof top units (RTUs) (Hou et al. 2016). Other than typical decomposition method, token-based

scheduling strategy was used in a simulation study with multi-zones sharing a chiller plant. This method solves several sub-problems including multiple zones, chiller, and duct pressure distributions with sequential manner while zone modules are optimized in parallel (Radhakrishnan et al. 2015; Radhakrishnan et al. 2016). In our study, the DMPC algorithm is developed based on the PJ ADMM, and implemented to an actual building to demonstrate optimal performance under realistic conditions.

CHAPTER 3. AGENT–BASED ESTIMATION FOR CONTROL ORIENTED BUILDING MODELS

3.1 Overview

The objective of the work presented in this chapter is to develop and demonstrate, for the first time, an agent-based framework for data-driven grey-box building models. The proposed method introduces building sub-system agents, and each sub-system agent uses information from sensors to solve a smaller-scale estimation problem, with a lower number of parameters compared to centralized schemes. Several models are considered for the sub-system agents and a systematic selection approach is established considering the root mean square error, the parameter sensitivity to output trajectory, and the parameter correlation. The final model is integrated from selected models for each agent. A classical decomposition approach, the dual decomposition, that takes advantage of the separable optimization problem with Lagrangian, is used to solve the maximum likelihood estimation problem in a distributed setting. Two methods are presented based on the distributed and decentralized estimation (Negenborn and Maestre 2014), resulting in a negotiated-shared parameter model and a free-shared parameter model respectively.

The developed agent-based system identification framework is demonstrated using a case-study of an open plan office space with multiple sub-systems (radiant floor, double façade, AHU) and uncontrolled occupant schedule. Additional case-studies are carried out for a localized radiant comfort system and parameter adaptation for different weather conditions and are discussed in Chapters 4 and 5.

3.2 Methodology

This section starts with the definition of the agent structure and then presents the formulation of the grey-box building sub-system models along with the methodology developed to improve the optimization process, and to establish the criteria for model quality. Finally, the shared parameter negotiation and agent-based estimation framework are described.

3.2.1 Agent definition

In the proposed framework, each agent represents a building sub-system type: (a) terminal comfort delivery such as radiant heating/cooling system, chilled beam, under plenum air distribution; (b) building envelope (double façade, curtain wall, etc); (c) zone, i.e. space represented with a single zone or multiple sub-zones for local comfort delivery. Each agent in the multi-agent system can access only a portion of the sensors but has the ability to share data and communicate with its neighbouring agents. The integrated system agent is assembled with information from sub-system agents. Also, there may be sensors deployed outside of the building for measuring and monitoring environment parameters (environment agent).

3.2.2 Estimation of sub-system models

A grey-box model is formed from the heat balance equations on each node. An example for a temperature node is presented in Equation 3.1. X, Cp, R, and Q represent the node temperature, the specific heat capacity, the resistance between two nodes, and the heat flux input to the node, respectively. α is the heat flux coefficient and represents the ratio of the thermal influence of each disturbance input to the state. The neighbouring temperature node is denoted as X_{adj}. Then the continuous time state-space equation is formulated with the state matrix A, input matrix B, state vector X, and input vector u (Equation 3.2). All environment data including outdoor air temperature and solar radiation as well as the controlled heating and cooling supply to the zone form the input vector u. Variables such as the capacity, resistance, and heat flux coefficient α form matrix A and B. The solution of this first order ordinary differential equation is a discretized form of state-space equation assuming that the control inputs are constant for each time-step (Equation 3.1). For this study, the time-step, k, is set to 5 minutes. The temperature of the next time-step is a linear function of the temperature and input at the current time-step and A_d and B_d matrix.

$$Cp_{node}\dot{X}_{node} = \sum \frac{X_{adj} - X_{node}}{R_{adj\sim node}} + \sum \alpha_{node}\dot{Q}_{node} \quad \text{(Eq 3.1)}$$

$$\dot{X} = AX + Bu \quad \text{(Eq 3.2)}$$

$$X_{k+1} = A_d X_k + B_d u_k \quad \text{(Eq 3.3)}$$

In general, the grey-box estimation problem is not linear nor convex in terms of estimate parameter and output temperature trajectory. Statistically, the model structure is a Maximum Likelihood

Estimator (MLE) that requires prior information for each estimate parameter, θ. A typical objective function is the summation of squared residual between the actual operation and the model prediction through all iterations, n. In this study, the square of the above function is used to expand the search space (Equation 3.4). The inverse of the capacity and resistance, and the heat flux coefficient, denoted with H, U and α (Equation 3.4), are estimate parameters, so each element in A_d and B_d matrix of the discrete-time state-space equation is in the form of multiplication of variables.

$$\text{minimize}\left(\sum_{k=1}^{n}(\hat{y}[k]-y[k])^2\right)^2$$

where:

$$X[k+1]=A_d(\theta)X[k]+B_d(\theta)u[k]$$

$$\hat{y}[k]=C_dX[k]$$

$$\theta=\left[Cp_1^{-1},\ldots,Cp_{n_{Cp}}^{-1},R_1^{-1},\ldots,R_{n_R}^{-1},\alpha_1,\ldots,\alpha_{n_\alpha}\right]=\left[H_1,\ldots,H_{n_H},U_1,\ldots,U_{n_U},\alpha_1,\ldots,\alpha_{n_\alpha}\right]$$

(Eq 3.4)

The explicit matrix expression is shown in Equation 3.5. The estimation trajectory is a linear function of the initial state and input trajectory. The lower-triangle matrix with A_d, B_d and C_d becomes larger as the estimation period is increased, and the estimation problem becomes more complex. Fmincon was used in Matlab environment among several optimization solvers for this constrained non-linear optimization problem. The active-set algorithm was selected (Mathworks 2015).

$$\text{minimize}\left(\left[\hat{Y}(\theta)-Y\right]^T\left[\hat{Y}(\theta)-Y\right]\right)^2$$

where:

$$\hat{Y}(\theta)=\begin{bmatrix}\hat{y}[1]\\ \hat{y}[2]\\ \vdots\\ \hat{y}[n]\end{bmatrix}=\begin{bmatrix}C_dA_d(\theta)\\ C_dA_d(\theta)^2\\ \vdots\\ C_dA_d(\theta)^n\end{bmatrix}x_0+\begin{bmatrix}C_dB_d(\theta) & 0 & \cdots & 0\\ C_dA_d(\theta)B_d(\theta) & C_dB_d(\theta) & \cdots & 0\\ \vdots & \vdots & \ddots & \vdots\\ C_dA_d(\theta)^{n-1}B_d(\theta) & C_dA_d(\theta)^{n-2}B_d(\theta) & \cdots & C_dB_d(\theta)\end{bmatrix}\begin{bmatrix}u[0]\\ u[1]\\ \vdots\\ u[n-1]\end{bmatrix}$$

$$\theta=\left[Cp_1^{-1},\ldots,Cp_{n_{Cp}}^{-1},R_1^{-1},\ldots,R_{n_R}^{-1},\alpha_1,\ldots,\alpha_{n_\alpha}\right]=\left[H_1,\ldots,H_{n_H},U_1,\ldots,U_{n_U},\alpha_1,\ldots,\alpha_{n_\alpha}\right]$$

(Eq 3.5)

This grey-box estimation has the following features: (a) Large number of parameters including the resistance, capacitance, and heat flux coefficient. (b) Large search region for each parameter; this large bound increases the chance to fall into a local minimum while there might be a global minimum. (c) Different sensitivity of each estimate parameter to the output trajectory so

parameters require different bounds, which requires trial and error based on intuition and engineering knowledge. Moreover, for the building estimation problem, typically a local minimum is found in the case of large air capacity that results in flat temperature when no or insufficient input excitation is given.

In this study, a sensitivity-based parameter range selection and range shift is implemented to update the parameter bound during the optimization process. In our approach, each parameter has a different search range that has the same sensitivity to the output so that optimal values are found based on impartial optimization for all parameters. Lower and upper bounds of each parameter are set with a bound range γ_p that gives the same perturbation to the output trajectory (Equation 3.6). This is based on the standard deviation of the experimental output trajectory as follows:

$$[\theta_{p,LB}, \theta_{p,UB}] = [\theta_p^{ini} - \theta_p^{ini}\gamma_p, \theta_p^{ini} + \theta_p^{ini}\gamma_p]$$

$$where:$$

$$\gamma_p = \underset{\gamma \in [0,0.99]}{\arg\min} \left(Y_{std} - \sqrt{\frac{\hat{Y}(\theta_p^{ini} + \theta_p^{ini}\gamma)^T \hat{Y}(\theta_p^{ini} - \theta_p^{ini}\gamma)}{n}} \right)^2 \quad \text{(Eq 3.6)}$$

Typically, the optimal parameter set is not inside the initial parameter range so a range shift method is introduced. The algorithm runs until all parameters are located inside the stop range ε, which is the ratio between the distance from the initial value and bound and the distance from the initial and optimal value in each iteration (Table 3.1). Figure 3.1 shows the parameter range shift algorithm for parameter θ_p. k represents the time and the value of ε is 0.01 for this study. During the initial iterations, optimized values are close to the upper or lower bound while as the iterative process evolves parameter bounds are shifted with a different magnitude. In this way, the optimal value of each parameter is found based on different moving steps according to its significance. Finally, all parameters are inside the stop range and the iteration loop is terminated.

Table 3.1 Iteration loop for the parameter range shift

$while \left\| (\theta_p^{k+1} - \theta_p^k) / (\theta_{p,UB}^k - \theta_p^k) \right\| < \varepsilon$
$\theta_p^{k+1} = \underset{\theta_p^k \in [\theta_{p,LB}^k, \theta_{p,UB}^k]}{\arg\min} \left(\left[\hat{Y}(\theta_p^k) - Y \right]^T \left[\hat{Y}(\theta_p^k) - Y \right] \right)^2$
$[\theta_{p,LB}^{k+1}, \theta_{p,UB}^{k+1}] = [\theta_p^{k+1} - \theta_p^{k+1}\gamma_p, \theta_p^{k+1} + \theta_p^{k+1}\gamma_p]$
end

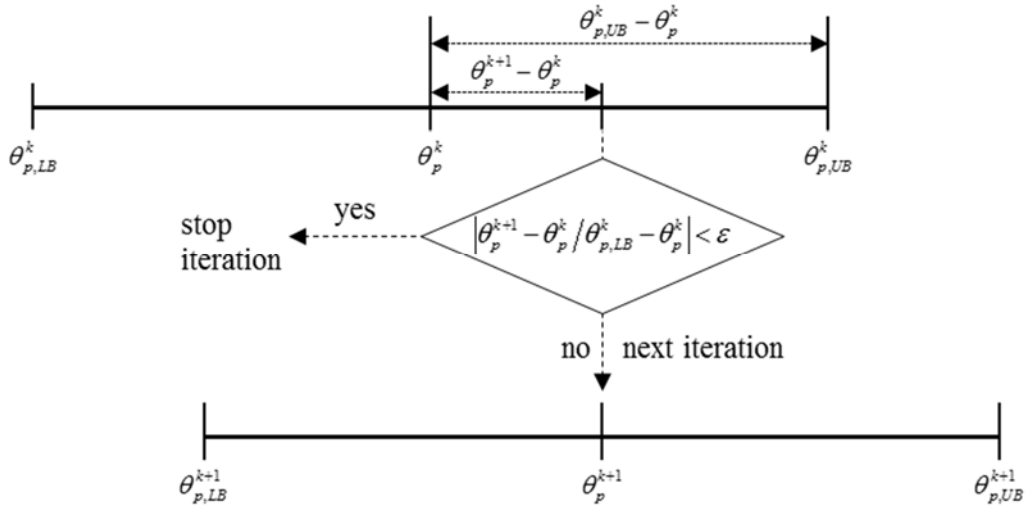

Figure 3.1 Graphical representation of the parameter range shift

3.2.3 Criteria for model quality

The agent-based estimation approach developed in this study, is based on the optimization of sub-system models for which, each agent uses its own sensor and the experimental trajectory for the boundary temperature from its adjacent agent. The final model is assembled without further optimization. Therefore, accurate and robust models are required in the sub-system modelling step. In this regard, several criteria, including the prediction error, parameter significance and parameter correlation, are considered to select the best model among several candidates.

The Root Mean Square Error (RMSE) that shows the error intuitively while maintaining the actual unit of the output data was used for the comparison of each sub-system model. $\hat{y}$, k, and n in Equation 3.7 represent the model output, time, and number of data.

$$RMSE = \sqrt{\frac{\sum_{k=1}^{n} \left(\hat{y}[k] - y[k]\right)^2}{n}} = \sqrt{\frac{\hat{Y}^T Y}{n}} \qquad \text{(Eq 3.7)}$$

The models are also compared based on the significance index, SI_p. Sensitivity of the output trajectory from the model parameter variation is denoted as sensitivity matrix S based on the parameter perturbation method (Equation 3.8) that enables the approximated calculation of sensitivity for the grey-box model where the output trajectory is not explicitly expressed with differentiable function according to each parameter (Del Barrio and Guyon 2003):

$$S_p = \frac{\partial \hat{Y}(\theta_p)}{\partial \theta_p} \approx \frac{\hat{Y}(\theta_p + \Delta\theta_p) - \hat{Y}(\theta_p)}{\Delta\theta_p} \quad \text{(Eq 3.8)}$$

$$\tilde{S}_p = \theta_p S_p \quad \text{(Eq 3.9)}$$

$$SI_p = \sqrt{\frac{\tilde{S}_p^T \tilde{S}_p}{n}} \quad \text{(Eq 3.10)}$$

The variation of each parameter comes from the sensitivity-based parameter range γ_p discussed in Section 3.2. Herein γ_p is recalculated with the optimized value rather than the initial parameter. More specifically, 50 % of the γ_p is multiplied with the parameter value ($\Delta\theta_p = 0.5\gamma_p\theta_p$). For a fair comparison between parameters with different units, the reduced sensitivity matrix is used (Equation 3.9) (Del Barrio and Guyon 2003). The significance index of parameter *p, SI*$_p$ is induced from the reduced sensitivity matrix, whose unit is°C (Equation 3.10).

Finally, the correlation index, *CI*$_p$ (Equation 3.11) is also introduced for the sub-system model *comparison*. The correlation coefficient shows how much each two parameters are correlated, which is denoted as ρ_{pq}. In this study, the Pearson product-moment correlation coefficient is used. K_{pq} and σ_p represent the covariance between two reduced sensitivities from two parameters of θ_p and θ_q, and the standard deviation of the reduced sensitivity from the parameter θ_p. $\bar{S}_p$ and $\bar{S}_q$ represent column vectors consisting of averaged values of the reduced sensitivity matrices $\tilde{S}_p$ and $\tilde{S}_q$. The obtained correlation coefficients are averaged for each parameter except that with itself, which is 1. In Equation 3.11 *m* represents the number of estimate parameters, and *p* and *q* represent the two pairs of estimate parameters. A model with parameters that have lower correlation index is considered to be superior.

$$CI_p = \frac{1}{m-1}\left(\sum_{q=1}^{m} \rho_{pq} - 1\right)$$

where:

$$\rho_{pq} = \frac{K_{pq}}{\sigma_p \sigma_q} = \frac{\left(\tilde{S}_p - \bar{S}_p\right)^T \left(\tilde{S}_q - \bar{S}_q\right)}{\sqrt{\left(\tilde{S}_p - \bar{S}_p\right)^T \left(\tilde{S}_p - \bar{S}_p\right)}\sqrt{\left(\tilde{S}_q - \bar{S}_q\right)^T \left(\tilde{S}_q - \bar{S}_q\right)}} \quad \text{(Eq 3.11)}$$

3.2.4 Shared parameter negotiation

In the agent-based estimation framework of this study, each agent has at least one sensor and boundary temperatures from neighboring agents or environment data such as the outdoor air temperature. Figure 3.2 presents an example of an integration of two sub-system agents. Each sub-system agent has a parameter of resistance for a given physical location, named as shared parameter in this study (shared resistances are denoted with dotted lines in Figure 3.2). All sub-system agents are estimated independently, yielding different values of the shared parameter which are denoted as $R_{23(i)}$ and $R_{23(j)}$. Since the final integrated system agent requires one value ($R_{23(int)}$) where a shared parameter exists, a parameter negotiation based on the dual decomposition is used to converge the different values from the sub-system model estimation to an identical value.

This type of distributed optimization problem is classified as Decoupled Cost but Coupled Constraints (DCCC) (Necoara, Nedelcu, and Dumitrache 2011). Decoupled cost is formed when the sensors are installed for all sub-agents and coupled constraints are shared parameters between each neighboring agent. In the dual decomposition method, the centralized optimization problem is transformed to Lagrangian dual function. The objective function of Lagrangian dual function consists of sub-problem's objective functions and consensus constraints of shared estimate parameters multiplied by the dual variable (Lagrangian multiplier). In this way, the problem is split into separate Lagrangian dual functions solved in parallel by updating the dual variables so the complicating (shared) variables are converged to the identical value (Nedi´c and Ozdaglar 2009).

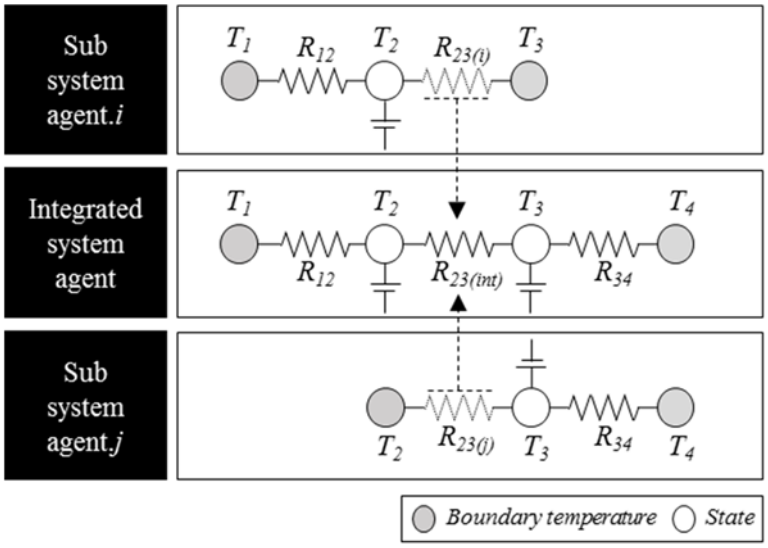

Figure 3.2 Example of sub-system and integrated system agents

Table 3.2 Dual decomposition algorithm for the negotiation between agent *i* and *j*

while $\theta_{ij(i)}^{k+1} = \theta_{ij(j)}^{k+1}$

$$\theta_i^{k+1} = \underset{\theta_i^k}{\operatorname{argmin}} \left(g_i(\theta_i^k) + \lambda_{ij}^k \theta_{ij(i)}^k \right)$$

$$\theta_j^{k+1} = \underset{\theta_j^k}{\operatorname{argmin}} \left(g_j(\theta_j^k) - \lambda_{ij}^k \theta_{ij(j)}^k \right)$$

$$\lambda_{ij}^{k+1} = \lambda_{ij}^k + \mu_{ij} \left(\theta_{ij(i)}^{k+1} - \theta_{ij(j)}^{k+1} \right)$$

end

The typical dual decomposition without bounds for all iterations was not successful in our preliminary study because of the non-convex nature of the objective function. Therefore, lower and upper bounds for the shared parameters are set based on the assumption that the optimal value is located between two bounds which are the optimized values from the previous iteration. The dual decomposition algorithm for the negotiation between two sub-system agents *i* and *j* is shown in Table 3.2. $\theta_{ij(i)}$and $\theta_{ij(j)}$ represent shared parameters that belong to agent *i* and *j*, respectively. A normalized form of the objective function $g(\theta)$, with a percentage of the relative difference between the optimal value from the sub-system agent $f(\theta^*)$ and the current optimal value $f(\theta)$, was introduced for a fair optimization of each agent:

$$g(\theta^k) = 100 \left(\frac{f(\theta^k) - f(\theta^*)}{f(\theta^*)} \right) \quad \text{(Eq 3.12)}$$

The dual variable λ is linearly updated with the time-step μ and the distance between the shared parameters $\theta_{ij(i)}$ and $\theta_{ij(j)}$. The initial λ and the time-step μ are set to 0 and 0.01, for this study.

3.2.5 Residual analysis

As discussed in Section 2 (Background), it may not be realistic to expect that the auto-correlation of the residual and cross-correlation between the input signal and residual based on experiments with the building in its actual operation mode (i.e. with uncertainty due to occupancy schedule, etc) is inside the high confidence range. Therefore, in this study residual analysis does not represent an absolute criterion but provides some useful information as a post processing technique. The equations of auto-correlation (Equation 3.13) and cross-correlation (Equation 3.14) functions are shown below:

$$\hat{\rho}_{rr}(h) = \frac{\sum_{k=1}^{n-|h|}\left(r^{k+h} - \bar{r}\right)\left(r^{k} - \bar{r}\right)}{\sum_{k=1}^{n}\left(r^{k} - \bar{r}\right)\left(r^{k} - \bar{r}\right)} \quad \text{(Eq 3.13)}$$

$$\hat{\rho}_{ru}(h) = \frac{\sum_{k=1}^{n-|h|}\left(r^{k+h} - \bar{r}\right)\left(u^{k} - \bar{u}_i\right)}{\sum_{k=1}^{n}\left(r^{k} - \bar{r}\right)\left(u^{k} - \bar{u}\right)} \quad \text{(Eq 3.14)}$$

r, u, and h represent the residual between the experiment and prediction, input such as boundary temperature or heat flux, and the lag. 75% of the total estimation data length was set for the number of lags (h) since we use experimental datasets, although previous studies based on simulation used a significantly lower number (Bacher and Madsen 2011; Jiménez, Madsen, and Andersen 2008; Kramer, Schijndel, and Schellen 2013). The confidence range was set based on 95% confidence band: $\pm 1.96/\sqrt{n}$.

3.2.6 Agent-based estimation

The agent-based estimation framework consists of two different methods; the negotiated shared-parameter and the free shared-parameter model, representing the distributed and decentralized approach respectively. Both start from sub-system model estimations. The outcome of the distributed method is a typical grey-box model where physical interpretation of the shared parameters is incorporated; different shared parameters from sub-system model estimations are negotiated to be identical. In the decentralized approach, the outcome is a ″pseudo grey-box" model without physical interpretation, as two different shared parameters from the sub-system model estimations are maintained.

3.2.6.1 Distributed method: negotiated-shared parameter model

Figure 3.3 presents the agent-based estimation framework of the distributed method. Sensor information and parameter information are delivered as shown by the dotted and solid arrow respectively. The initial estimate parameter θ^0 comes from the initial parameter agent, and may include information from the building drawings, literature, or a building audit. With this initial parameter, all sub-system models are estimated as discussed in Section 3.2. All models for each sub-system agent are compared to each other with three criteria including the RMSE, significance index *SI*, and correlation index *CI*, and the best models are selected (Section 3.3). As each sub-

system agent is optimized, the shared parameters for the selected best models are negotiated to be identical based on the dual decomposition method. In this step, the sensitivity-based parameter range is fixed at the final (optimized) value from the sub-system agent. Then, sub-system agent optimizations are carried out independently for fine tuning, by fixing the shared parameters to estimate the rest of the parameters, to improve the accuracy of sub-system models. Finally, the integrated model is assembled and tested with RMSE and residual analysis of auto-correlation and cross-correlation.

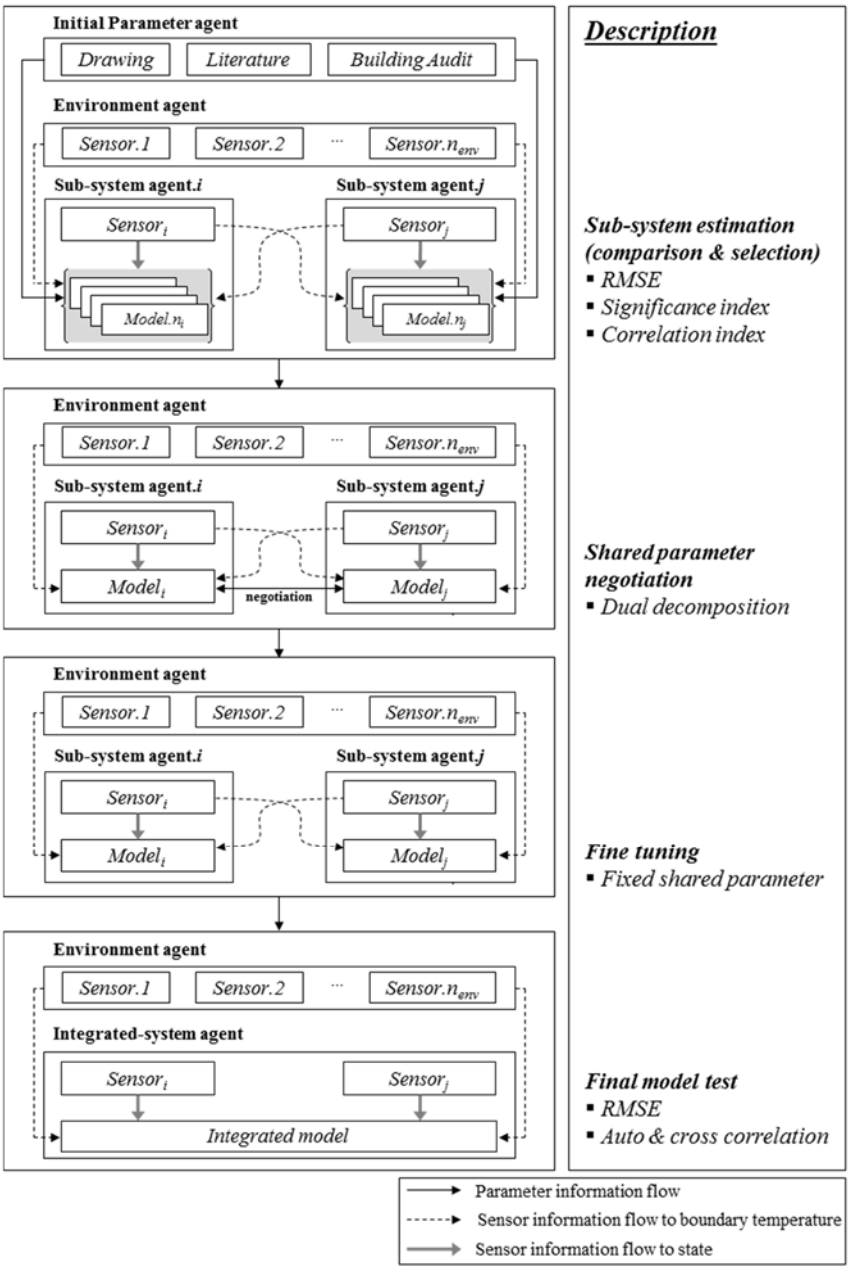

Figure 3.3 Agent-based estimation framework (distributed method)

3.2.6.2 Decentralized method: free-shared parameter model

Figure 3.4 shows the information flow of the decentralized estimation. The initial steps are the same with the distributed estimation but the shared parameters are not negotiated. Therefore, coupled elements in off-diagonal parts of a state matrix have different value ($R_{23(i)}$ and $R_{23(j)}$) originate from each sub-system agent. A generic example, for the integrated-system agent in Figure 3.2, is shown in Equation 3.15.

$$A = \begin{bmatrix} -\frac{1}{Cp_2}\left(\frac{1}{R_{12}} + \frac{1}{R_{23(i)}}\right) & \frac{1}{Cp_2}\left(\frac{1}{R_{23(i)}}\right) \\ \frac{1}{Cp_3}\left(\frac{1}{R_{23(j)}}\right) & -\frac{1}{Cp_3}\left(\frac{1}{R_{23(j)}} + \frac{1}{R_{34}}\right) \end{bmatrix} \quad \text{(Eq. 15)}$$

All sub-system agents are estimated independently using boundary temperatures for the adjacent agent from the experimental data. Thus, the integrated model yields good results once each sub-model shows good agreement with the experiment data. In other words, well-estimated sub-system models guarantee the prediction accuracy of the integrated model regardless of the agreement of shared parameters. However, the physical meaning of shared parameters is compromised.

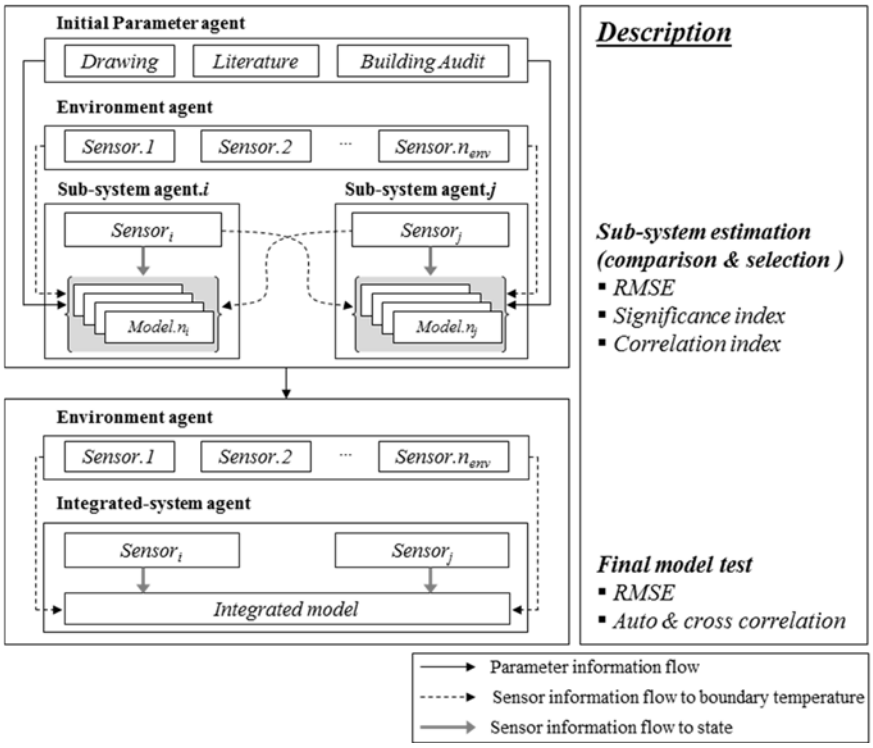

Figure 3.4 Agent-based estimation framework (decentralized method)

3.3 Case study: single zone modelling

This section presents a case-study for the implementation of the agent-based system identification framework. It starts with a description of the test-bed and the data collection process and then presents the model estimation and selection for each sub-system and the integrated system.

3.3.1 Experiment

An open plan office space (9.9 m by 10.5 m) that can host up to 20 occupants is a Living Laboratory and was considered as test-bed for this study (Figure 3.5). Its main features are a radiant floor slab and a south facing double façade system with 1.52 m cavity. A Building Management System (BMS) is available through the installed Tridium JACE controllers and Niagara/AX software framework (Tridium Inc), which in addition to a variety of internet-enabled features gives the ability to monitor, control, and automate all the building systems regardless of manufacturer or communication protocols.

Figure 3.5 Exterior view of the building and test-bed (Living Lab 1)

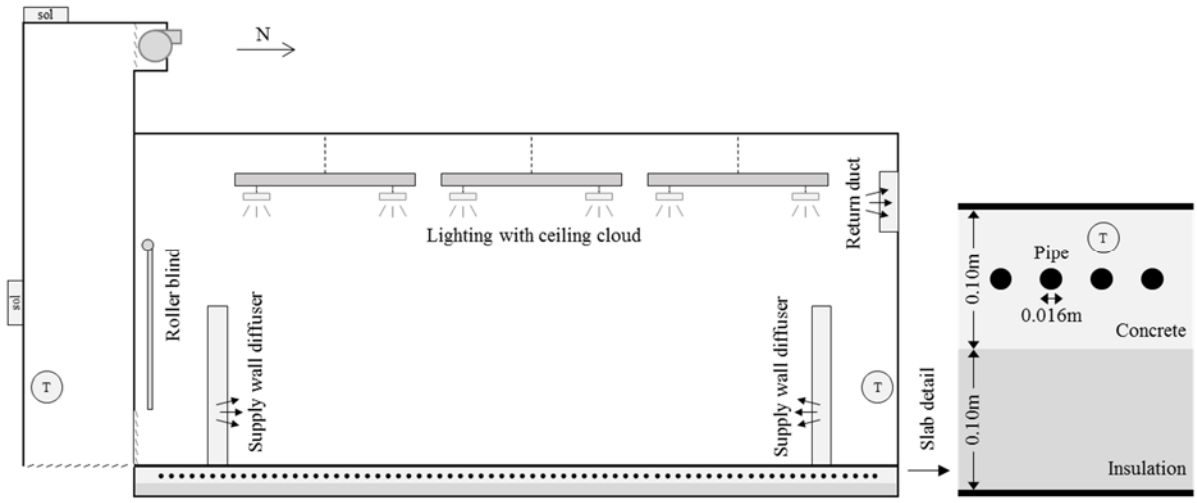

Figure 3.6 Section view of the open-plan office space with details of the floor slab (notation: T and sol represent the sensors for temperature and solar radiation)

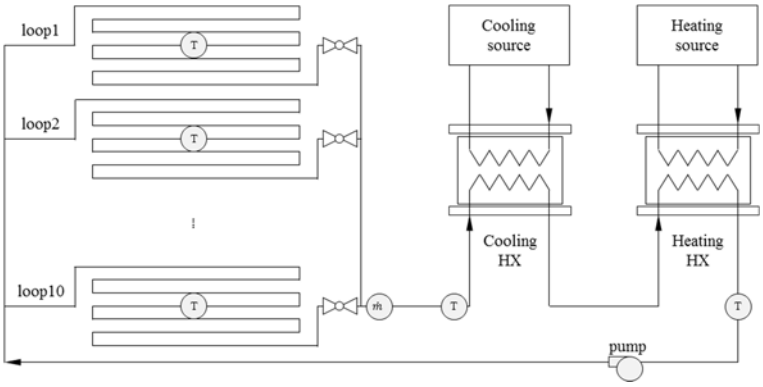

Figure 3.7 Hydronic circuit of the radiant floor system (notation: T and ṁ represent the sensors for temperature and flow rate)

All sensor locations are illustrated in Figure 3.6 which presents a section view of the office. Details of the hydronic circuit for the radiant floor system are shown in Figure 3.7. Thermistors were used to measure the outdoor air temperature on the roof (BAPI, BA/10K-3, ±0.2% @0~70°C), the cavity air temperature in the double façade (BAPI, BA/10K-3, ±0.2% @0~70°C), and the room air temperature (BAPI, BA/BS2-WTH-SO, ±0.3°C @ 25°C). The solar radiation was measured with two LI-COR 200-SL pyranometers (resolution of 0.1 W/m^2 and accuracy of 3%) mounted on the exterior glass surface (vertical) and the roof of the double façade (horizontal). Resistance Temperature Detectors (RTDs) were used for measuring the air temperature of the duct (ACI, A/TT1K-6, ±0.5% @-40~85°C), pipe water temperature of the radiant floor (ACI, A/TT1K-5, ±0.5%), and slab temperature inside the concrete (ACI, A/TT1K-LTS, ±0.3°C @ 0°C). The slab is divided into 10 sections. An RTD sensor with copper shielding is embedded at the center of each section, around 1.9 cm from the top surface. The average reading of 10 RTD sensors was used for the estimation. The radiant floor in this office space has been constructed to provide local control and sensing capabilities, since this is a research Living Laboratory. In this study, although the average value of 10 RTD sensors was used, their difference was less than 1°C. Therefore, one or two sensors would be sufficient for this experiment and hence, the methodology can be generalized to typical buildings. The pipe circuit after the pump consists of 10 parallel loops in the concrete slab, which are merged prior to the heat exchanger (Figure 3.7). The supply and return water temperature was measured at the inlet and outlet side of the heat exchanger. The water flow rate was measured with a turbine flow meter (ONICOM, F-1110, ±1 @ 3~30ft/s) installed before the heat exchanger.

Occupants (graduate students) have different schedules which was not monitored and no information was stored for the internal heat gains including the equipment and people except the power consumption of the electric lighting, which was measured in the BMS system. A roller shade installed on the inside surface of the window was fixed at a low position to decrease the uncertainty due to the solar gains and to eliminate the need to account for the time varying resistance between the cavity and room that was used in previous studies (Gwerder and Gyalistras 2013; Sun et al. 2010). The double façade has two vents on the lower section; one is between the cavity and outside and the other is between the cavity and the room. An exhaust fan with vent is located on the upper section of the façade. All vents were closed during the experiment and the fan was switched off so natural and mechanical ventilation in the cavity were not considered in this study. The room was conditioned using the radiant floor system by controlling the supply water temperature with PID so the air temperature set-point was met, while the water flow rate was fixed at 0.046 cubic meter per minute (12 gallon per minute), which is the maximum flow rate for the given pressure setpoint of 0.69 bar (10 pound per square inch) of the pipe. The air temperature set-point was modified every 2 hours, based on a randomly selected value between 21 to 24°C. This is not the PRBS method but it was found to provide sufficient excitation to the system. The AHU provides ventilation to the room with supply air temperature equal to the set-point temperature through three cylinder wall diffusers located in the three corners of the room and one rectangle wall diffuser on northern wall. Room air temperature, controlled by the radiant floor system, was not regulated well with variant set point temperature due to the large capacity of the floor so heating and cooling was provided from the AHU and acted as a disturbance. The system identification experiment was carried out between June 1 and 20. Data collected during the first five days from the start of the experiment was used for estimation and data from the following fifteen days for validation. The estimation set is followed by the validation set not to repeat the calculation of initial states where there is no sensor installed. All data were averaged every 5 minutes.

3.3.2 Sub-system model estimation and selection

With a centralized estimation approach, a large number of estimate parameters, roughly between 12 and 24 depending on the model structure, is unavoidable. Also, each sub-system has different dynamics, e.g. the magnitude of fluctuation of double façade air temperature is much larger than

that of room air and slab temperature so the centralized estimation provides good results only for the double façade. Thus, in the agent-based approach, the single zone building model is represented by three different sub-system agents, namely, the double façade agent, radiant floor agent, and room agent.

In the modeling framework developed in this study, sub-system models are simplified linear state-space models that approximate with adequate resolution, the full dynamics; their structures represent a compromise between simplicity and preservation of physical sense. All parameters are time-invariant, temperature-independent, and some of them are lumped according to the model structure. Unknown initial values for states without sensor measurements are estimate variables as well. Radiative heat transfers between surfaces are not considered. Initial conduction resistances are originated from the drawing when available, and capacitances are based on the air volume. Initial values of the heat flux coefficient (α) are calculated between 0 and 1, based on standard building properties and prior experience. For the significance index comparison of each sub-system model, all values are summed according to the estimate parameter type, i.e. U, H, and α. For the correlation index comparison of each sub-system model, averaged values along with the minimum and maximum of all estimate parameters are shown.

3.3.2.1 Double façade agent

Two sub-system model structures are considered for the double façade agent including first and second order models (Figure 3.8). T_{cav} and $T_{ext.win}$ represent the cavity temperature where the installed sensor is located and the exterior window surface temperature for which no sensor information is available. A third order model that might have another state on the interior window between the cavity and the room is not considered in this study because the dynamics between two neighboring agents is assumed to be represented with a time-invariant resistance without any state for the shared parameter negotiation. Boundary temperatures from the outdoor environment (T_{out}) and the adjacent room agent (T_{room}), along with the solar radiation ($Q_{sol,ver}$) are used as known inputs. The heat flux input on each state is multiplied by the corresponding coefficient ($\alpha_{sol.ext.win}$ and $\alpha_{sol.cav}$). An initial value for the convective heat transfer coefficient on the double façade side was adopted from the literature (Park et al. 2004) and for the room side from TRNSYS type 56 (TRNSYS 17 2010). Figure 3.9 shows the model comparison for the double façade agent; it consists of five figures and the x-axis represents the model number. The first figure shows the

RMSE of the estimation (E) and validation set (V). The second, third and fourth figures show the significance index of each parameter type, and the fifth figure shows the correlation index. Figure 3.10 shows the estimation (5 days, 1~1440) and validation (15 days, 1441~5760) results. Model 2 has lower error in the estimation period but the validation set shows almost the same accuracy for both models. The significance index does not provide a clear indication but parameters of model 1 are less correlated to each other. Model 1 with one state that does not require initial state information for unmeasurable points has been selected to be the best model.

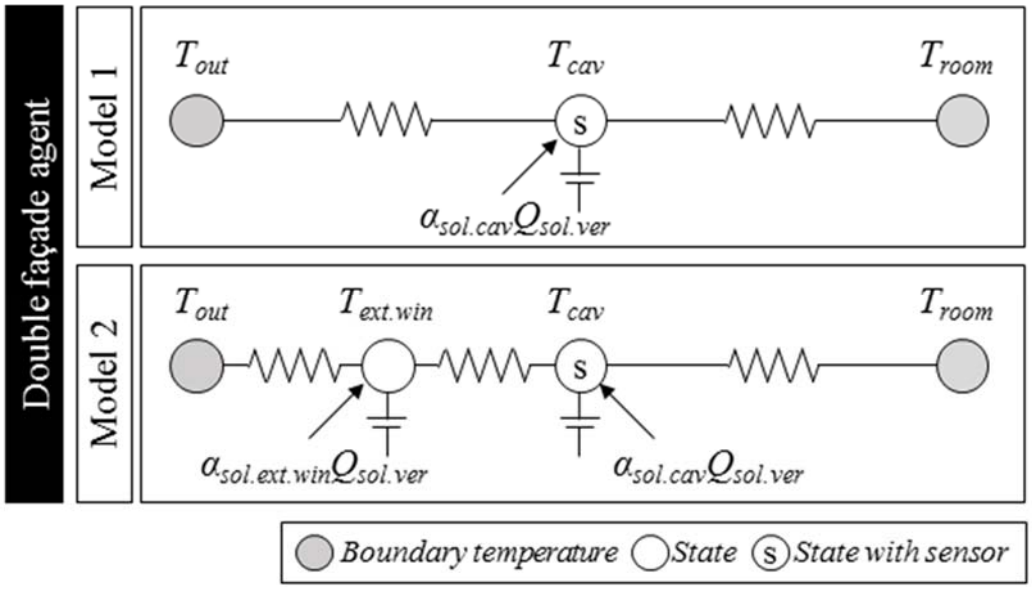

Figure 3.8 Structure of double façade agent models

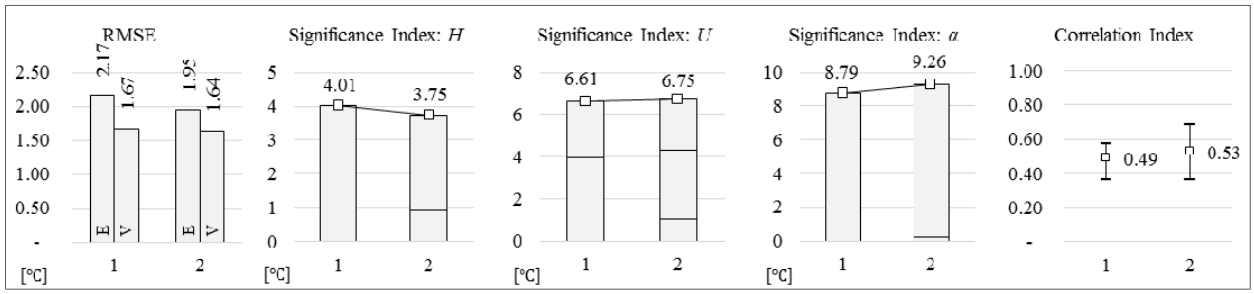

Figure 3.9 Model comparison of double façade agent (E and V represent estimation and validation)

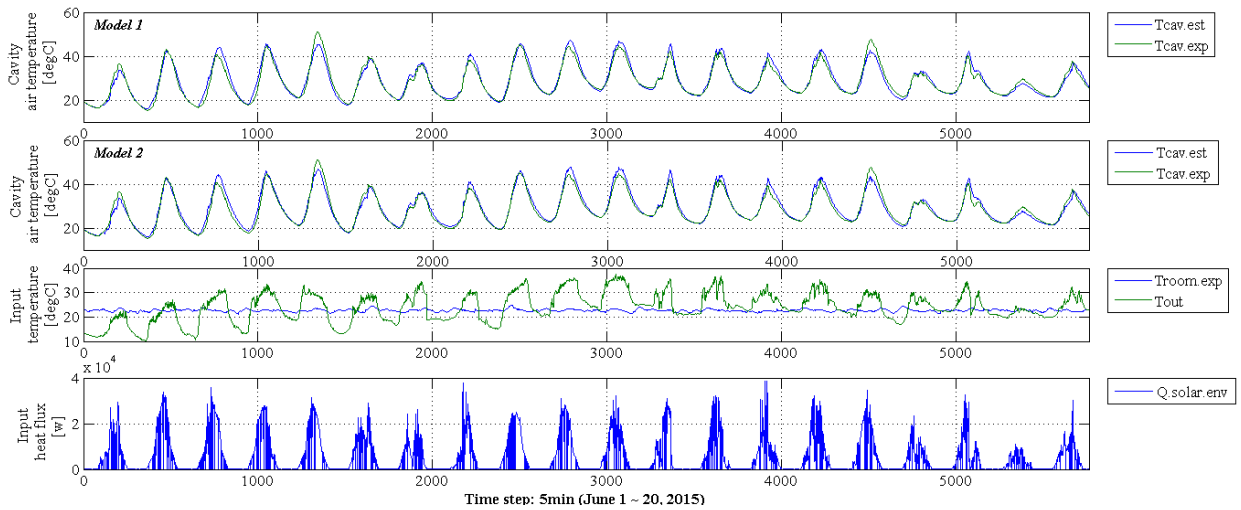

Figure 3.10 Estimation (1~1440) and validation (1441~5760) results for the double façade agent models

3.3.2.2 Radiant floor agent

Three sub-system model structures are considered for the radiant floor agent including two second order models and a third order model (Figure 3.11). T_{slab} represents the concrete temperature where the RTD sensors are located. In model 1 there is no additional parameter below T_{source} since there is insulation (10 cm) and air plenum (60 cm) below the slab so this boundary is assumed to be adiabatic. In model 2, constant temperature of 21°C for the adjacent zone in the floor below is considered (T_{adj}) while model 3 has an additional state where the insulation and air plenum are located, denoted as T_{sink}. The air temperature from the room agent (T_{room}) is the boundary input and the heat flux from the hot water to the concrete through the pipe (Q_{rad}) is the controlled input. The disturbance inputs for the heat flux due to transmitted solar radiation and lighting ($Q_{sol.ver}$ and Q_{light}) are considered along with their corresponding coefficients ($\alpha_{sol.slab}$ and $\alpha_{light.slab}$). Low-order models developed for radiant floor systems in the literature adopted a model structure with the hot water temperature as boundary input (Feng et al. 2015; Nghiem et al. 2012; Nghiem, Pappas, and Mangharam 2013; Široký et al. 2011; Sourbron, Verhelst, and Helsen 2013); some of them used the supply water temperature as a boundary temperature for control (Široký et al. 2011; Sourbron, Verhelst, and Helsen 2013) and others used the water flow rate with on/off control (Feng et al. 2015; Nghiem et al. 2012; Nghiem, Pappas, and Mangharam 2013). The model structure developed in this study has Q_{rad} as control input. In this way, both the supply water temperature and water flow rate could be controlled according to the sequence of Q_{rad}. All initial values including the conduction resistance and capacity are based on the design drawings. However, the exact material

properties of concrete and insulation were not available, so assumptions were made, e.g. the concrete and insulation types are typical, and the pipe is located in the middle of the concrete slab. The convective heat transfer coefficient between the floor and the air is a constant value based on the European standard (European Standard (UNI EN 1264-5) 2009).

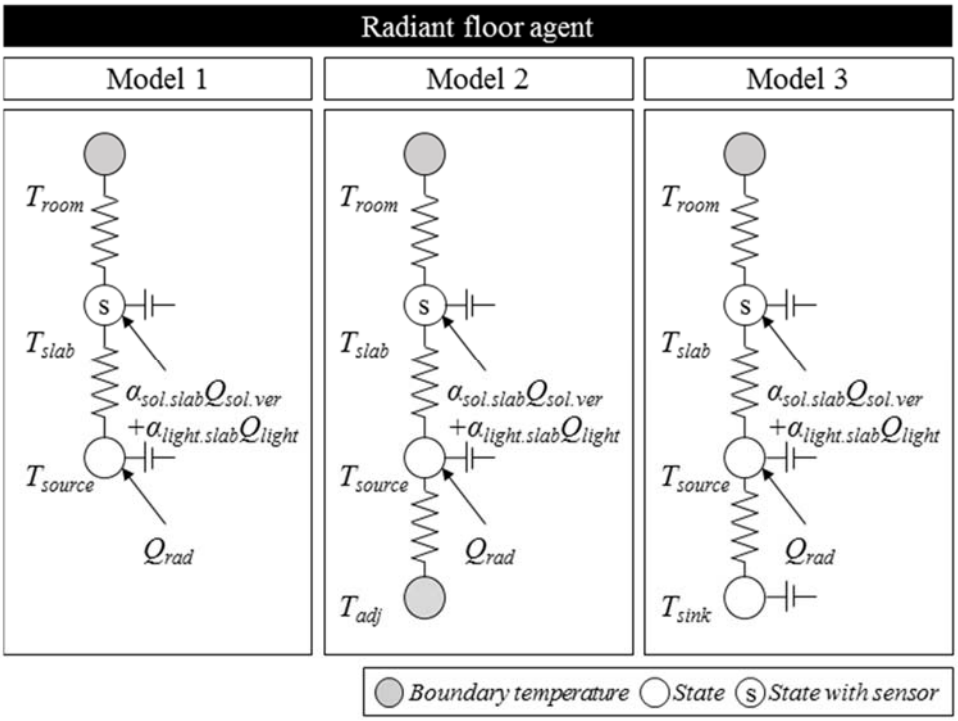

Figure 3.11 Structure of radiant floor agent models

Figure 3.12 shows the comparison with the RMSE, significance index, and correlation index for the radiant floor agent models and Figure 3.13 presents the estimation and validation results. The significance and correlation index of model 2 and 3 did not provide clear evidence for the model selection. The RMSE was sufficient to discard model 1; its predictions does not follow the experimental data because its structure is too simple to reflect the actual heat transfer phenomena below the slab. On the contrary, model 2 and model 3 could capture this dynamics using a constant temperature for the adjacent zone or an additional state. Model 3, shows the best performance, as its prediction follows the experiment trajectory with low error for the entire period so it was selected to be the best model. The significance index for α is very small that it is neglected in the integrated model.

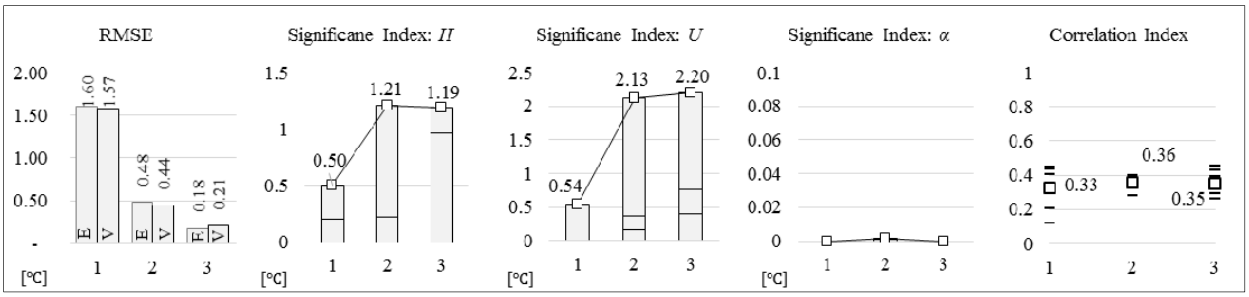

Figure 3.12 Model comparison of radiant floor agent (E and V represent estimation and validation)

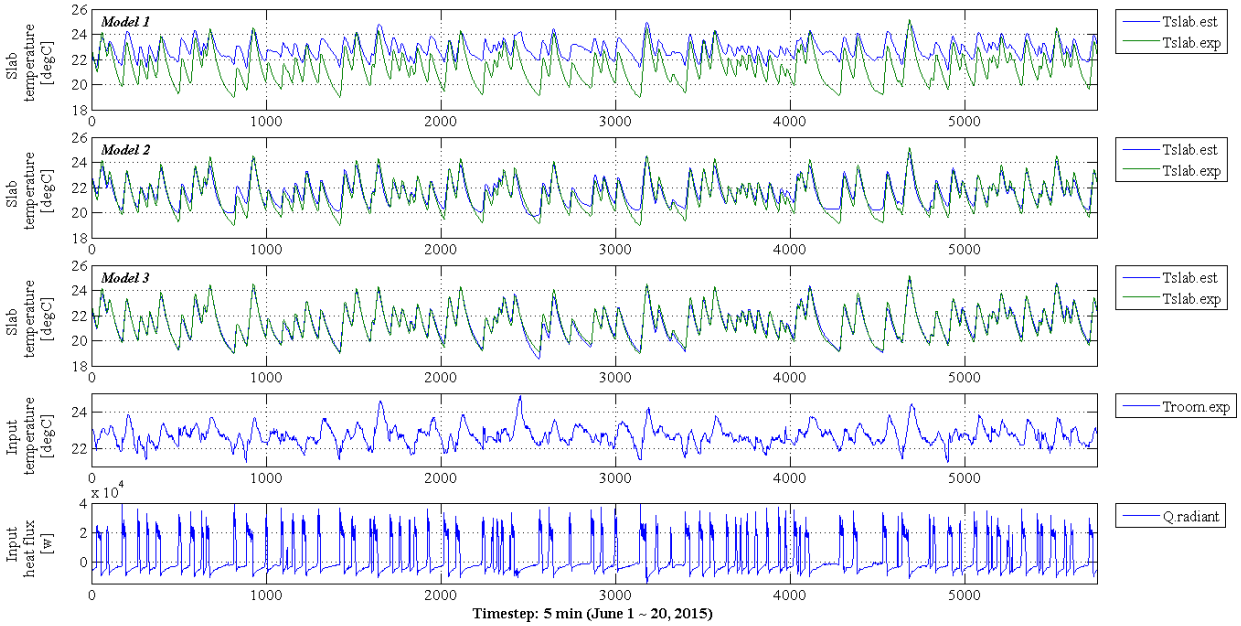

Figure 3.13 Estimation (1~1440) and validation (1441~5760) results for the radiant floor agent models

3.3.2.3 Room agent

Three sub-system model structures are considered for the room agent including first, second, and third order models (Figure 3.14). The outdoor air temperature (T_{out}) is used as a boundary temperature along with the two temperatures from the two adjacent agents of the double façade (T_{cav}) and radiant floor (T_{slab}). T_{env}, $T_{ext.env}$, and $T_{int.env}$ are envelope temperatures considered in models 2 and 3 (Figure 3.14). The transmitted and incident solar radiation ($Q_{sol.ver}$ and $Q_{sol.hor}$, respectively) and lighting (Q_{light}) heat gains are used as disturbance inputs multiplied by the corresponding coefficients ($\alpha_{sol.room}$, $\alpha_{sol.env}$, $\alpha_{sol.ext.env}$, *and* $\alpha_{light.room}$,). The internal heat gain ($Q_{int,heat}$) consists of heat flux values for computers, monitors and people (adopted from Hosni, Jones, and

Xu. 1999; Wilkins and Hosni 2011). $Q_{int,heat}$ is multiplied by the heat flux coefficient (α_{ppl}), which represents the number of people and it is an estimate parameter. The heat flux from the air handling unit (Q_{AHU}) is an input to the room air temperature (T_{room}). The room air temperature varies according to the temperature difference with adjacent mediums through convection and radiation. However, relatively direct changes are made due to AHU since a portion of the room air is displaced with heating and cooling injection. Therefore, the inverse of the air capacity in the input matrix (B), which is multiplied to the heat flux input from the air system of the state-space equation, is treated as a separate estimate parameter in addition to that in the state matrix (A). The first-order model considers only the room air temperature as state variable, which can be justified by the fact that is a high performance building so the external wall is well insulated (including two insulation layers and the air space). The second and third order models are more detailed in terms of including the inputs to the state that represents the envelope temperature. All initial values are from the European standard (European Standard (UNI EN 1264-5) 2009), literature (Park et al. 2004), and TRNSYS type 56 (TRNSYS 17 2010) for the floor surface, wall surface, and double façade side surface, respectively.

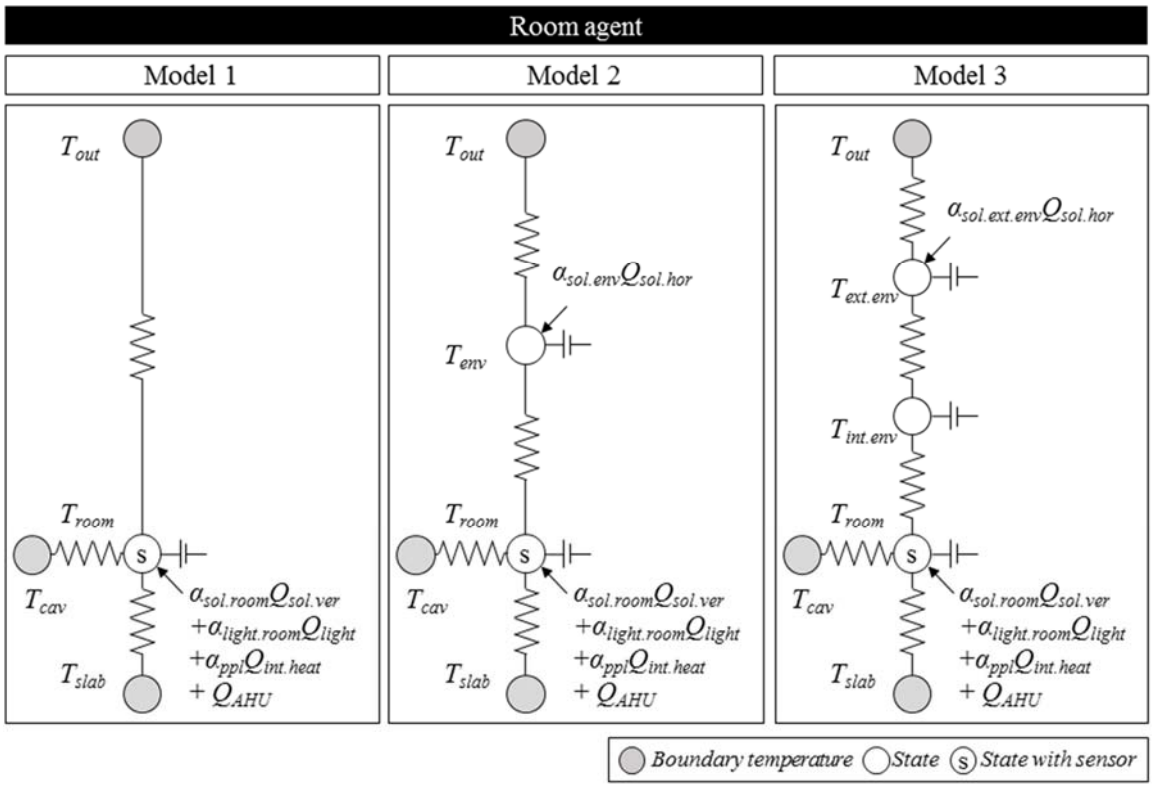

Figure 3.14 Structure of room agent models

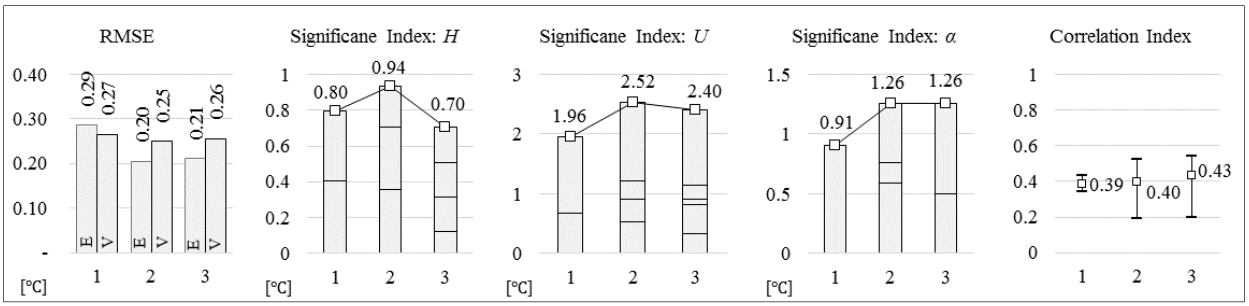

Figure 3.15 Model comparison of room agent (E and V represent estimation and validation)

Figure 3.15 shows the comparison with the RMSE, significance index, and correlation index for the room agent models and Figure 3.16 presents the estimation and validation results. All models are good in terms of the RMSE. However, model 1 is less accurate than model 2 and model 3, and all significance indices are lower because the resistance between outdoors and the room, and the coefficients multiplied to Q_{light} and Q_{solar} are very small and could be neglected. Model 3 has lower significance indices and larger correlation indices compared to model 2. Therefore, model 2 has been selected to be the best model.

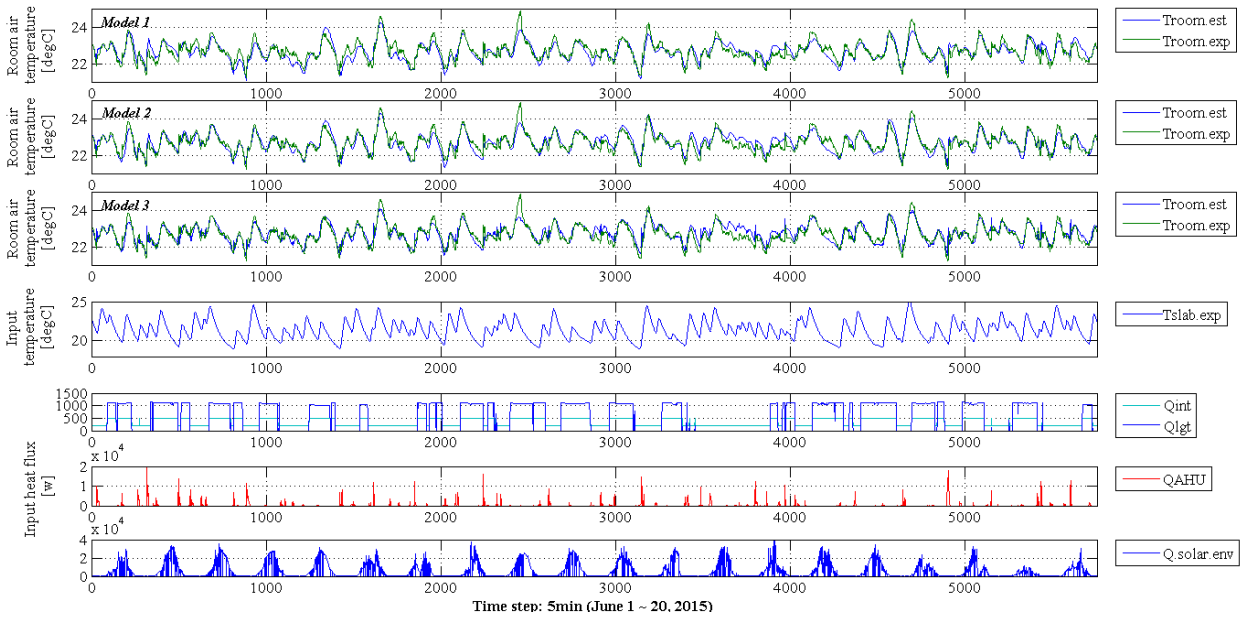

Figure 3.16 Estimation (1~1440) and validation (1441~5760) results for the room agent models

3.3.3 Integrated-system model

Figure 3.17 shows the thermal network of the integrated-system agent. The first order, third order, and second order models from the double façade, radiant floor, and room agent are assembled to the integrated-system agent. It has one boundary temperature corresponding to the outdoor air (T_{out}) and six states; three of them, i.e. the cavity air (T_{cav}), room air (T_{room}) and slab temperature (T_{slab}) have information from sensor data. Two different models are discussed in the following sections.

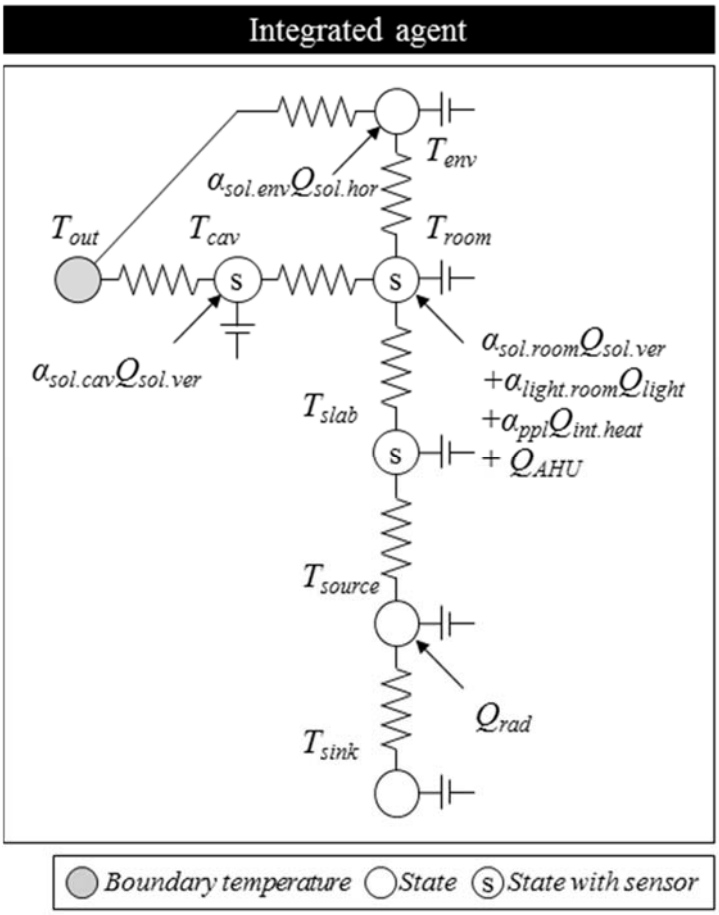

Figure 3.17 Structure of integrated agent model

3.3.3.1 Negotiated-shared parameter model

Table 3.3 shows the dual decomposition algorithm for this case-study. *i*, *j*, and *k* represent double façade, radiant floor, and room agent. All values and procedures were set as explained in the methodology (Section 3.4). The number of the estimated variables are 4, 7, and 12 for the double façade agent, radiant floor agent, and room agent, respectively. Two of them are shared parameters (complicating variables) which result in four copies for three sub-system agents; one for the double

façade agent, one for the radiant floor agent, and two for the room agent. Therefore, it is a sparse problem in terms of the number of complicating variables (2) compared to that of all variables (23) and reasonable to apply the decomposition theory.

Table 3.3 Dual decomposition algorithm for the case-study

while $\theta_{ij(i)}^{k+1} = \theta_{ij(j)}^{k+1}$ and $\theta_{jk(j)}^{k+1} = \theta_{jk(k)}^{k+1}$

$$\theta_i^{k+1} = \underset{\theta_i^k}{\operatorname{argmin}} \left(g_i(\theta_i^k) + \lambda_{ij}^k \theta_{ij(i)}^k \right)$$

$$\theta_j^{k+1} = \underset{\theta_j^k}{\operatorname{argmin}} \left(g_j(\theta_j^k) - \lambda_{ij}^k \theta_{ij(j)}^k + \lambda_{jk}^k \theta_{jk(j)}^k \right)$$

$$\theta_k^{k+1} = \underset{\theta_k^k}{\operatorname{argmin}} \left(g_k(\theta_k^k) - \lambda_{jk}^k \theta_{jk(k)}^k \right)$$

$$\begin{bmatrix} \lambda_{ij}^{k+1} \\ \lambda_{jk}^{k+1} \end{bmatrix} = \begin{bmatrix} \lambda_{ij}^{k} \\ \lambda_{jk}^{k} \end{bmatrix} + \begin{bmatrix} \mu_{ij} & 0 \\ 0 & \mu_{jk} \end{bmatrix} \begin{bmatrix} \theta_{ij(i)}^{k+1} - \theta_{ij(j)}^{k+1} \\ \theta_{jk(j)}^{k+1} - \theta_{jk(k)}^{k+1} \end{bmatrix}$$

end

Figure 3.18 shows the evolution of shared parameters (upper two graphs) and dual variables (lower two graphs). The first shared parameter ($\theta_{ij(i)}$ and $\theta_{ij(j)}$), which is the inverse of resistance between the double façade agent and room agent, is converged in fourteenth iterations. The second shared parameter ($\theta_{jk(j)}$ and $\theta_{jk(k)}$), the resistance between the room agent and radiant floor agent, is converged in eighth iterations. In the meantime, the two dual variables (λ_{ij} *and* λ_{jk}) are converged to a constant value.

Figure 3.19 represents the estimation and validation results of negotiated-shared parameter model. The three upper graphs show the comparison between the model prediction (blue line) and the experiment (green line) for the three agents. The two lower graphs present the exogenous and control input, which are the outdoor air temperature and heat flux input from the air system, solar radiation, and radiant floor system. The RMSE of the estimation period is 2.16, 0.29, and 0.24°C, and that of the validation period is 1.71, 0.46, and 0.37°C for cavity air, room air, and slab temperature, respectively. The estimation result is fairly robust and stable as the validation maintains its good prediction even for a period of 20 days which was considered to test the model, as information about the internal heat gain due to equipment and occupancy schedule was not available, and also the final integrated model is not estimated but built based on the information

from the sub-system (agent) models. Estimated values for all parameters are presented in Table 3.4.

An integrated model (Figure 3.17) developed based on standard centralized estimation, failed to provide accurate predictions for the room and slab temperatures. Also, integrated models assembled with the agent negotiation approach, did not provide accurate predictions, when sub-system models with inferior performance (e.g. model 2 for the double façade agent, model 1for the room agent, model 1 for the radiant floor agent), based on the criteria presented in Section 3.3, were used. These two comparisons (results not shown) confirm the merits of the sub-system model evaluation and distributed system identification presented in this work.

Table 3.4 Estimated values of negotiated-shared parameter model

H_{cav}	1.13E-6	$U_{out\sim cav}$	51.92	$\alpha_{sol.cav}$	0.08
H_{slab}	3.53E-8	$U_{cav\sim room}$	29.07	$\alpha_{sol.room}$	3.77E-19
H_{source}	3.61E-7	$U_{room\sim slab}$	527.58	$\alpha_{sol.env}$	0.17
H_{sink}	4.14E-17	$U_{slab\sim source}$	1402.44	$\alpha_{light.room}$	0.14
H_{room}	2.43E-7 *(rad+conv)*	$U_{source\sim sink}$	249.39	α_{ppl}	1.91
	8.00E-8 *(conv)*	$U_{room\sim env}$	21.75		
H_{env}	6.31E-8	$U_{out\sim env}$	269.36		

*H (°C/J) represents the inverse of capacity corresponding to the temperature node (indicated by the subscript) and U (W/°C) the inverse of resistance between the temperature nodes in Figure 3.17.

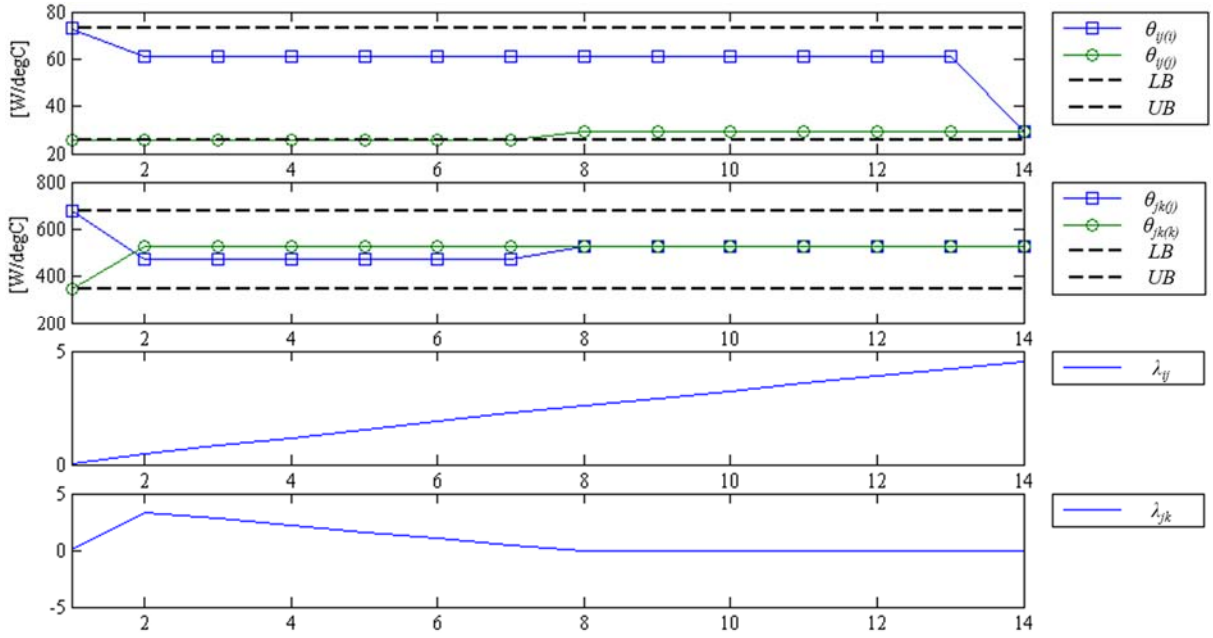

Figure 3.18 Evolution of shared parameters and dual variables

Residual analysis including auto-correlation and cross-correlation has been used as post processing for the estimation period. The confidence range is set at ±0.0517 based on the 95% confidence standard deviation. Figure 3.20 shows a sample auto-correlation function of the residual from each agent and Figure 3.21 shows a sample cross-correlation function between the input and residual. All of them are outside of the confidence range, which are illustrated as two parallel lines, even though 75% of data length was examined.

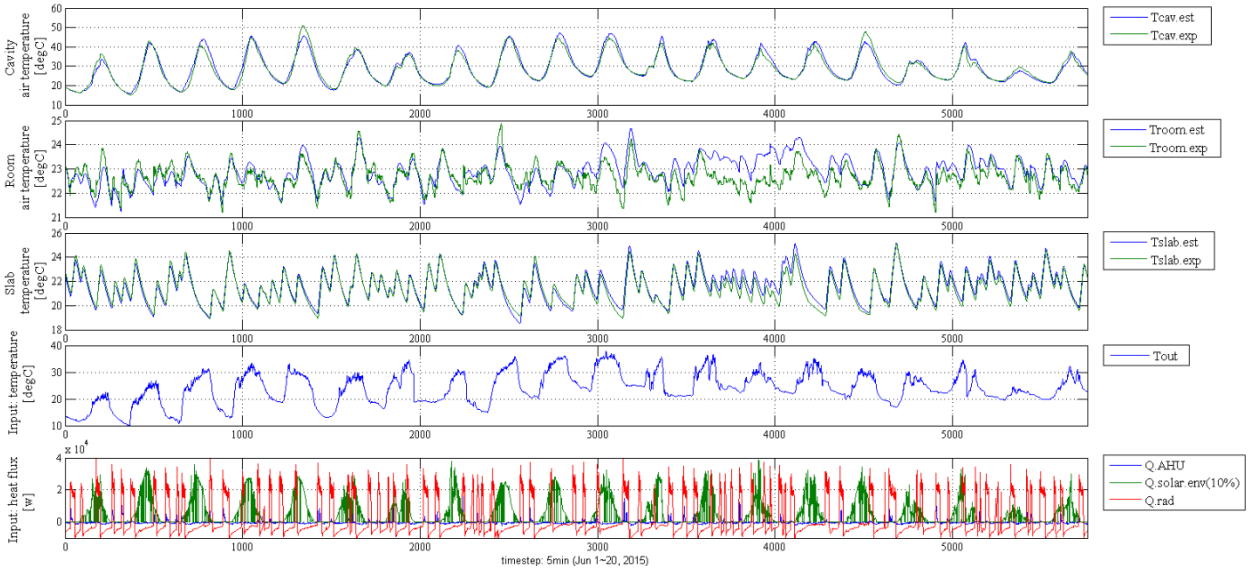

Figure 3.19 Estimation (1~1440) and validation (1441~5760) results of negotiated-shared parameter model

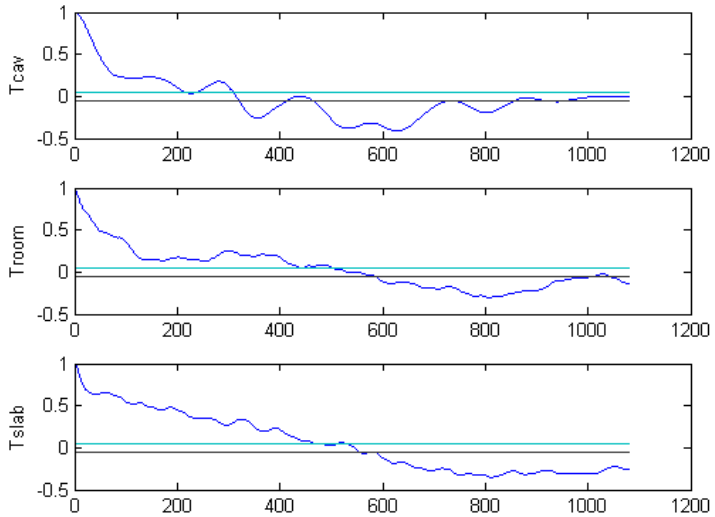

Figure 3.20 Sample auto-correlation function of the residual (negotiated-shared parameter model)

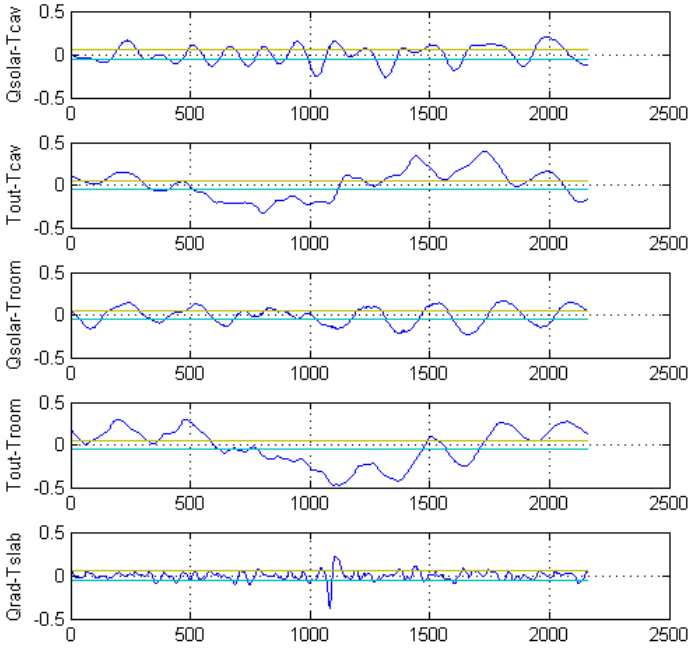

Figure 3.21 Sample cross-correlation function between input and residual (negotiated-shared parameter model).

3.3.3.2 Free-shared parameter model

Figure 3.22 represents the estimation and validation results for the free-shared parameter model. The structure is the same with that explained for Figure 3.19. The RMSE of the estimation period is 2.16, 0.23, and 0.15°C, and that of the validation period is 1.68, 0.36, and 0.30°C for the cavity air, room air, and slab temperature, respectively. The prediction of the free-shared parameter model is slightly better than that of the negotiated-shared parameter model in both the estimation and validation period. Therefore, it has been shown that the physical meaning of the shared parameter model is compensated with a small loss in accuracy of the prediction, which however, is not significant considering the complexity of the integrated-system model. Estimated values for all parameters are presented in Table 3.5. Figure 3.23 and 3.24 show the sample auto-correlation and cross-correlation function for the free-shared parameter model, based on the same setting and structure used in the negotiated-shared parameter model. All results are generally similar with those obtained with the negotiated-shared parameter model but the auto-correlation of the room agent and the radiant floor agent are slightly better than the negotiated-shared parameter model.

Table 3.5 Estimated values of free-shared parameter model

H_{cav}	4.68E-07	$U_{out\sim cav}$	123.93	$\alpha_{sol.cav}$	0.19
H_{slab}	3.47E-08	$U_{cav\sim room}$	72.87 (double façade agent)	$\alpha_{sol.room}$	1.89E-17
H_{source}	3.48E-07		25.48 (room agent)	$\alpha_{sol.env}$	0.17
H_{sink}	4.63E-12	$U_{room\sim slab}$	679.76 (room agent)	$\alpha_{light.room}$	0.18
H_{room}	1.97E-7 (rad +conv)		345.24 (radiant floor agent)	α_{ppl}	2.74
	7.91E-8 (conv)	$U_{slab\sim source}$	1371.31		
H_{env}	8.37E-08	$U_{source\sim sink}$	280.28		
		$U_{room\sim env}$	34.4		
		$U_{out\sim env}$	300.43		

*H (°C/J) represents the inverse of capacity corresponding to the temperature node (indicated by the subscript) and U (W/°C) the inverse of resistance between the temperature nodes in Figure 3.17.

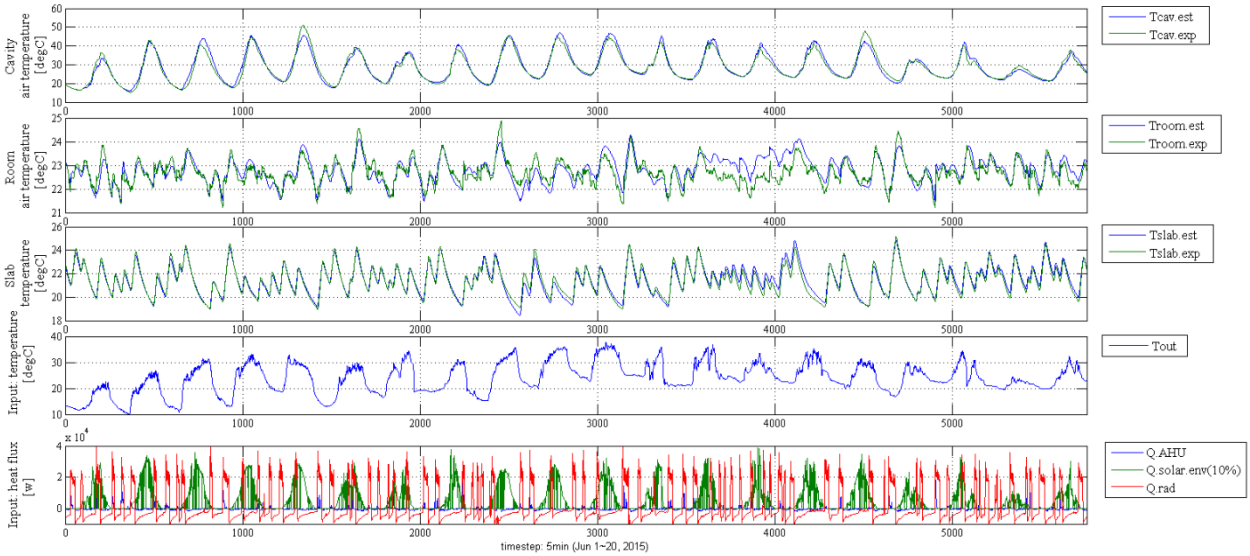

Figure 3.22 Estimation (1~1440) and validation (1441~5760) results of free-shared parameter model.

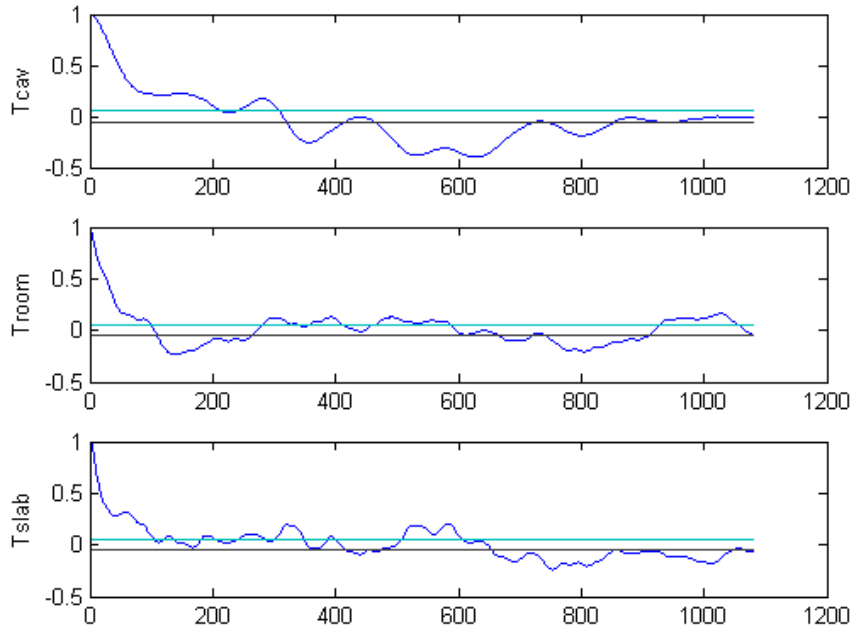

Figure 3.23 Sample auto-correlation function of residual (free-shared parameter model).

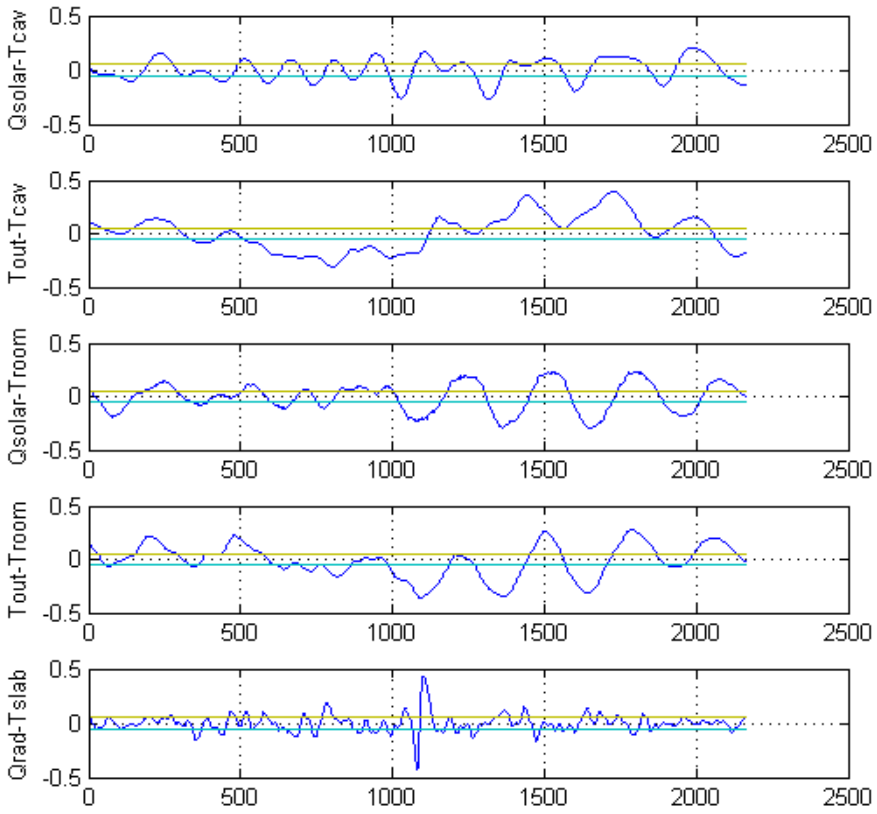

Figure 3.24 Sample cross-correlation function between input and residual (free-shared parameter model).

3.4 Chapter conclusions

In this chapter, an agent-based estimation framework for data-driven building models has been introduced. An experimental case-study of a single-zone occupied office space with multiple sub-systems (radiant floor, double façade, AHU) has been used to demonstrate the new approach. The results indicate that the agent-based estimation is a potential solution for control-oriented models of building systems that can be easier to develop and integrate whereas the conventional centralized approach could not provide accurate predictions for all states. The main conclusions are summarized as follows:

- Sensitivity-based parameter range selection and shift was implemented and the optimization results for the sub-systems grey-box model estimation show that the chance for a global minimum is increased. Different structures of sub-system models were compared and the selection criteria based on model prediction error as well as the parameter sensitivity to output trajectory and parameter correlation proved to guarantee the accuracy of the integrated system model.
- Integrated system models were assembled based on distributed and decentralized method. The distributed model requires the negotiation for the shared parameter but the decentralized model uses a different parameter value from sub-system agents. Both models show fairly good prediction accuracy in the validation set. However, in the free-shared parameter model the physical meaning may be compromised.
- The residual analysis of auto-correlation and cross-correlation for both integrated agent models show that even though the residuals are small, the 95% confidence range for experiment-based estimation with unmeasured uncertainty due to occupancy and internal heat gains cannot be met.

The experimental datasets used in this study are confined to the summer season although cooling and heating were used alternately. To overcome this limitation, adaptive estimation could be implemented in the future. The agent-based estimation is a suitable approach for this implementation. For example, each agent could incorporate adaptive parameters that need to be updated according to environmental conditions, such as outdoor air temperature, and control scheme. All sub-agents would be self-tuned by validating their prediction with measured data.

CHAPTER 4. EVALUATION OF THE ENERGY PERFORMANCE OF A RADIANT FLOOR SYSTEM WITH MODEL PREDICTIVE CONTROL - IMPLEMENTATION IN AN OFFICE BUILDING AND COMPARISON WITH BASELINE CONTROL AND AIR DELIVERY SYSTEM

4.1 Overview

The objective of the work presented in this chapter is to provide a detailed evaluation of the energy and cost saving potential of radiant floor systems with MPC. The developed zone MPC controller includes data-driven building models estimated and validated for the heating and cooling seasons, and an optimizer based on constraint quadratic programming with hard comfort bounds, which yields an exact numerical solution with predicted exogenous disturbances. The MPC strategy is implemented in an occupied office building with a chiller and boiler as HVAC sources. Its performance is evaluated by comparison with (i) feedback simulation (ii) MPC simulation, and (iii) experimental results from neighboring thermal zones where an air system with feedback is used for conditioning.

4.2 Test-bed

The test-bed used in this study is an open-plan office space (9.9 m by 10.5 m) that can host up to 20 occupants, and it is one of the Living Labs at Herrick building of Purdue campus. An exterior view of the building and section view with HVAC details are shown in Figures 4.1 and 4.2. The main features of the test-office are a radiant floor slab and a south-facing double façade system. The radiant floor has been constructed to provide cooling and heating with sensing capabilities. Steam and chilled water are delivered to the heat exchanger from the campus plant. Temperature sensors (ACI, A/TT1K-LTS, ±0.3°C) are embedded in each concrete slab and in the heat exchanger to monitor the supply and return water temperature. A turbine-type flow meter (ONICOM, F-1110, ±1%) is installed between the pipe and the heat exchanger. In addition, four RTD sensors (Digi-Key, 10K ohm, ±1%) and thermocouples (Omega, T-type, ±0.5°C) are installed in the room to capture the detailed dynamics of the thermal zone. The room has four wall diffusers for ventilation that are served from an Air Handling Unit (AHU). The vents and fan of

the double façade were kept closed during this study. A standard BMS is available through the installed Tridium JACE controllers and Niagara/AX software framework (Tridium Inc).

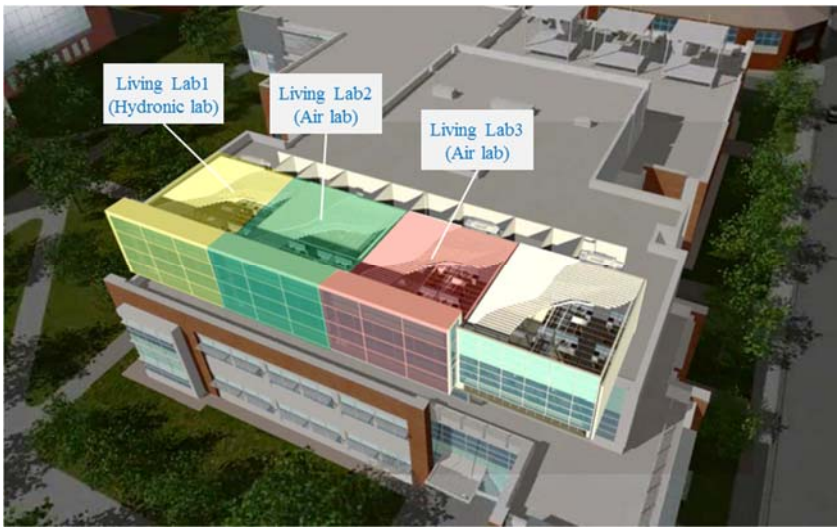

Figure 4.1 Three living labs at Herrick building

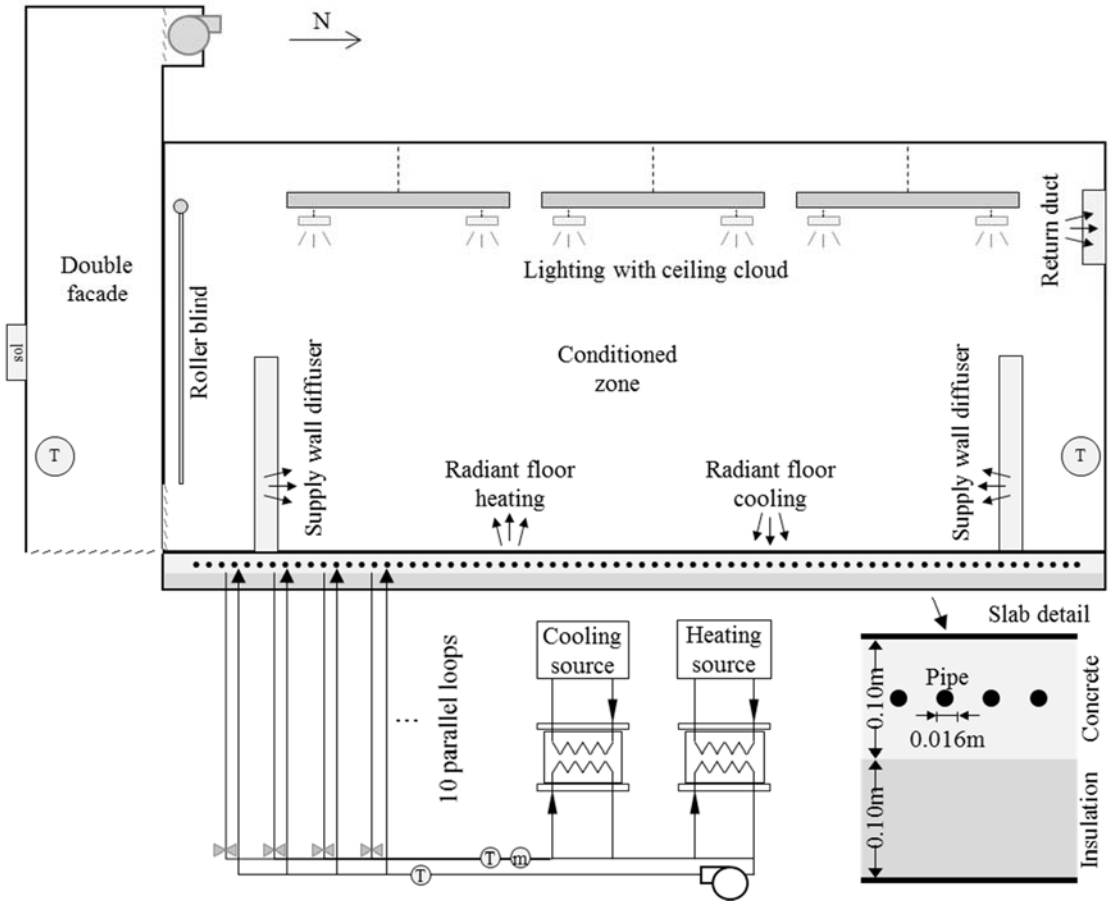

Figure 4.2 Test-bed with radiant floor system

4.3 Data-driven building model

A data-driven grey-box building model is constructed based on the state-space formulation (Equation 4.1). The model includes five states. T_{cav} and T_{room} represent the cavity and room air temperature, and T_{sur}, T_{so}, and T_{si} represent the concrete temperature; lower case *sur*, *so*, and *si* refer to the slab surface, slab core where the pipe is located, and lower slab temperatures. The solar radiation on south face (Q_{sol}) multiplied with coefficients α_{cav}, α_{room}, α_{sur} is used as input to T_{cav}, T_{room}, and T_{sur}. The Q_{AHU} and Q_{rad} are controlled inputs to T_{room} and T_{so} while the exogenous disturbance from the internal gains (equipment, lighting, and people), Q_{int}, multiplied with coefficients β_{room} and β_{sur} is input to T_{room} and T_{sur}.

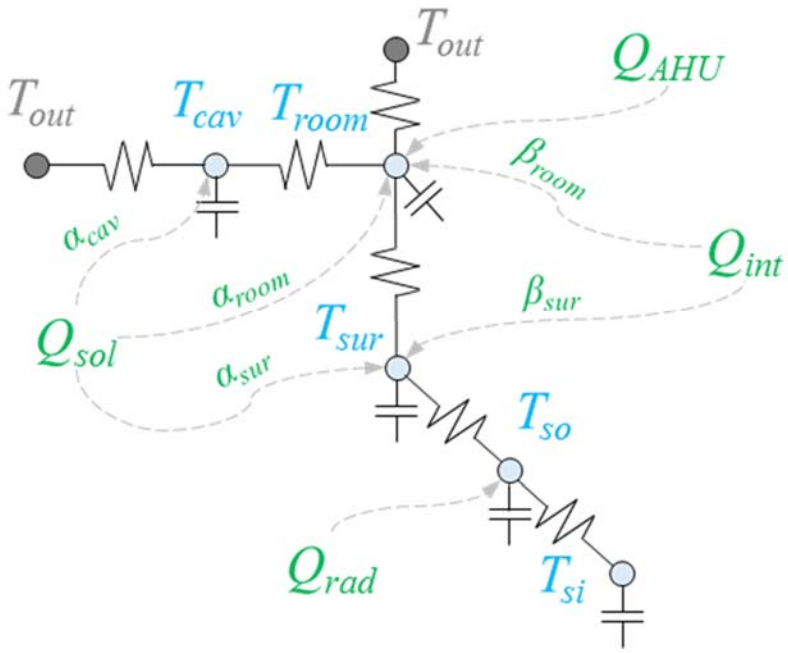

Figure 4.3 Grey-box model structure

$$x[n+1] = A_d x[n] + B_{d,w} w[n] + B_{d,q} q[n] \qquad \text{(Eq 4.1)}$$

$$\underbrace{\begin{bmatrix} x[1] \\ x[2] \\ \vdots \\ x[n] \end{bmatrix}}_{\mathbf{X}} = \underbrace{\begin{bmatrix} A_d \\ {A_d}^2 \\ \vdots \\ {A_d}^n \end{bmatrix}}_{\mathbf{\Omega_x}} \underbrace{x[0]}_{\mathbf{x_0}} + \underbrace{\begin{bmatrix} B_{d,w} & 0 & \cdots & 0 \\ A_d B_{d,w} & B_{d,w} & \cdots & 0 \\ \vdots & \vdots & \ddots & \vdots \\ {A_d}^{n-1} B_{d,w} & {A_d}^{n-2} B_{d,w} & \cdots & B_{d,w} \end{bmatrix}}_{\mathbf{\Omega_w}} \underbrace{\begin{bmatrix} w[0] \\ w[1] \\ \vdots \\ w[n-1] \end{bmatrix}}_{\mathbf{w}} + \underbrace{\begin{bmatrix} B_{d,u} & 0 & \cdots & 0 \\ A_d B_{d,u} & B_{d,u} & \cdots & 0 \\ \vdots & \vdots & \ddots & \vdots \\ {A_d}^{n-1} B_{d,u} & {A_d}^{n-2} B_{d,u} & \cdots & B_{d,u} \end{bmatrix}}_{\mathbf{\Omega_u}} \underbrace{\begin{bmatrix} u[0] \\ u[1] \\ \vdots \\ u[n-1] \end{bmatrix}}_{\mathbf{u}}$$

(Eq 4.2)

Once this state-space formulation (Equation 4.1) is stacked in time series, the control input (**u**) and temperature trajectories (**X**) are in an explicit linear relation, which is a suitable form for implementation in the optimization algorithm (Equation 4.2). With this formulation, estimation is carried out with a distributed system identification approach that is described in detail in Chapter 3. The thermal zone is disassembled into sub-systems and smaller scale of estimation problems are solved in parallel and then integrated while tuning different shared parameters between sub-systems to become identical using dual decomposition method. Figure 4.4 shows the modelling results. RMSE of the model for the cooling season are 0.47 and 0.70°C for air and slab surface temperatures. The accuracy of the model for the heating season are 1.02 and 1.09°C for the air and slab surface temperatures. A model for the air delivery system is estimated for the cooling season, which yields an RMSE of 0.63 and 0.48°C.

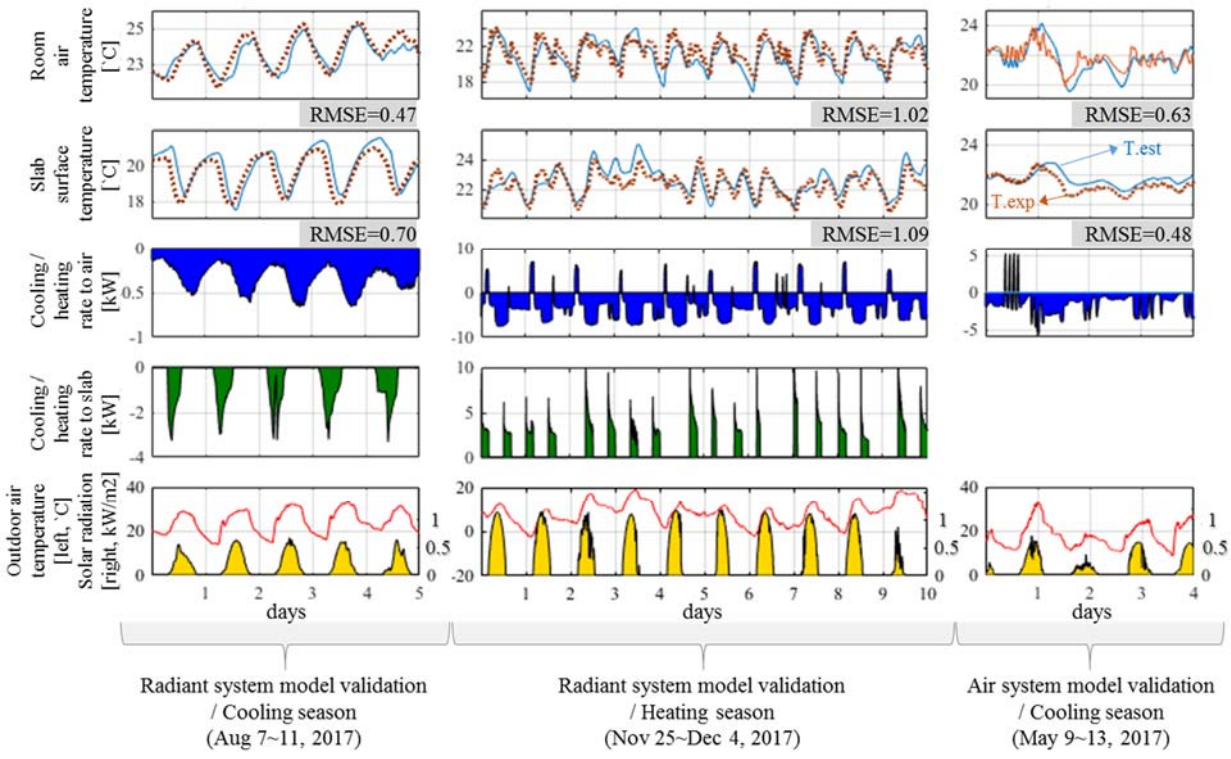

Figure 4.4 Modelling validation results

4.3.1 HVAC system

The cooling and heating source in the actual test-bed are provided from the campus plant. For the implementation and simulation, an air-cooled chiller model is assumed for the cooling season while a boiler is used for heating season. Performance data of the air-cooled chiller are adopted from the EnergyPlus engineering reference (EnergyPlus 2015) and the Energy Input Ratio (EIR)

method is used based on the catalogue data of an actual product (Trane CGAM20). The nominal capacity ($Q_{ref,cap}$) and coefficient of performance ($C_{ref,COP}$) are 68.9 kW and 2.67, respectively. For our case-study, the capacity is scaled down to 8 %. The electricity consumption of the chiller is a multiplication of three polynomials (f in Equation 4.3) that represent the capacity, COP, and Part Load Ratio (PLR). The capacity and COP curves are biquadratic and require two control inputs. The leaving water temperature ($T_{leaving}$) is fixed at 13°C which yields a quadratic polynomial and the optimization problem has a convex form. The COP is plotted in Figure 4.5 as a function of outdoor air temperature, leaving water temperature and PLR. Lower outdoor air temperature and higher leaving water temperature result in higher COP. As for the PLR, any ratio larger than 30% results in high COP.

$$f_{chiller} = f_{Cap} \cdot f_{COP} \cdot f_{PLR}$$

$$where: \begin{cases} f_{Cap} = Q_{ref,Cap} \cdot Curve_{biquad}\left(T_{leaving}, T_{outdoor}\right) \\ f_{COP} = \dfrac{1}{C_{ref,COP}} \cdot Curve_{biquad}\left(T_{leaving}, T_{outdoor}\right) \\ f_{PLR} = Curve_{quad}\left(\dfrac{Q_{load}}{f_{Cap}}\right) = Curve_{quad}\left(PLR\right) \end{cases} \quad \text{(Eq 4.3)}$$

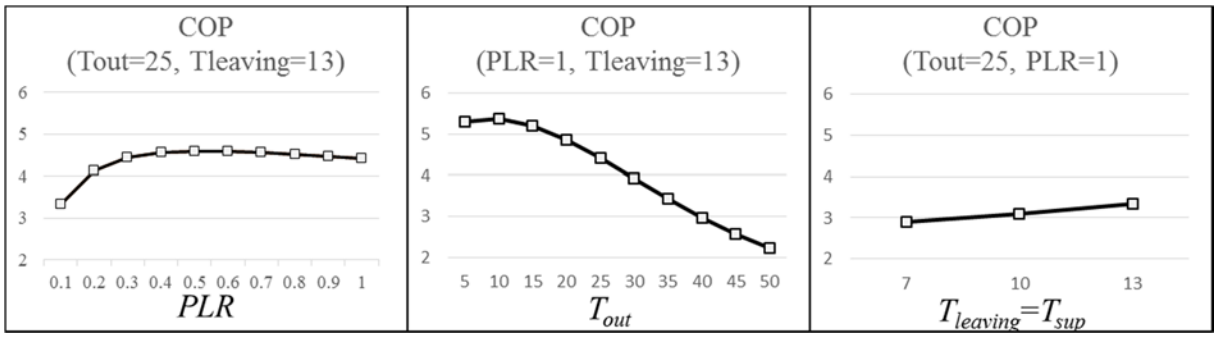

Figure 4.5 COP of air-cooled chiller

4.3.2 MPC formulation

The MPC formulation for the cooling application is shown in Equation 4.4. The objective function is the electricity cost consumed by the chiller, while the fan and pump electricity consumption is neglected. The decision variable **u**, which is the control input to the model, is the trajectory of PLR in a given prediction horizon, 24hours. $f_{chiller}$ represents the electricity consumption of the HVAC source, which is a convex function as the PLR is the control input. TOU (Time of Use) electricity price is multiplied to the electricity consumption. Multiple inequality constraints are applied. The first constraint (Equation 4.4), represents the temperature bound of the conditioned zone; $\mathbf{T_{bound}}$ is

the upper or lower temperature bound, and $\mathbf{C_T}$ is the matrix multiplied to all states to extract the target temperature states. Additional bounds are used for certain states of the system, for example, the slab temperature in the radiant system, and the capacity of the HVAC source. $\mathbf{\Omega}$ represents the predefined matrices as shown in Equation 4.2. Finally, this constraint quadratic programming is solved with *quadprog* in Matlab environment (MathWorks 2014).

$$\begin{aligned} &\min \varepsilon_{cost} \cdot f_{chiller}(\mathbf{u}) \\ &s.t. \begin{bmatrix} \mathbf{C_T} \cdot \mathbf{\Omega_u} \cdot \mathbf{f_{cap}} \\ \vdots \end{bmatrix} \mathbf{u} \le \begin{bmatrix} \mathbf{T_{bound}} - \mathbf{C_T} \cdot (\mathbf{\Omega_T} \cdot \mathbf{T_0} + \mathbf{\Omega_w} \cdot \mathbf{w}) \\ \vdots \end{bmatrix} \end{aligned} \quad \text{(Eq 4.4)}$$

For the heating application, the objective function is the summation of heating rate input to the slab. Optimization for the MPC is formulated with linear programming (Equation 4.5) and is solved with *linprog* in Matlab environment (MathWorks 2014). f_{boiler} refers to all-ones row matrix. The same inequality constraints with cooling application are applied.

$$\begin{aligned} &\min f_{boiler} \cdot \mathbf{u} \\ &s.t. \begin{bmatrix} \mathbf{C_T} \cdot \mathbf{\Omega_u} \\ \vdots \end{bmatrix} \mathbf{u} \le \begin{bmatrix} \mathbf{T_{bound}} - \mathbf{C_T} \cdot (\mathbf{\Omega_T} \cdot \mathbf{T_0} + \mathbf{\Omega_w} \cdot \mathbf{w}) \\ \vdots \end{bmatrix} \end{aligned} \quad \text{(Eq 4.5)}$$

4.4 MPC performance

4.4.1 MPC implementation settings

This section presents information on disturbances and constraints that were used for the implementation. For the disturbance prediction, the occupant heat gain is set to 65 W for a sedentary working person based on ASHRAE Standard 55 (ASHRAE 2013). The equipment heat gain for each occupant is calculated to be 50W based on measurements (historic data for weekends and weekdays) for the total power consumption and the actual number of occupants. The occupancy schedule is from 08 am to 10 pm considering the actual occupants of the test-bed. The air system provides ventilation by regulating the supply air temperature to be equal to the average of the lower and upper temperature bounds. The relative humidity of the room is set to 40% via the cooling coil control in AHU to eliminate the potential risk for condensation on the floor due to the low surface temperature. In this case, the reheat coil is ON to increase the supply air

temperature set-point to offset the latent cooling rate as the AHU input is not considered in MPC calculation. TOU electricity price is considered for cooling; \$0.16/kWh and \$0.067/kWh were used for the peak (12pm~6pm) and off-peak (otherwise) hours.

The operative temperature, which is a linear combination of the air and Mean Radiant Temperature, is used to control the space. It is calculated based on a weighted average of the air and slab temperature as the air flow rate in the zone is less than 0.2m/s (ASHRAE 2013). For this purpose, a detailed experiment was conducted with an array of sensors including a globe meter and five thermocouples at various heights from the floor, to determine the two weighting coefficients. These are used in the actual MPC implementation for estimating the operative temperature (based on recommendations from ASHRAE 55 (ASHRAE 2013) using readings from the RTD sensor (at 0.6 m height from the ground) for the air temperature and from the thermocouple (TC) for the slab surface temperature. The weighting coefficients were estimated to be 0.77 and 0.23 for the air and slab surface temperature for cooling. Those for heating were 0.85 and 0.15. The RMSE between the experiment and estimation of the operative temperature are 0.12 and 0.41°C.

The vertical temperature difference between the head and ankle are used to quantify the thermal asymmetry (ASHRAE 2013) in cooling case. This metric is used to define the limit of the maximum difference between the air and slab surface temperature which is set to be 7°C based on recent studies with human test-subjects and a thermal manikin experiment (Krajčík et al. 2013; Krajčík et al. 2016). Also, the low-bound of the slab surface temperature is set to 15°C based on (Wang et al. 2009) to eliminate potential thermal discomfort of the occupants. This temperature bound for the floor affects the maximum cooling capacity of the radiant floor system as a large cooling rate is feasible when the concrete temperature is high and vice versa. Based on initial experiments, the maximum available cooling capacity for all floor slab sections was around 5kW when the slab surface temperature is 15°C so this was set as an inequality constraint in the optimization problem. The maximum slab temperature was set to be 29°C for heating based on (ASHRAE 2013) and the corresponding maximum heating capacity of the radiant floor system is set to 12.5kW.

A schematic for the DMPC implementation is shown in Figure 4.6. MPC calculations are performed in a server computer with Matlab that has access to weather forecast data for 24 hours prediction. The optimal cooling and heating rates are calculated and sent to Niagara server through Modbus communication. Then the valves for each section in the radiant floor system are activated

to satisfy the signal in each loop for a given time-step, 30 min. After each time-step, sensor data for the zone and slab temperatures, the control and exogenous input are sent to the server computer, for the state estimation by the Kalman filter.

Weather forecast data including outdoor air temperature, relative humidity, and cloud cover are extracted from the National Oceanic and Atmospheric Administration (NOAA) web-site to a server computer. The following model was used for calculating the global horizontal irradiance (*GHI)* based on cloud cover forecast (Seo 2010):

$$GHI = I_0 \cdot \sin(h) \cdot \{C_0 + C_1(CC) + C_2(CC)^2 + C_3(T_{out(k)} - T_{out(k-3)}) + C_4(RH) + C_5 \cdot V_{wind}\} + d \quad \text{(Eq 4.6)}$$

GHI is calculated based on the solar constant (I_0, 1355 W/m^2), solar altitude angle (h), outdoor air temperature (T_{out}, k is time-step), cloud cover (CC), relative humidity (RH), wind speed (V_{wind}), and regression coefficients (C_0, C_1, C_2, C_3, C_4, C_5, and d) that are estimated for different climate zones in the literature (Seo 2010). Coefficients for zone Cfa (warm temperature, fully humid, and hot summer) were selected considering the location of the test-bed. Then the solar irradiance incident on the south façade is calculated from *GHI* using the *Solar Radiation Process* algorithm (Type 16 in TRNSYS) (TRNSYS 18 2017).

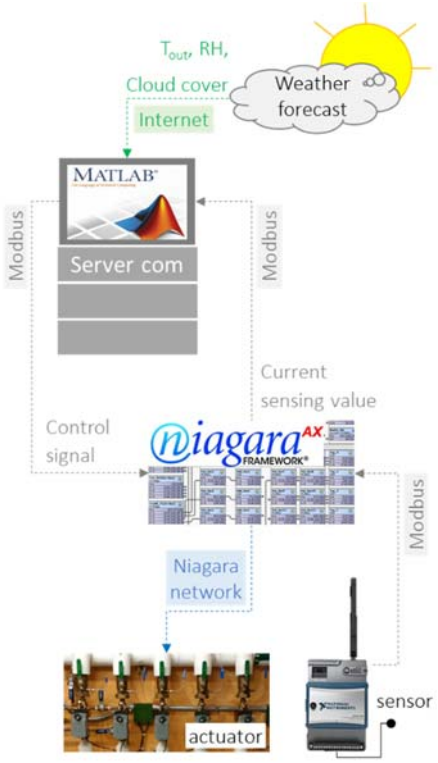

Figure 4.6 Data communication for MPC

The initial states for the unmeasured temperatures are calculated with the Kalman filter (Stengel 1994). The predicted error covariance (P in Equation 4.7) is updated from the previous time-step (P^{-}) with the state matrix (A_d) and the covariance matrix of process noise (Q) which is set based on the estimation results (averaged value of RMSE for the air and slab) in Section 4.3. The Kalman gain (K in Equation 4.8) is calculated with predicted error covariance and a covariance matrix of sensor noise (R in Equation 4.8) which is set based on temperature sensor accuracy. H is the matrix that extracts observed states from all states. Then the state (x) is updated based on the predicted state ($\hat{x}$) obtained from building dynamics (Equation 4.1) and the actual measurement (Y) along with the Kalman gain (Equation 4.9). Then the error covariance matrix (P^{+}) is updated to calculate the Kalman gain of the next iteration (Equation 4.10).

$$P = A_d P^{-} A_d^{T} + \mathrm{Q} \quad \text{(Eq 4.7)}$$

$$K = PH^{T}(HPH^{T} + \mathrm{R})^{-1} \quad \text{(Eq 4.8)}$$

$$x = \hat{x} + K(Y - H\hat{x}) \quad \text{(Eq 4.9)}$$

$$P^{+} = (I - KH)P \quad \text{(Eq 4.10)}$$

4.4.2 Simulation settings

Simulations are performed for evaluating the performance of the MPC controller for the cooling and heating seasons. The time-step is set to 5 min for all simulations including the feedback and MPC to capture realistic feedback dynamics whereas MPC implementations were carried out with 30 minutes of time-step. The MPC simulation is conducted for each day and the last state is an input to the initial state for the next day so it runs sequentially for a given period. The same disturbances for the weather and internal heat gain used in implementation were also applied for the simulations. All simulations have five days of warm-up period.

4.4.3 MPC performance in cooling season

4.4.3.1 Implementation results

Figure 4.7 shows the implementation results for 10 consecutive days in the cooling season (Aug. 13–22, 2017). The five-days warm-up period is excluded from the graph. The operative, room air, and slab surface temperatures along with their lower and upper-bounds are shown with control and exogenous inputs (heating rate to the slab, outdoor air temperature, and solar radiation). The

temperature is calculated using the maximum, average, and minimum value of measurement from the 4 sensors in the zone. There are small violations (6th and 8th day) of the operative temperature bound which means that some areas of the zone are not perfectly conditioned. However the difference is minor and the average value is inside the bound, which is used for the implementation. Also, the slab surface shows a relatively large range of temperature deviation. This is because the radiant floor consists of 10 loops and corresponding areas and pipe lengths are different so the cooling rates provided to each loop are not identical.

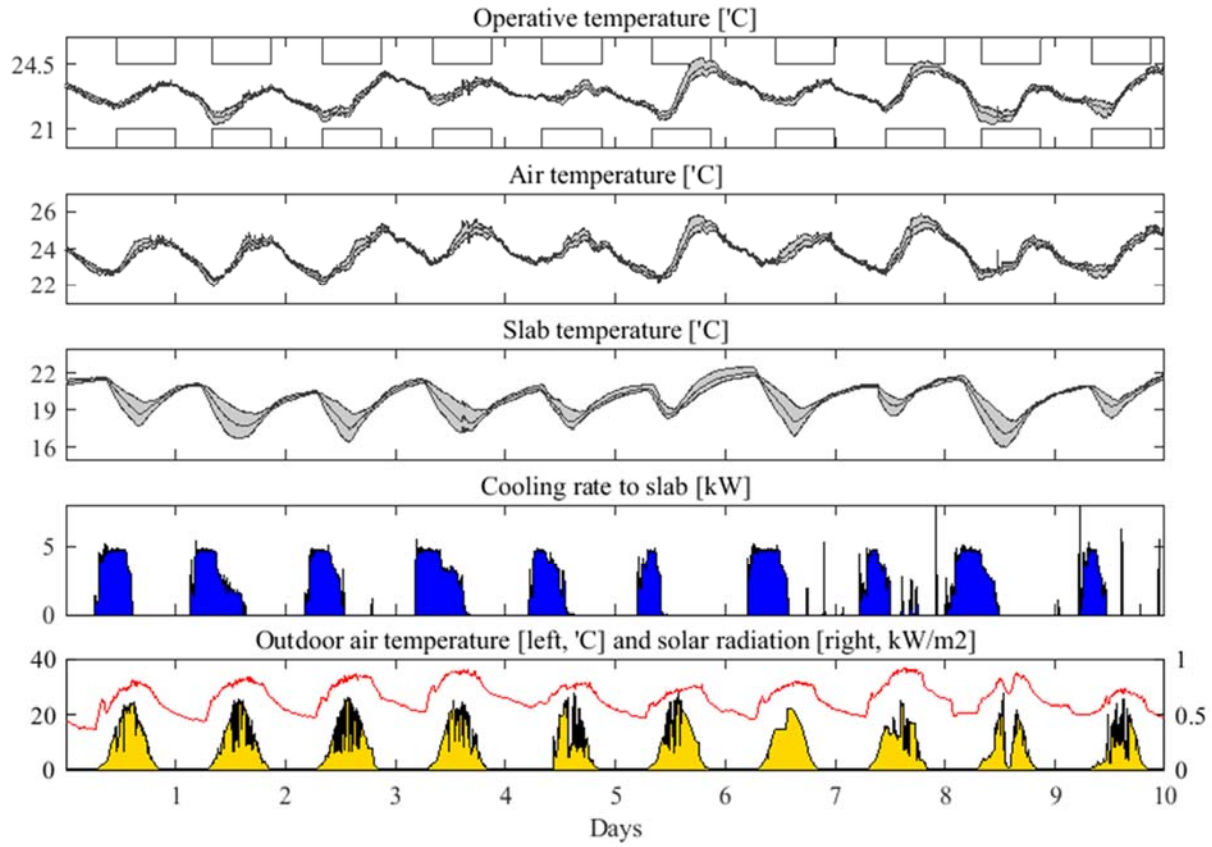

Figure 4.7 MPC implementation results for the cooling season (Aug. 13–22, 2017)

4.4.3.2 Performance comparison with feedback control

MPC simulation (green) and implementation (red) results are compared with simulation feedback control (blue) to investigate the ideal and actual MPC performances. Figure 4.8 presents the operative temperature profiles as well as the cooling rate, COP and outdoor environment, and Table 1 shows the total energy and cost for 10 days of simulations and implementation. In operation with feedback control, the radiant cooling system turns ON when the actual operative

temperature is higher than the set-point temperature which is an average of lower and upper bounds to regulate the temperature inside the bounds. For this reason, different than the operation with the MPC controller, the cooling system remains ON until the end of occupied period when feedback control is used and the corresponding COP is low due to the high outdoor air temperature in the daytime. The MPC simulation shows pre-cooling at night and thereby higher COP is utilized with lower outdoor air temperature. Also, the radiant cooling system turns OFF in advance based on the optimization so the operative temperature at the end of occupied hour matches the upper comfort bound. As a result, 14% of cooling energy use reduction is achieved (333 VS 288kWh) in ideal MPC simulation. The corresponding electricity and cost savings are 23 and 45% compared to the feedback strategy (76 VS 59kWh and $7.2 VS $4.0). Considerable cost savings are achieved due to the pre-cooling with TOU price, and cooling is used mainly during the off-peak hours. In the implementation, significant energy and cost reductions (16 and 34%) are achieved (76 VS 64 kWh, $7.2 VS $4.7) which is a comparable to the performance of the ideal MPC.

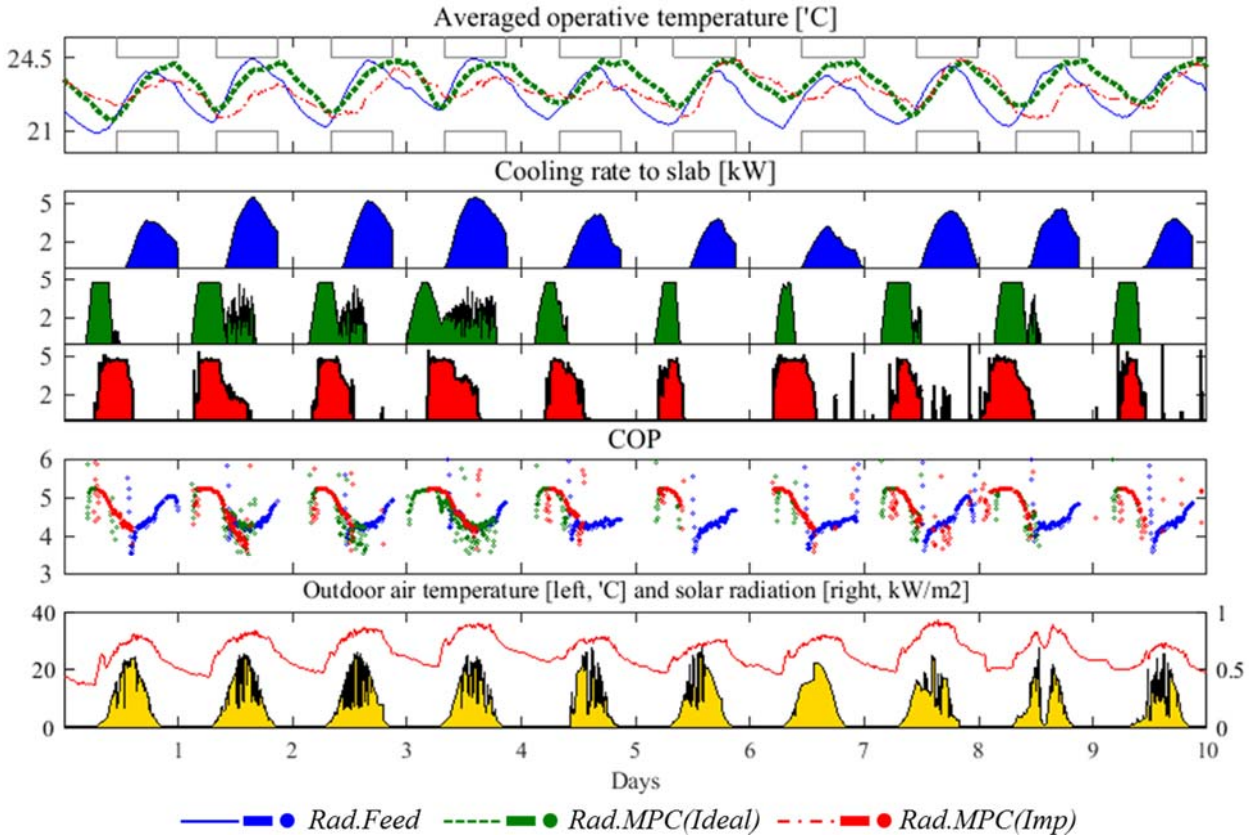

Figure 4.8 Performance comparison of MPC with feedback control

Table 4.1 Total energy consumption and cost for feedback control and MPC cases

	Rad.Feed	*Rad.MPC(Ideal)*	*Rad.MPC(Imp)*
Cooling consumption [kWh]	333	288	307
Electricity consumption [kWh]	76	59	64
Cost [$]	7.2	4.0	4.7

4.4.3.3 Performance comparison with air system

In this section, the performance of the radiant floor system with MPC strategy is compared with a typical air delivery system. For the air system, the decision variable for the MPC calculation is PLR and the cooling rate is input to the room air temperature node directly (T_{room} in Figure 4.3). The same HVAC source, an air-cooled chiller, is used in the objective function. The fan energy consumption is not considered. Figure 4.9 represents the operative temperature profiles with respect to cooling rate, COP and outdoor environments, and Table 2 shows total energy and cost for 10 days of simulations and implementation. Two control strategies for the air system with feedback (blue) and MPC (green) strategy are compared with the MPC implementation results (red) for radiant floor system. For the air system, MPC consumes more cooling and electricity than feedback control whereas 10% of total cost reduction was estimated ($9.5 VS $8.5). On the other hand, significant cooling energy, electricity, and cost reduction (18, 35, and 50%) was achieved in the MPC implementation for the radiant floor system compared to the air system with feedback control. Despite the optimized control of the air system, its cost saving potential is limited compared to the radiant floor system as pre-cooling is used to reduce the cost while consuming more cooling energy and electricity. This is due to the lower thermal capacity of the zone air compared to the concrete slab where the cooling could be stored longer as a heat sink. Also, as shown in Figure 4.5, another saving source is the higher efficiency of the chiller plant that feeds relatively low temperature of leaving water to the slab.

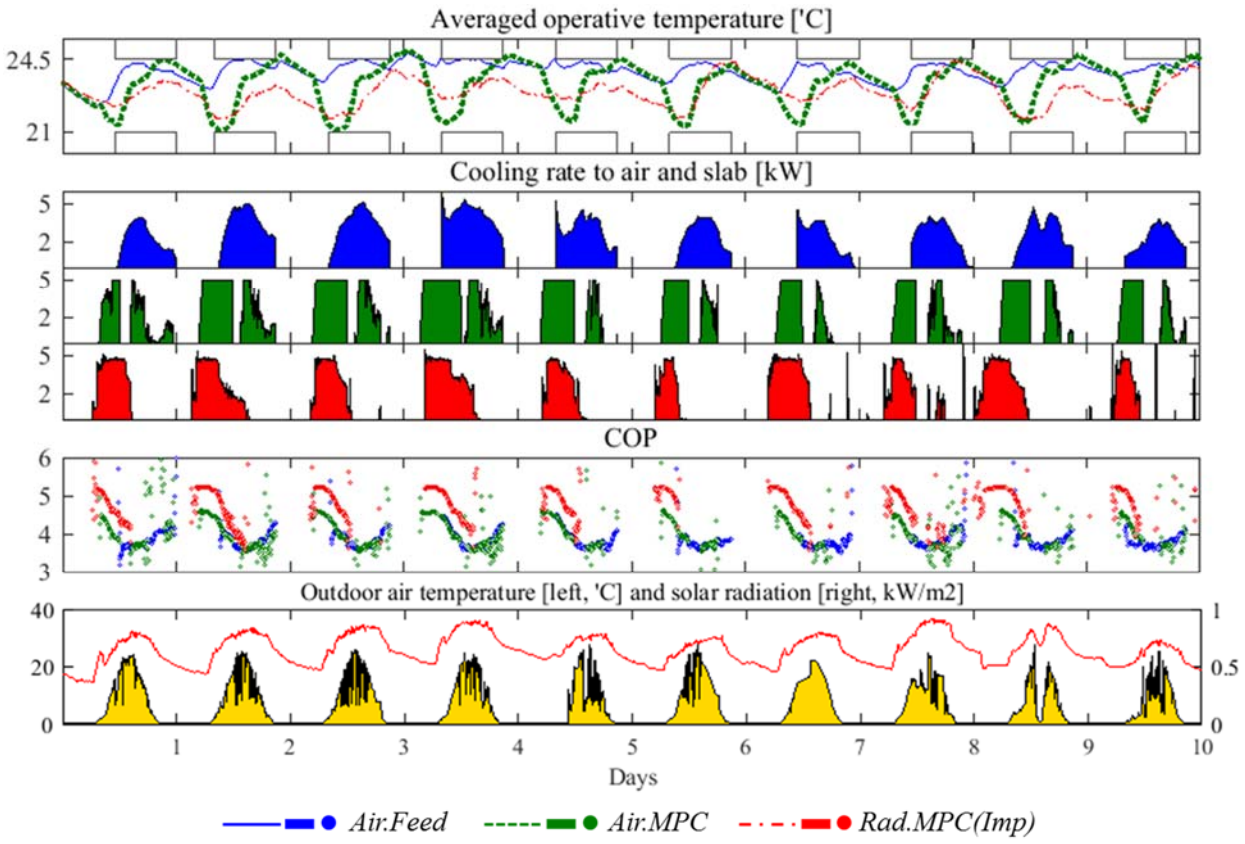

Figure 4.9 Performance comparison between the radiant and air delivery systems

Table 4.2 Total energy consumption and cost for air and radiant cases

	Air.Feed	*Air.MPC*	*Rad.MPC(Imp)*
Cooling consumption [kWh]	377	430	307
Electricity consumption [kWh]	99	108	64
Cost [$]	9.5	8.5	4.7

4.4.3.4 Side-by-side comparison with air system

MPC implementation results are compared with experimental data from other zones, namely the Living Labs 2 and 3 (LL2 and LL3) that have identical room dimensions and construction and air-based thermal conditioning systems. Figure 4.10 shows operative temperature profiles along with disturbances including the outdoor air temperature, solar radiation, and internal equipment heat gain. A comparison during the exact same period was not practically feasible as different experiments were conducted in LL2 and LL3 during the implementation period. Instead, several days with similar disturbances including outdoor environments and internal heat gain were

selected from the cooling season. Set-point temperatures of LL2 and LL3 were 22.5 and 22.0°C and conditioned for 24 hours but the daily energy consumption and cost were calculated only for the occupied period (08am ~ 10pm).

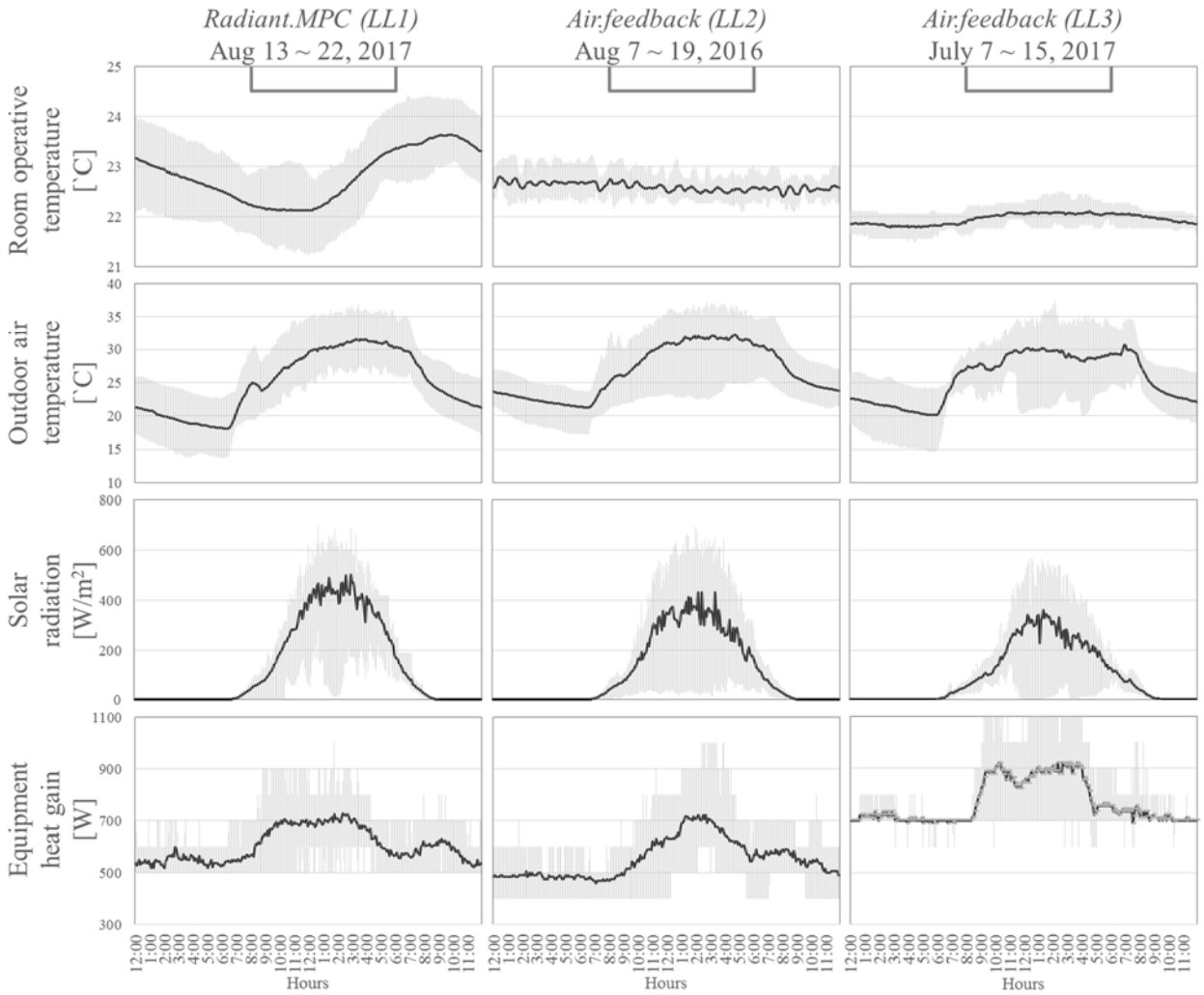

Figure 4.10 Temperature and disturbance inputs of experiment for cooling case

Figure 4.11 represents the daily electricity consumption for three cases with respect to the range of the maximum outdoor air temperature. LL3 shows the highest consumption due to the lower set-point temperature and more equipment heat gain. In all cases, MPC consumes less electricity. The averaged daily electricity consumption is 6.4, 11.7, and 16.0kWh and the corresponding cost \$0.47, \$1.40, and %1.92. The radiant floor with MPC strategy can reduce the electricity consumption and cost around 45~60 and 66~75% compared to the air system with feedback control.

The higher saving potential of this side-by-side comparison than the comparison against the simulations (50%) in the previous section (Section 4.4.3.3) is the result of the lower set-point temperature used in LL2 and LL3; the air temperature was regulated close to the MPC upper-bound in the simulated feedback control whereas actual zones were conditioned with mid (LL2) or biased down (LL3) set-points.

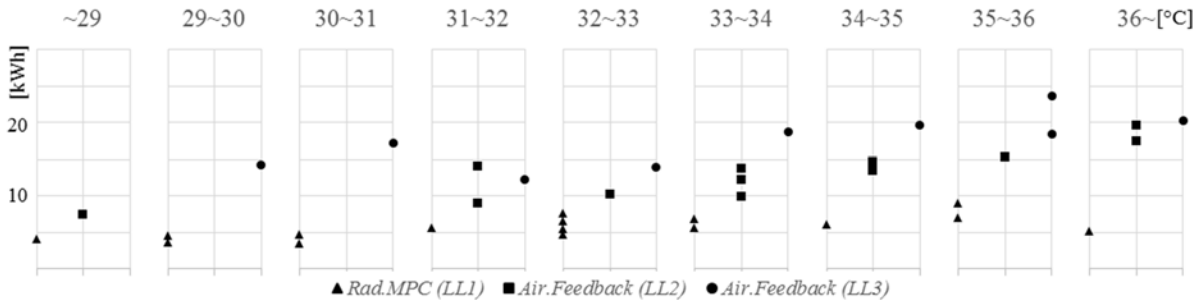

Figure 4.11 Daily electricity consumption with maximum outdoor air temperature for cooling experiment

4.4.4 MPC performance in heating season

4.4.4.1 Implementation results

Figure 4.12 shows the implementation results for 10 consecutive days in the heating season (Jan. 27 – Feb. 5, 2018). The five-days warm-up period is excluded from the graph. The operative, room air, and slab surface temperatures along with their lower and upper bounds are shown with the control and exogenous inputs (heating rate to the slab, outdoor air temperature, and solar radiation). The temperature is calculated using the maximum, average, and minimum value of measurement from the 4 sensors in the zone. During the 8th day of the implementation period, the vent between the cavity and the room was opened for maintenance so the room air temperature was not regulated properly. The slab surface temperatures shows larger deviation compared to the cooling season because the temperature sensors that are close to the double façade are affected by the solar radiation due to the low altitude angle.

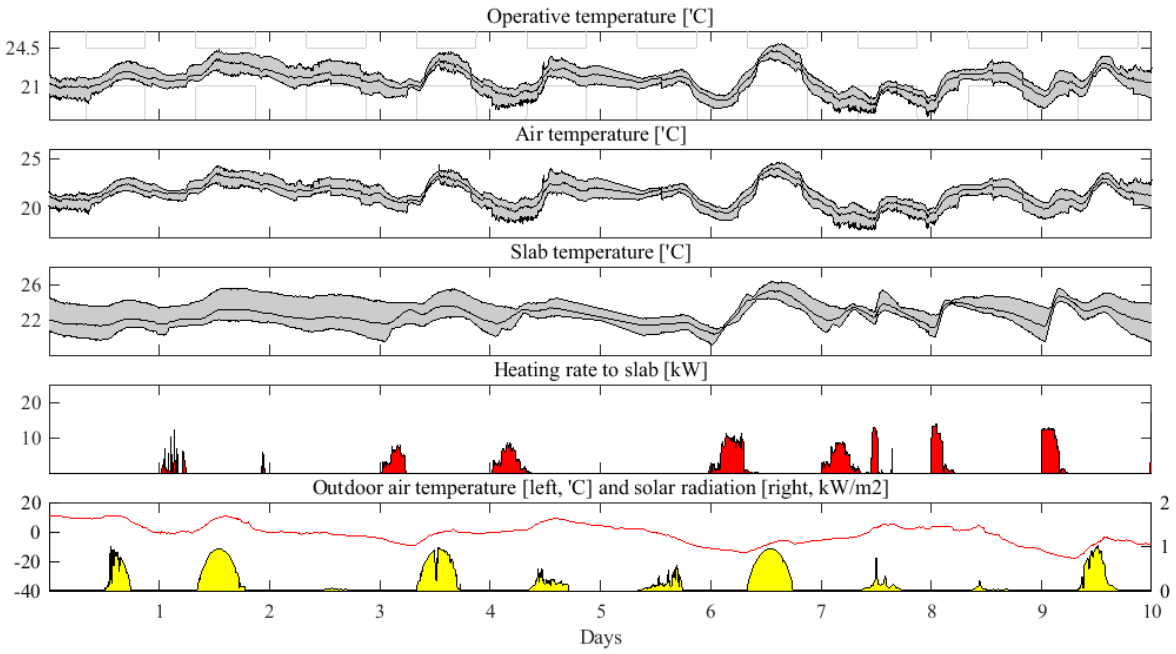

Figure 4.12 MPC implementation results for heating season (Jan. 27 – Feb. 5, 2018)

4.4.4.2 Performance comparison with feedback control

MPC simulation (green) and implementation (red) results are compared with simulation feedback control (blue) to investigate the ideal and actual MPC performances of the radiant floor heating system. Figure 4.13 represents shows the operative temperature profiles as well as the cooling rate and outdoor environment. In feedback control, heating turns ON when the actual operative temperature is higher than the set-point temperature which is an average of lower and upper bounds to regulate the temperature inside the bounds. Also, heating is activated in advance of occupied hours to satisfy the comfort bound in the morning; 2 hours was used by trial simulation with given specific data of 10 days. However it was challenging to maintain the comfort inside the bounds with feedback control, and overheating occurs especially in 10th day. In the case of MPC, optimal heating is provided so the operative temperature is as close as possible to the lower comfort bound in the morning so overheating in the daytime is minimized. Finally, 20% of heating energy saving was achieved (297 VS 237 kWh) in ideal case. In the implementation, comparable energy reductions (16%) with the ideal case was achieved.

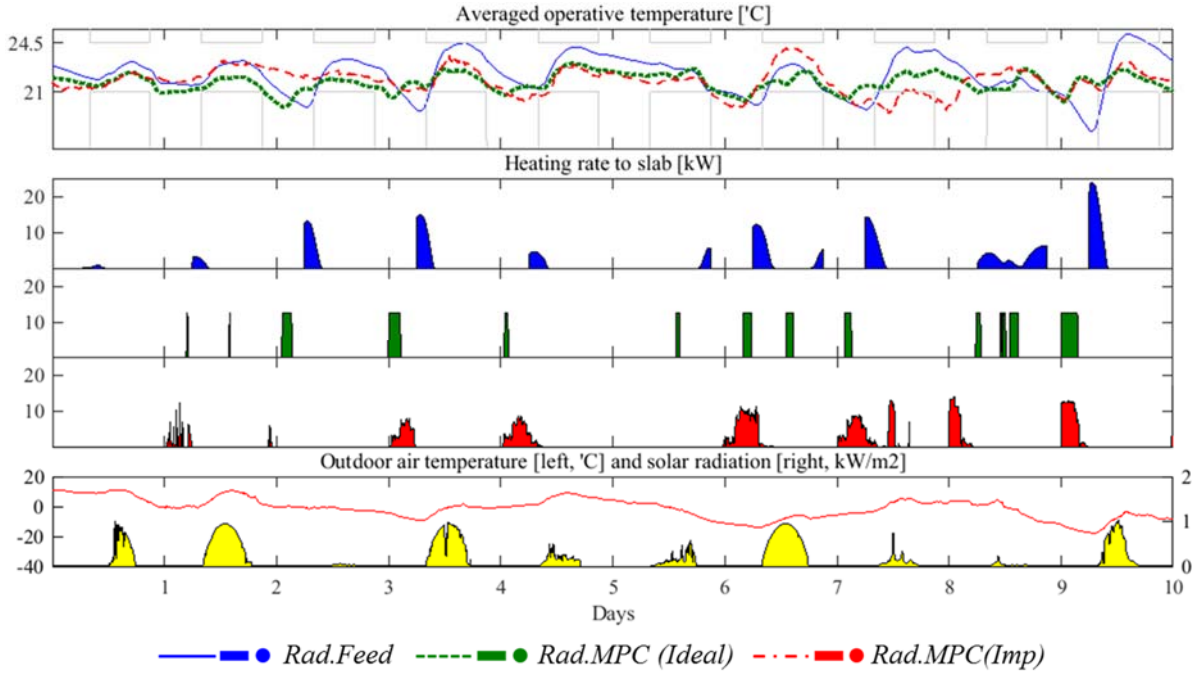

Figure 4.13 Performance comparison between MPC and feedback control

4.4.4.3 Side-by-side comparison with air system

MPC implementation results are compared with experimental data from LL3 that has air-based thermal conditioning system. Four days (1st, 3rd, 6th and 8th) in MPC implementation were excluded due to the negligible heating load and malfunction. In LL3, even for the heating season, cooling load was required from time to time during the daytime due to the solar gain with low altitude angle, internal heat gain and high insulated building design. For this reason, severe cold and cloudy days (6 days) were selected where only the heating energy was consumed. Figure 4.14 shows operative temperature profiles along with disturbances including the outdoor air temperature, solar radiation, and internal equipment heat gain. Set-point temperatures of LL3 was 22.2°C, and conditioned for 24 hours but the daily energy consumption was calculated only for the occupied period (08am ~ 10pm).

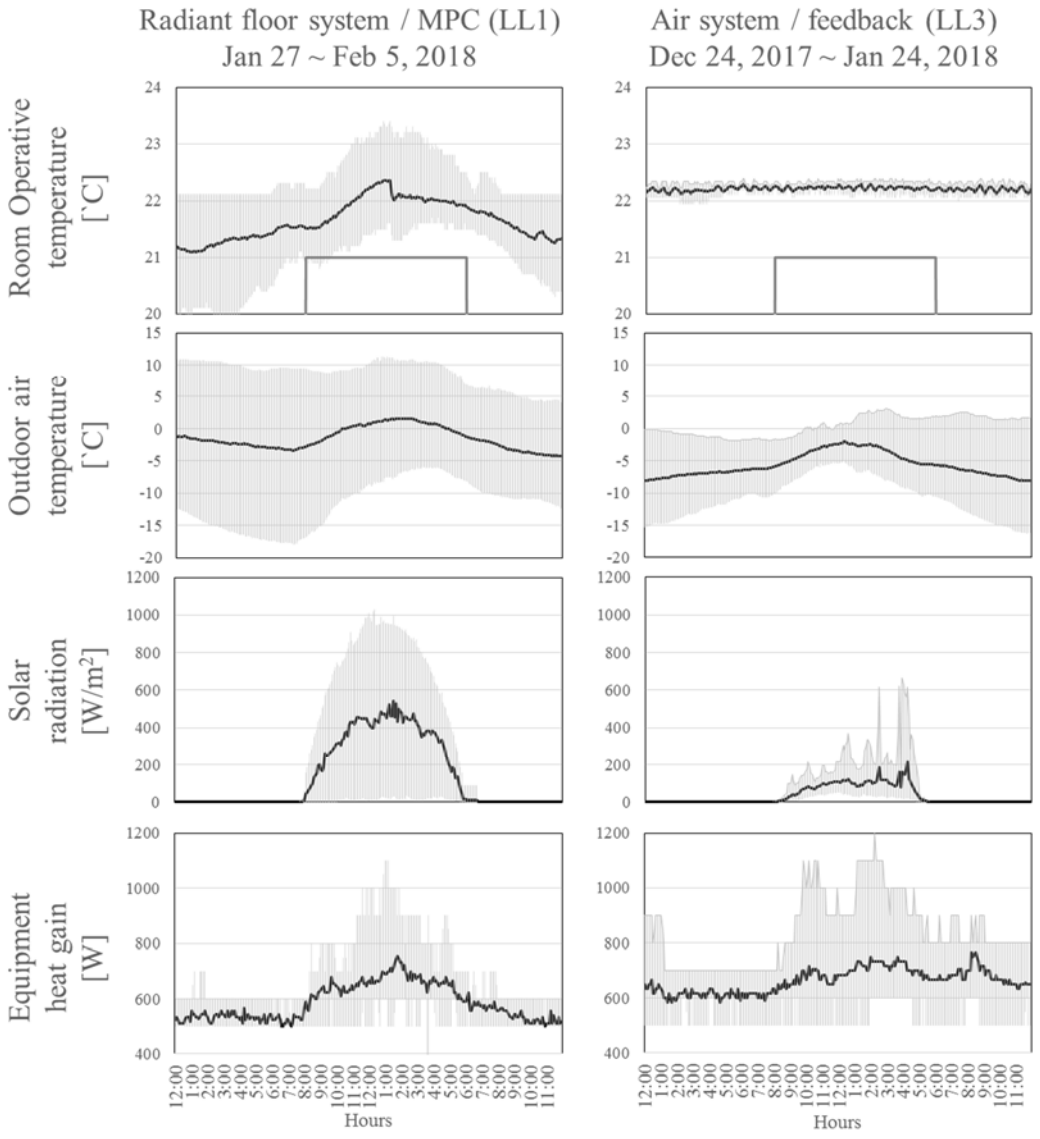

Figure 4.14 Temperature and disturbance inputs of experiment for heating case

Figure 4.15 represents the daily energy consumption for two cases with respect to the range of the maximum outdoor air temperature. Feedback control with air system in LL3 consumes more than radiant floor with MPC in most days. Averaged daily energy consumption of 6 days for each case are 32.2 and 45.6kWh, and 29% of energy reduction is achieved in MPC implementation compared with conventional air system. This higher saving potential than previous comparison with simulation case might be originated not only from the optimized control but also higher set-point temperature (22.2°C) of the air system, low outdoor air temperature, and less solar gain as shown in Figure 4.14.

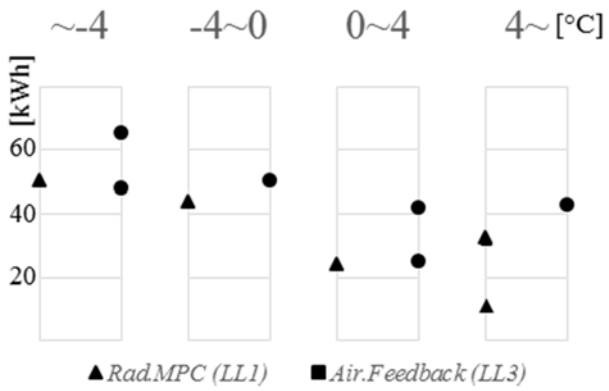

Figure 4.15 Daily consumption with maximum outdoor air temperature for heating experiment

4.5 Chapter conclusions

In this chapter, a detailed evaluation of the energy and cost saving potential of a radiant floor system with MPC was presented. Data-driven building models were estimated, validated, and implemented to an actual test-bed with an open-plan office space. Significant energy and cost savings were calculated through comparisons with simulation and experimental cases. The main findings and limitations are summarized as follows:

- In cooling implementation, cost saving of radiant floor system with MPC is about 34% compared to the simulated feedback control. This is due to the utilization of pre-cooling with higher chiller efficiency when the outdoor air temperature is low along with lower electricity price at night.
- Compared to an air delivery system with feedback control, the cost saving potential of radiant and air system with MPC is 50 and 10%respectively.
- In heating implementation of radiant floor system, the energy saving of MPC is about 16% compared to the feedback control.
- Further saving potential is observed in side-by side comparison between the implementation results and the experiment of adjacent room where the air system is serving for heating and cooling cases.

In optimization formulation of this study, an exact numerical solution is found via constraint linear or quadratic programming with hard comfort bounds. It is free from trial and error to find the suitable weights, typically multiplied to the energy consumption and comfort violation terms in

the objective function of nonlinear optimization problems. Therefore, the demonstrated saving potential of implemented MPC via the comparison with simulations and experimental case studies are reliable and not subject to potential errors due to local minima. Also, this optimization formulation has lower computational cost compared to typical nonlinear optimization. It is fast enough even with a short time step; e.g., 5min in this study. Thereby this approach is suitable for distributed or cooperative optimization methods for large-scale problems that require light computation while facilitating communications between local problems.

This formulation, however, is not able to utilize a maximum input bound. Especially, for the radiant floor system, maximum input to the slab is decided with maximum water flow rate of a pump, effectiveness of the slab, and current concrete temperature around the pipe area which is a state in model structure so input bound (maximum capacity) in a given prediction horizon is unknown. In this study, this bound is fixed at certain values (5 and 12.5 kW for cooling and heating cases) with minimum and maximum slab temperature bounds in conservative fashion. Nevertheless, sufficient saving potential was achieved.

In this study, averaged values from historical data were used for calculating the number of occupants and schedule. Ideal control performance cannot be attained due to the prediction error of disturbance as well as the building model discrepancy. In the future, it is expected that user-interactive technology will facilitate the interaction between the occupants and BMS so the occupants' information could be estimated via statistical methods.

CHAPTER 5. A DISTRIBUTED APPROACH TO MODEL PREDICTIVE CONTROL WITH APPLICATION TO RADIANT COMFORT DELIVERY SYSTEMS IN OFFICE SPACES WITH LOCALIZED THERMAL ENVIRONMENTS

5.1 Overview

The objective of the work presented in this chapter is to develop and demonstrate a multi-agent system approach to tractable optimal control of high performance buildings. A distributed optimization algorithm inspired by the Proximal Jacobian Alternating Direction Method of Multipliers (PJ-ADMM) is used in the distributed model predictive controller (DMPC) and multiple MPCs run iteratively while exchanging control input information until they converge. For the distributed system identification, the agent-based approach presented in Chapter 3, is extended to develop data-driven models for a new configuration of an open plan office with localized comfort delivery. The work presented in this chapter aims to demonstrate the potential of the agent-based approach for developing control-oriented models in complex cases, such as office buildings with high resolution thermal environments. This chapter also addresses challenges associated with the control complexity along with the growing input dimension in such configurations and demonstrates DMPC implementation into an actual building test-bed for the first time.

5.2 Distributed MPC algorithm

In thermal environment control of buildings, the objective function is the HVAC energy consumption. The decision variable **u**, which is the control input to the model, is the trajectory of Part Load Ratio (PLR) in a given prediction horizon. f_{HVAC} represents the electricity consumption of the HVAC source, which is a convex function when the PLR is the control input. The dimension of the trajectory is increased with the number of zones or systems that are connected to the shared HVAC source. The centralized MPC algorithm is formulated as a convex optimization problem (Equation. 5.1) with several linear inequality constraints. The first constraint represents the temperature bound of the conditioned zone; $\mathbf{T_{bound}}$ is the upper or lower temperature bound, and $\mathbf{C_T}$ is the matrix multiplied to all states to extract the target temperature states. Additional bounds can be used for certain states of the system, for example, slab temperatures in radiant systems. The

last constraint is set for the capacity of the HVAC source. $\mathbf{\Omega}$ represents the predefined matrices as shown in Equation 4.2.

$$\min f_{HVAC}\left(\begin{bmatrix}\mathbf{I} & \mathbf{I} & \cdots\end{bmatrix}\begin{bmatrix}\mathbf{u_i}\\ \mathbf{u_{i+1}}\\ \vdots\end{bmatrix}\right)$$
$$s.t.\begin{bmatrix}\mathbf{C_T}\cdot\mathbf{\Omega_{u,i}} & \mathbf{C_T}\cdot\mathbf{\Omega_{u,i+1}} & \cdots\\ \vdots & \vdots & \cdots\\ \mathbf{I} & \mathbf{I} & \ddots\end{bmatrix}\begin{bmatrix}\mathbf{u_i}\\ \mathbf{u_{i+1}}\\ \vdots\end{bmatrix}\leq\begin{bmatrix}\mathbf{T_{bound}}-\mathbf{C_T}\cdot\left(\mathbf{\Omega_T}\cdot\mathbf{T_0}+\mathbf{\Omega_w}\cdot\mathbf{w}\right)\\ \vdots\\ \mathbf{u_{max}}\end{bmatrix} \quad \text{(Eq 5.1)}$$

Algorithm 5.1 is the distributed MPC used in our study. It is inspired by the Proximal Jabcobian Alternating Direction Method of Multipliers (PJ-ADMM) (Hou et al. 2016), which is a variant of the classical ADMM method. The optimization in each controller is regulated with a proximal term and the control inputs of other agents (neighbors) are transferred from the previous iteration for parallel computing. Multiple optimizations for each agent (referred to as agent *i*) run in parallel until the convergence criteria are satisfied. In this formulation, the coupled cost is decomposed by fixing the control input of other agents ($\sum \mathbf{u}_{neighbors}^{k-1}$) so the dimension of the control input ($\mathbf{u}_i^k$) is reduced according to the number of agents. Decomposition is feasible as information from other agents is transferred from the previous iteration (referred to as step *k-1*). This enables parallel optimization, which would not be otherwise possible, as the objective function is evaluated with all control input trajectories from other agents. The same inequality constraints with centralized MPC are set.

Each agent searches for the optimal control inputs while exchanging information with other agents. The regulation term with multiplier ϕ_i is added to the objective function to encourage the convergence of the iterated control inputs. This multiplier is a vector which is updated with the deviation of two control input trajectories. In initial iterations, it is small so each agent calculates its objective function with less restriction. Then, as the iteration evolves, the regulation term becomes large and, the algorithm converges when the maximum value of the deviation of two control input trajectories is smaller than the stop criteria, ε_{stop}. The way Algorithm 5.1 updates the regulation term (ϕ_i) helps speed up the convergence speed, however, it comes at the price of sacrificing optimality performance.

Algorithm 5.1

1: initialize $\left(\mathbf{u}_\mathbf{i}^0,\ \ldots,\boldsymbol{\phi}_\mathbf{i}^0,\ \ldots\right)$

2: repeat following optimizations in parallel

$$\left|\begin{array}{l}
3:\ \mathbf{u}_\mathbf{i}^k = \arg\min_{\mathbf{u_i}}\left(f_{HVAC}\left(\mathbf{u}_\mathbf{i} + \sum \mathbf{u}_{neighbors}^{k-1}\right) + \boldsymbol{\phi}_\mathbf{i}^{k-1}\left\|\mathbf{u}_\mathbf{i} - \mathbf{u}_\mathbf{i}^{k-1}\right\|^2\right) \\
4:\ s.t. \begin{bmatrix} \mathbf{C_{T,i}}\cdot\boldsymbol{\Omega}_\mathbf{u,i} \\ \vdots \\ \mathbf{1} \end{bmatrix}\cdot\mathbf{u}_\mathbf{i}^k \le \begin{bmatrix} \mathbf{T_{bound}} - \mathbf{C_{T,i}}\cdot\left(\boldsymbol{\Omega}_\mathbf{T}\cdot\mathbf{T_0} + \boldsymbol{\Omega}_\mathbf{w}\cdot\mathbf{w} + \sum \boldsymbol{\Omega}_{neighbors}\cdot\mathbf{u}_{neighbors}^{k-1}\right) \\ \vdots \\ \mathbf{u_{max}} - \sum \mathbf{u}_{neighbors}^{k-1} \end{bmatrix} \\
5:\ \boldsymbol{\phi}_\mathbf{i}^k = \boldsymbol{\phi}_\mathbf{i}^{k-1} + \sigma\left|\mathbf{u}_\mathbf{i}^k - \mathbf{u}_\mathbf{i}^{k-1}\right| \\
\vdots
\end{array}\right.$$

6: until $\max\left(\left\|\begin{bmatrix} \mathbf{u}_\mathbf{i}^k \\ \mathbf{u}_\mathbf{i+1}^k \\ \vdots \end{bmatrix} - \begin{bmatrix} \mathbf{u}_\mathbf{i}^{k-1} \\ \mathbf{u}_\mathbf{i+1}^{k-1} \\ \vdots \end{bmatrix}\right\|\right) \le \varepsilon_{stop}$

5.3 Application of DMPC to optimal building climate control

In this section, we present the application of our multi-agent system approach into an actual test-bed. First, we describe the test-bed and the system identification for developing the building model. Then, we provide details for the DMPC implementation including the HVAC system, exogenous inputs and constraints, and we describe the data communication process. Finally, we discuss the performance of the DMPC controller with regards to thermal environment control and energy saving potential.

5.3.1 Test-bed

We explore the potential of the radiant system to provide localized thermal conditioning for the cooling season. For this purpose, the room is divided into four thermal zones corresponding to four sections of the radiant floor as shown in Figure 5.1. Each floor section consists of two pipe loops that are controlled together. RTD sensors (Digi-Key, 10K ohm, 1%) and thermocouples (Omega, T-type, ±0.5°C) are installed in each section (0.6 m height from the floor and on floor) to measure the air and slab surface temperatures (Figure 5.1). Ultrasonic flow meters (TUF-2000M, ±1%) and thermocouples (Omega, T-type, ±0.5°C) are attached and inserted at each pipe loop to capture the cooling rate for each section (Figure 5.2). The room has four wall diffusers for ventilation that are

connected to an Air Handling Unit (AHU). The vents and fan of the double façade were kept closed during this study. A standard BMS is available through the installed Tridium JACE controllers and Niagara/AX software framework (Tridium Inc).

5.3.2 Building model

The system identification experiment was conducted using the four room sections from the south to north direction as shown in Figure 5.1. To ensure sufficient excitation, cooling was provided to alternate floor sections for about six to twelve hours and the minimum surface temperature for the floor was 18~19°C. The room was occupied most of the day time so the air temperature was maintained with the ventilation system between 22 and 24°C.

The typical (centralized) estimation approach is not feasible for this system due to the large number of estimate parameters and the different magnitude of state trajectories in each sub-system including the double façade, the four thermal zones and the radiant floor. Therefore, a distributed system identification approach is deployed with six sub-system models (represented by six agents) representing the four thermal zones, the radiant floor and the double façade. The six sub-system models are initially estimated in parallel, reducing the scale of the estimation problem, and then integrated in a plug-and-play manner. The structure of the integrated model (Figure 5.3) consists of 17 states and 27 resistances (17C27R) with one boundary temperature which is the outdoor air temperature. Figure 5.3 shows only a portion of the model by excluding the repeated structure for simplicity. Resistances between the air nodes are fixed according to the ventilation flow rate assuming the air is well-mixed since the wall-supply diffusers are distributed in four corners. The model structure of each thermal zone has one state and three or four resistances (1C3R or 1C4R). The radiant floor is treated as one agent. It consists of 12 states and 18 resistances (12C18R). The thermal capacity of each floor section is weighted with its area and the resistances between the four concrete sections ($R_{s,hor}$ and $R_{s,ver}$ in Figure 5.3) are identical. Thus, the estimation is carried out with three states and three resistances to simplify the optimization problem. Internal heat gains from the equipment, occupants, and lighting are distributed to each section evenly. 90 % of equipment and occupant heat gain and 60% of lighting heat gain is an input the air node. The remaining portions (10 and 40% respectively) are inputs to the slab surface temperature node.

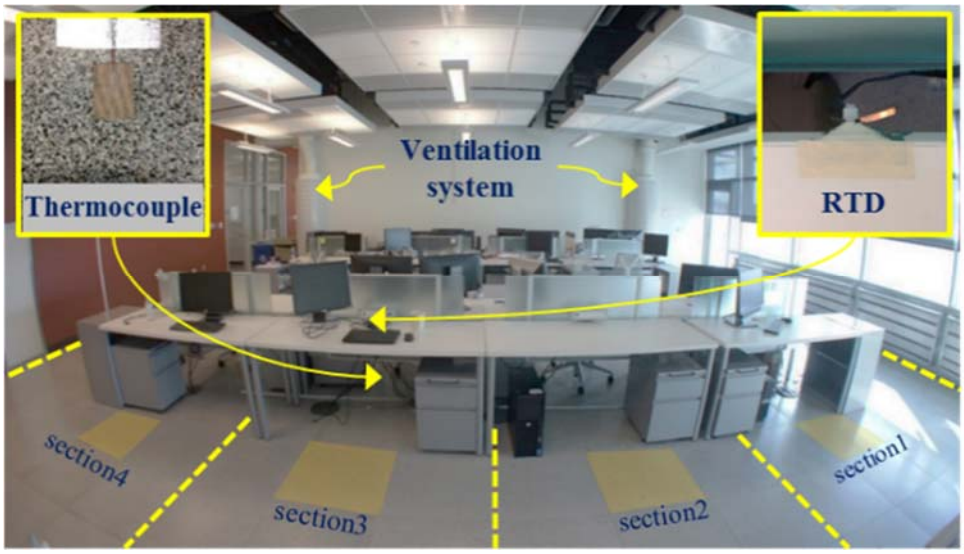

Figure 5.1 interior fish eye view of living lab 1

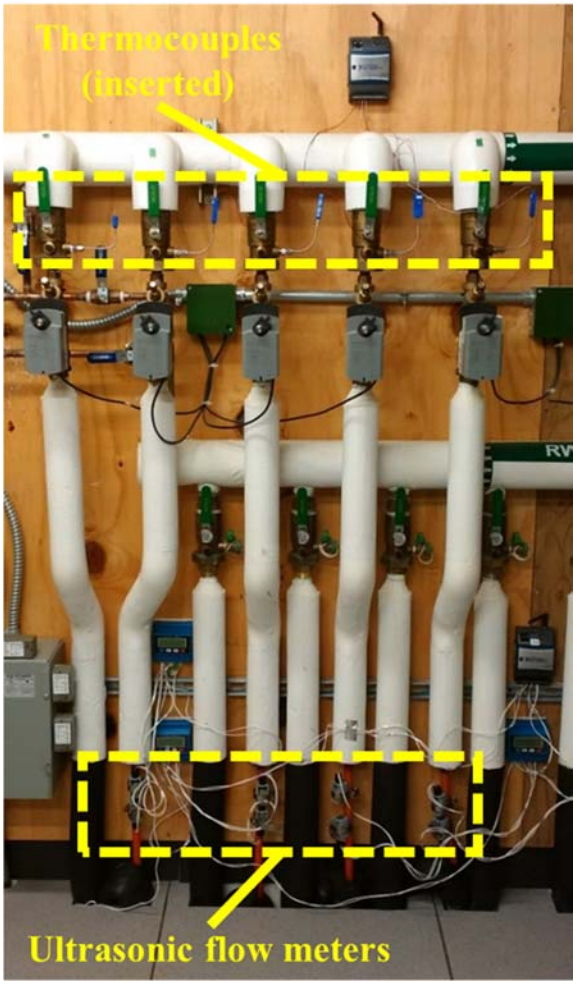

Figure 5.2 Pipe loops of the radiant floor system with temperature and flow meters installed.

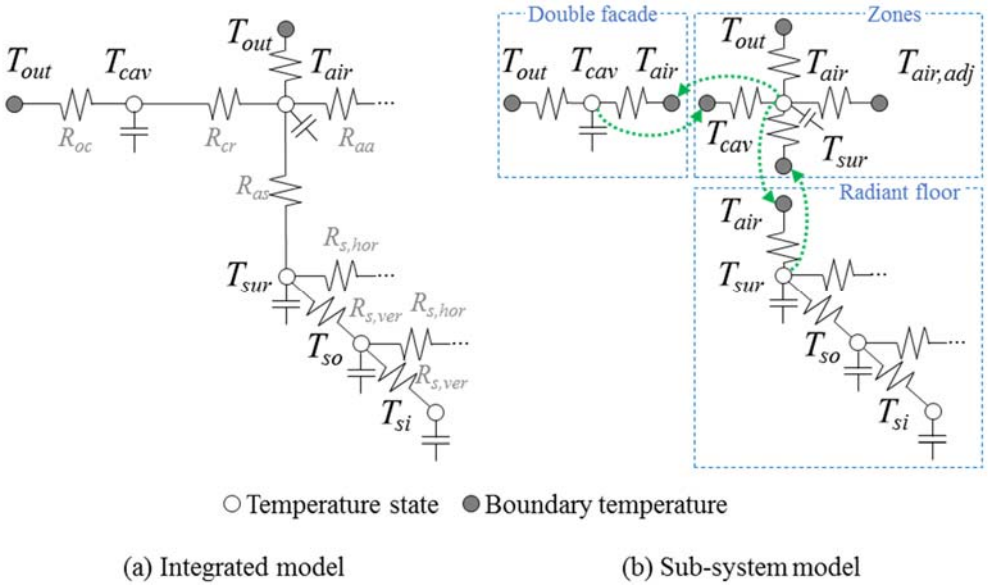

Figure 5.3 Integrated and sub-system model structure

The initial unmeasured temperature state for the internal concrete nodes (T_{so} *and* T_{si}) is assumed to be the same with the slab surface temperature. Six optimizations run in parallel with six sub-system models (agents). This yields different values for the shared estimate parameters between sub-systems. The dual decomposition method (explained in Section 3.3.4) is used to iterate the solution of the optimization problem until the deviation of the shared parameters is less than 5% of their value, in which case, they are assumed to be identical. Figure 5.4 shows the evolution of the shared parameters and reveals that 16 iterations are needed for the negotiation.

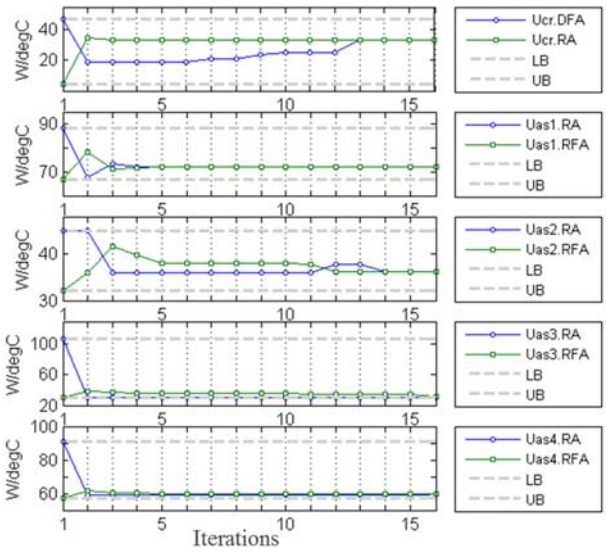

Figure 5.4 Evolution of shared parameters

Figure 5.5 shows results for one estimation set and two validation sets. Air and surface temperatures are shown on the left and right respectively along with the heat flux and temperature input at the bottom. The estimation period includes three days during which the radiant floor cooling system was ON and two days with free floating conditions. The Root Mean Square Error (RMSE) during the estimation period for the air and slab surface temperature in each section ranges from 0.43 to 0.58℃, and from 0.45 to 0.68℃, respectively. The model was validated with two different datasets as shown in Figures 5.5 (b) and (c). During this period, the radiant floor cooling system was ON in alternate sections for eight hours and free floating was used for four hours between turns. When this process was completed for all sections, another 12 hours of free floating was provided. Two cycles were used for the two different validation sets, respectively. For the first validation set, the RMSE of the air and slab surface temperature ranges from 0.55 to 0.82℃, and from 0.44 to 0.92℃, respectively (Figure 5.5 (b)). The corresponding ranges for the second validations set are 0.58 to 0.66℃, and 0.44 to 0.92℃ (Figure 5.5 (c)). This accuracy is considered to be reasonably good considering the complexity of the model.

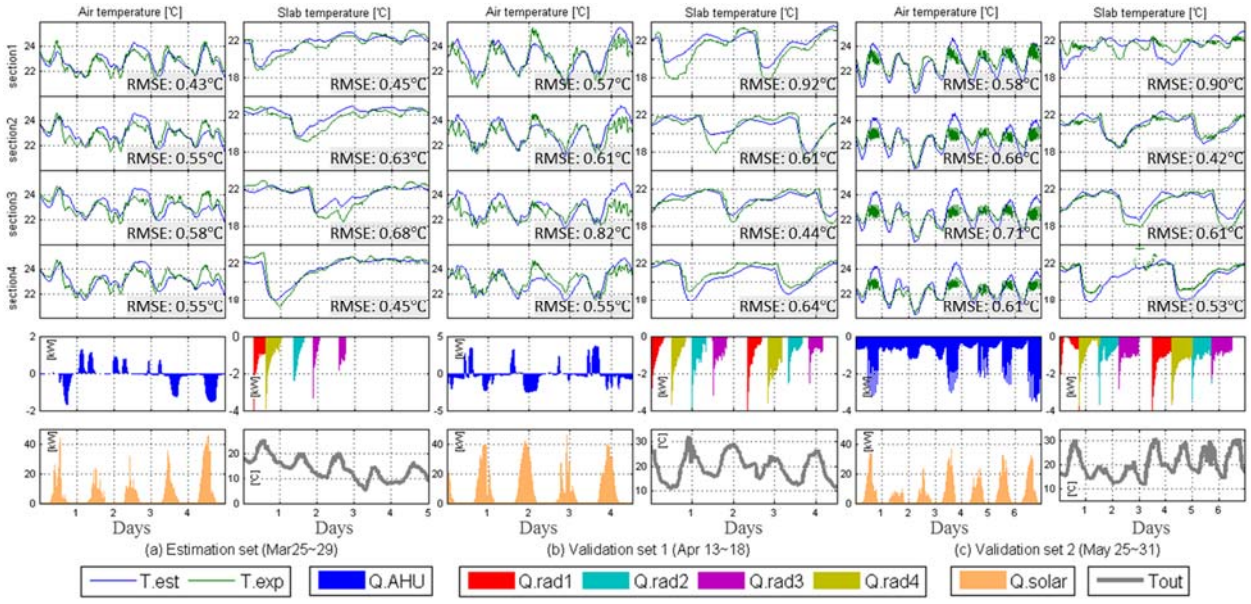

Figure 5.5 System identification results

5.3.3 DMPC implementation

5.3.3.1 HVAC system and objective function

Same HVAC system (Air-cooled chiller) and implementation settings were applied with previous chapter; details are explained in Section 4.3.3 and 4.3.5. However, in this chapter, air-cooled chiller

is serving four room sections with parallel radiant loop (Figure 5.6) and control input is PLR provided to each section. The electricity consumption of the chiller consists of the objective function with a regulation term as explained in Section 5.3 (Algorithm 5.1). The initial control input trajectory $\mathbf{u}^0$ and multiplier $\boldsymbol{\phi}^0$ are set to zero, and the step size and stop criteria (σ and ε_{stop} in Algorithm 5.1) are set to 50 and 0.0002.

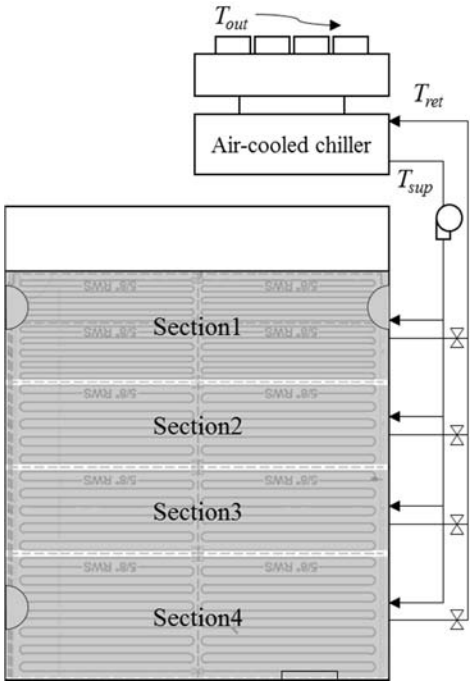

Figure 5.6 Test-bed with virtual air-cooled chiller (left)

5.3.3.2 Implementation settings

Four phases were considered during the implementation with different settings for the operative temperature bounds as shown in Table 5.1. For the first two phases, relatively large temperature bounds were used to ensure proper operation of the system, while the bounds for phase 3 were significantly different among the different sections to evaluate the potential for localized thermal environment control. For phase 4, lower bounds were set to see if relatively low operative temperature preferences could be met.

Table 5.1. Lower and upper bounds of the operative temperature [°C]

	phase 1	phase 2	phase 3	phase 4
room section1	22.0~25.0	21.0~24.0	22.5~25.5	20.5~23.5
room section2	22.0~25.0	21.0~24.0	unoccupied	19.0~22.0
room section3	21.0~24.0	22.0~25.0	19.5~22.5	19.0~22.0
room section4	21.0~24.0	22.0~25.0	19.5~22.5	unoccupied

Figure 5.7 shows the implementation results for 11 consecutive days (September 16-26, 2017). The room air (Tar), slab surface (Tsl), and operative temperatures (Top) along with lower and upper bounds are shown for all sections along with the corresponding control and exogenous inputs. The gap on the graph for day 8 is due to data loss associated with a server communication failure. The operative temperature bounds for all sections are mostly satisfied for phase 1 and 2. Some exceedance hours due to upper bound violations are observed in phase 4. Although the operative temperature bounds are hard constraints in the optimization problem, the maximum cooling rate was provided occasionally when the temperature is violated.

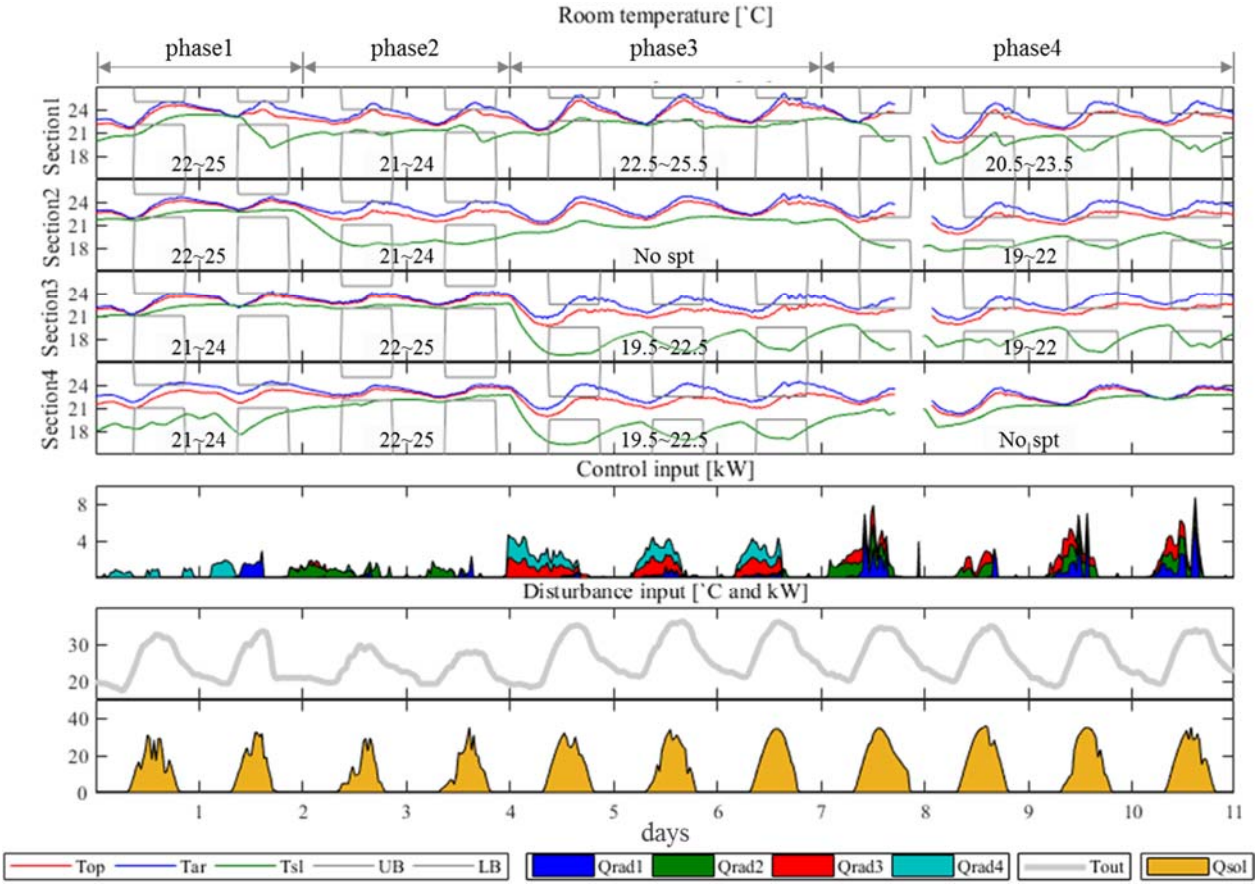

Figure 5.7 DMPC implementation results for four phases with different temperature bounds (September 16-26 2017)

5.3.3.3 Control performance analysis

In this section, results from the DMPC implementation in an actual test-bed are compared with simulations for two feedback and two MPC control strategies, introduced in Figure 5.8. The simulations are used for evaluating the performance of the DMPC algorithm and the DMPC controller. For feedback control, the room is considered to be represented by a single thermal zone and it is conditioned using a temperature bound that corresponds to the average of the values used in the four sections for the DMPC implementation (21.5~24.5, 20.5~23.5, and 19.5~22.5°C). For the first feedback controller (*Baseline-zone)*, all local sections are conditioned regardless of the occupancy unlike all the other cases in which localized conditioning is used for the occupied sections. The second feedback controller (*Baseline-local)* conditions only occupied sections. This comparison aims to investigate the energy saving potential of occupancy-based localized conditioning. To evaluate the DMPC algorithm, two simulation cases including CMPC and DMPC are used to investigate potential gaps between the theoretical and actual performance of the system. In simulation, MPC runs for each day and the last state is an input to the initial state for the next day so 11 consecutive MPCs run sequentially for 11days. The same disturbances for the weather and internal heat gain and algorithm settings, such as initial parameters ($\mathbf{u}^0$ and $\boldsymbol{\phi}^0$), step size (σ) and stop criteria (ε_{stop}), used in implementation were also used for the simulations.

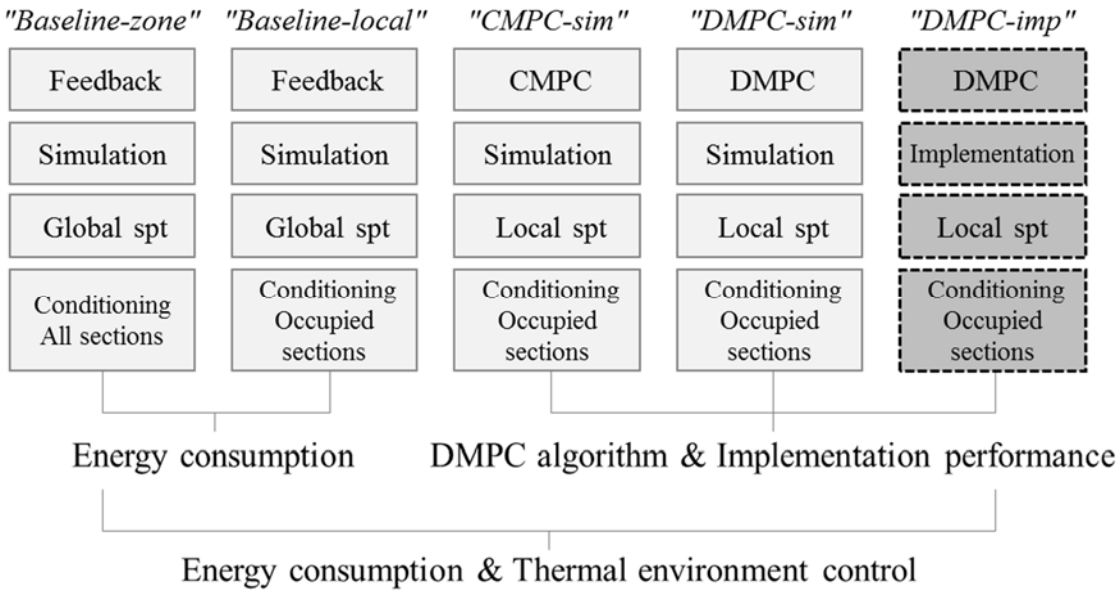

Figure 5.8 Different control scenarios used for the DMPC algorithm evaluation and the DMPC performance analysis

5.3.3.4 DMPC algorithm evaluation

Figure 5.9 shows the evolution of the objective function value and the residual for the regulation term of *DMPC sim*. Each line represents the optimization of one day. Residual represents the maximum value of the regulation term which is the deviation between the decision variables of the current and the previous iterations. Mostly, high fluctuations of the residual are seen for the initial iterations, and then they decrease. The algorithm requires13 to 157 iterations to converge which takes less than 5 min for each time-step which is sufficient for implementation in actual controllers, as the time-step for this study is 30 min.

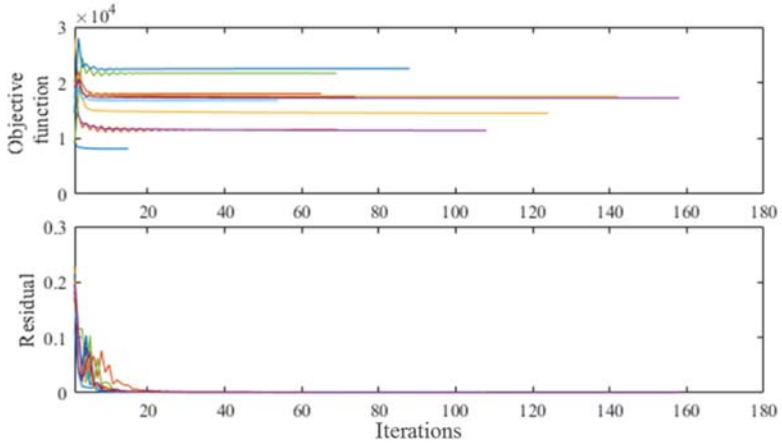

Figure 5.9 Evolution of objective function and residual in DMPC sim

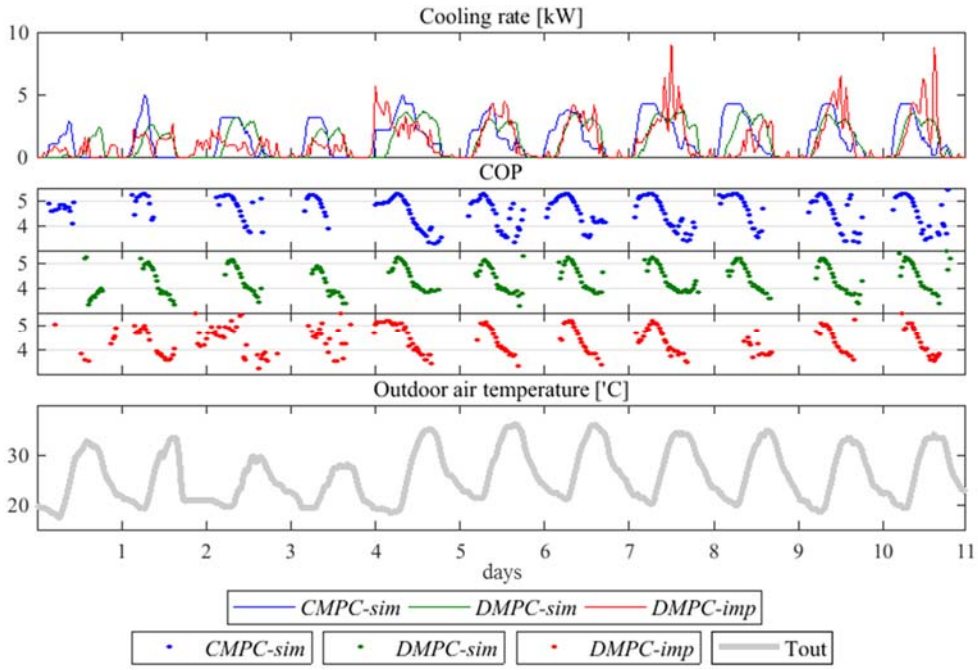

Figure 5.10 DMPC algorithm evaluation

Table 5.2. DMPC algorithm evaluation

Case	*CMPC-sim*	*DMPC-sim*	*DMPC-imp*
Cooling energy consumption[kWh]	350	327	314
Electricity consumption [kWh]	74	76	72

Figure 5.10 shows the cooling rate and COP variation during the test-period for the MPC simulations and DMPC implementation while Table 2 presents a summary of the results. Compared to CMPC, *DMPC-sim* results in lower cooling rate but higher electricity power consumption as the pre-cooling effect is less utilized. However, this compromise in DMPC controller performance is acceptable as the electricity consumption is increased by 2.8% only. As for the DMPC implementation, the cooling rate and electricity consumption is less compared to *DMPC-sim*; this is because the temperature bounds during implementation were not completely satisfied (see Section 4.3.4). Nevertheless, the pre-cooling effect is clearly seen with a higher COP and the total energy consumption is similar with the simulation; therefore, most of the potential benefits were captured in the implementation. If the room temperature would be perfectly regulated in implementation, the energy consumption would be the same with the simulation, which is a theoretical performance bound based on perfect disturbance prediction.

5.3.3.5 DMPC performance analysis

In this section, we investigate the energy saving potential of the occupancy-based control and DMPC by comparison with two feedback strategies. Table 3 shows the total cooling energy consumption and electricity consumption. The occupancy-based localized feedback control (*baseline-local*) saves 4.8% compared to the *baseline-zone* for the specific occupant schedule presented in Table 1; the unoccupied period for the local sections is 84 hours, i.e.16% of the total. When the MPC is implemented using different set-points (temperature bound) and occupancy-based conditioning, which is *DMPC-imp*, around 27 % of electricity savings are possible compared to *Baseline-zone*. This is illustrated in Figure 5.11, which shows the operative temperature profiles with different bounds for all sections along with the cooling rate to the radiant floor and the COP variation. Compared to feedback control, DMPC utilizes pre-cooling so the chiller operates during the night or early in the morning to take advantage of the higher COP due to low outdoor air temperature. The variation of COP shows these distinct differences (Figure 5.11). Also, the MPC strategy itself saves 19 % of cooling energy (390 versus 314kWh) due to the large thermal capacity

of the radiant floor system; as for the feedback control, cooling is provided from the slab to the room after the occupied hour.

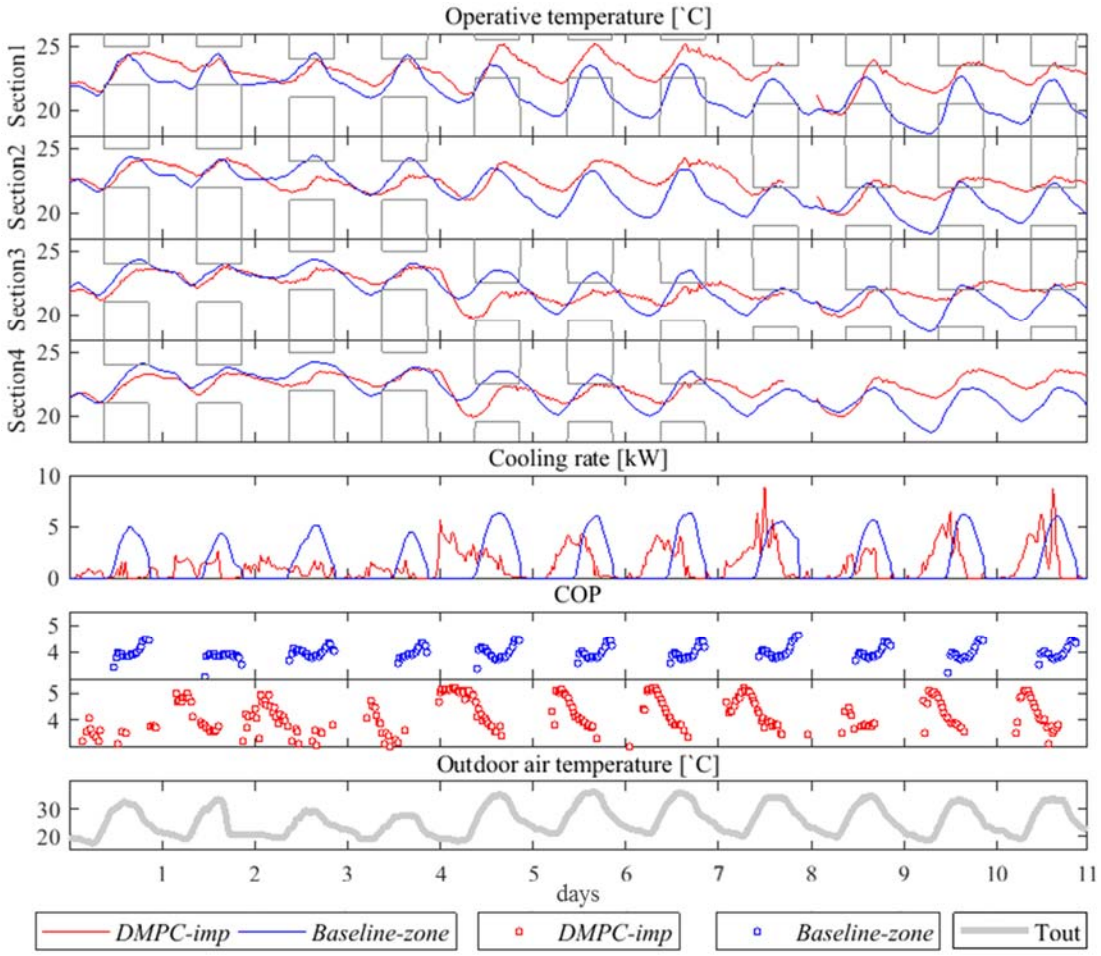

Figure 5.11 DMPC energy performance analysis

Table 5.3. DMPC energy performance analysis

Case	*Baseline-zone*	*Baseline-local*	*DMPC-imp*
Cooling energy consumption [kWh]	390	372	314
Electricity consumption [kWh]	99	94	72

The baseline feedback control *(Baseline-zone)* is compared with the *DMPC-sim* strategy that facilitates localized control based on different occupant preferences. The differences are quantified using the summation of operative temperature exceedance hours (°C·h) during occupancy and the results are presented in Table 4. For phase 1 and 2, the temperature exceedance with the *Baseline-zone* control is small because the temperature bounds of the different thermal zones are similar (21~24°C and 22~25°C). However, when the bounds are significantly different (19.5~22.5 and 22.5~25.5°C in phase 3; 19~22 and 20.5~23.5°Cin phase 4), the temperature exceedance hours

with the *Baseline-zone* control are increased. No temperature exceedance is observed in sections 2 and 4 for phase 3 and 4 as they were not occupied and thereby not conditioned. The total temperature exceedance hours for a period of 11 days are 64.7°C·h for the feedback control (*Baseline-zone*) and 22.2°C·h for *DMPC-imp*, i.e. 65.8% less. If different global temperature bounds such as the maximum or minimum value of the local bounds are implemented, the total exceedance hours of *Baseline-zone* are 191.3 or 45.6°C·h respectively which are still higher compared to *DMPC-imp*.

Table 5.4. Temperature exceedance comparison between Baseline-zone and DMPC-imp [°C·h]

	Baseline-zone				*DMPC-imp*			
	phase1	phase2	phase3	phase4	phase1	phase2	phase3	phase4
section1	0.3	1.7	17.9	5.5	0.2	0.0	1.1	2.5
section2	0.0	1.8	-	2.8	0.1	0.0	-	13.3
section3	1.3	0.0	15.3	2.5	0.0	0.0	0.0	3.8
section4	0.2	0.0	15.4	-	0.0	0.0	1.1	-

5.4 Limitations

During the implementation, disturbance prediction such as occupant's schedule and internal heat gain profiles were estimated based on historical data. Also, the solar irradiance forecast is calculated with a deterministic model based on the climate zone of the actual test-bed. In future work, a more precise method for the solar irradiance forecast using site-specific data could be used (e.g. (Liu et al. 2018)), along with statistical methods for occupant's schedule (Jia and Spanos 2016; Liao and Barooah 2010; Yang et al. 2014; Zhang et al. 2010).

In this chapter, we introduced scalable control functions and demonstrated localized thermal environment control in open-plan spaces using a radiant floor system with distributed sensing and data communication capabilities. Different comfort bounds are reported in the literature (Krajčík et al. 2013; Krajčík et al. 2017; Wang et al. 2009; Nevins and Feyerherm 1967) while recommendations for comfortable operative temperature ranges in ASHRAE 55 (ASHRAE 2013) might not be applicable for radiant floor systems. In the future, we will leverage on-going work on learning algorithms for occupants' thermal preferences (Lee et al. 2017; Lee et al. 2018) and the research presented in this chapter will be extended to integrate occupants' feedback in DMPC controllers.

In the case-study presented in this chapter, a standard BMS system was used for the implementation of the DMPC algorithm. Although the MPC computations run sequentially in a single server computer, parallel computing is realized as the information from other agents comes from the previous iterations. In the future, the developed algorithm can be implemented using new low-cost devices such as series of small single-board computers. It is envisioned that smart building features with distributed sensing, occupant interaction, data communication and computing abilities could be widely adopted if intelligence is embedded into physical devices (Cai et al. 2016a). The research presented in this chapter is the first step in this direction.

5.5 Chapter conclusions

In this chapter, a multi-agent system approach for smart thermal environment control of office buildings was presented. The study has shown that the distributed system identification algorithm based on dual decomposition method yields building models with good prediction accuracy even

for complex environments such as open-plan spaces with multiple individually controlled comfort delivery systems.

Using a data-driven model and weather forecast, the DMPC controller was implemented to optimize the operation of an air-cooled chiller while providing different operative temperature bounds for each radiant floor loop. The control input for each radiant loop (agent) was calculated individually through the information exchange between agents and then provided to the actual BMS. The comparison with a centralized control approach shows that the DMPC algorithm captures most of the energy saving potential of the system. This approach is scalable so it can be generalized to larger scales of building systems such as multiple zones or building clusters. In this case, demand charge needs to be considered with electricity price information. Compared to feedback control, DMPC saves around 27% of the electricity consumption by utilizing the higher COP of the chiller through the pre-cooling period. At the same time, different thermal environments were achieved by facilitating local conditioning in open-plan office spaces.

CHAPTER 6. CONCLUSIONS AND FUTURE WORK

6.1 Main Achievements

This thesis introduces and demonstrates a new agent-based approach to optimal control of high performance buildings. From the application perspective, the focus is thermal environment control of open-plan office spaces. Radiant floor systems are evaluated as high performance features and used as test-beds to demonstrate the proposed agent-based framework for zone and local environment control.

More specifically, key achievements of this doctoral thesis are:

- An agent-based estimation framework for data-driven building models. This includes identifying agents, their function and network structure, and estimating model parameters for both individual agents in the system, using information locally known or observable by each agent, and their connections. The proposed method introduces building sub-system agents, which are optimized independently, by solving locally a nonlinear programming problem while the information is exchanged between the agents. Then, they are integrated into one model with further parallel optimizations by applying the dual decomposition method.
- Two case-studies using the Living Laboratories at Purdue's Herrick Building as test-beds to validate the estimated control-oriented models under realistic operation conditions. The results show that the model prediction accuracy of the new approach is fairly good for implementation in predictive control while models can be developed and integrated with improved efficiency, flexibility and scalability, compared to centralized approaches. The distributed system identification algorithm based on dual decomposition method yields building models with good prediction accuracy even for complex environments such as open-plan spaces with multiple individually controlled comfort delivery systems. This approach provides a viable solution for control-oriented building models that can be easier to develop and integrate whereas the conventional centralized approach could not provide accurate predictions for all states.
- A DMPC algorithm for intelligent control of office buildings with high resolution thermal environments. The developed algorithm is inspired by the Proximal Jacobian Alternating

Direction Method of Multipliers (PJ-ADMM) with multiple MPCs run iteratively while exchanging control input information until they converge. With this tractable approach, agents solve individual optimization problems in parallel, through information exchange and broadcasting, with a smaller scale of the input and constraints, facilitating optimal solutions with improved efficiency.

- DMPC implementation into an actual building test-bed. The developed algorithm is tested using field data from an occupied open-plan office space with localized comfort delivery along with distributed sensing, control, and data communication capabilities. The comparison with a centralized control approach shows that the DMPC algorithm captures most of the energy saving potential of the system. Although the MPC computations run sequentially in a single server computer, parallel computing is realized as the information from other agents comes from the previous iterations.
- Detailed evaluation of the energy and cost saving potential of radiant floor systems with MPC to reveal its potential as high performance feature in office buildings.
    - The developed zone (centralized) MPC controller includes data-driven building models estimated and validated for the heating and cooling seasons, and an optimizer based on constraint quadratic programming with hard comfort bounds which yields an exact numerical solution with predicted exogenous disturbances. The implementation in an occupied office building with a chiller and boiler as HVAC sources shows significant energy and cost savings through comparisons with baseline air delivery systems and controls.
    - In the DMPC implementation, the control input for each radiant loop (agent) was calculated individually through the information exchange between agents and then provided to the actual BMS. The developed DMPC controller is capable of providing thermal environments with high resolution, thereby improving occupant satisfaction, while achieving more than 27% reduction in electricity consumption compared to baseline feedback control.

6.2 Future work

The overall agent-based methodology developed in this thesis could be packaged into a toolbox integrated into open-source building control platforms, existing building management systems, or

embedded into new smart devices. It is a scalable solution that can be extended to other smart and connected environments, e.g., multiple building systems, multi-zone buildings, building clusters integrated with power grids and automobiles.

It is envisioned that smart building features with distributed sensing, occupant interaction, data communication and computing abilities could be widely adopted if intelligence is embedded into physical devices. In this regard, the developed DMPC algorithm can be implemented using new low-cost devices such as series of small single-board computers (e.g., Raspberry Pi) and could be packaged into a toolbox integrated in advanced open-source building control platforms (e.g., Voltron). Also, it is expected that the human-related technology facilitates the interaction between the occupants and BMS so the occupants' information could be estimated via statistical methods which improve the accuracy of the MPC controller. Moreover, as the occupant is regarded as a service user and participant for improving the energy performance of the building, untapped energy saving potential is anticipated from the utilizing the comfort-and-energy trade off.

In the future, low cost devices of single board computer with sensors and occupants interaction protocol will be configured to provide the localized thermal environment with fine granularity as well as integrate the occupant in the loop to obtain the comfort feedback and occupancy information. Thereby we can leverage on-going work on learning algorithms for occupants' thermal preferences as well as the relation of comfort and energy-related feedback provided to individual occupants.

REFERENCES

Agbi, Clarence, Zhen Song, and Bruce Krogh. 2012. "Parameter Identifiability for Multi-Zone Building Models." *Proceedings of the IEEE Conference on Decision and Control*, 6951–56. doi:10.1109/CDC.2012.6425995.

Ahn, Byung-Cheon, and Jae-Yeob Song. 2010. "Control Characteristics and Heating Performance Analysis of Automatic Thermostatic Valves for Radiant Slab Heating System in Residential Apartments." *Energy* 35 (4): 1615–24. doi:10.1016/j.energy.2009.11.007.

Ahn, Byung-Cheon. 2011. *Developments in Heat Transfer: Radiant floor heating system.* InTech.

Arteconi, A., D. Costola, P. Hoes, and J.L.M. Hensen. 2014. "Analysis of Control Strategies for Thermally Activated Building Systems under Demand Side Management Mechanisms." *Energy and Buildings* 80 (September): 384–93. doi:10.1016/j.enbuild.2014.05.053.

ASHRAE, ANSI/ASHRAE Standard 55-2013, Thermal comfort Conditions for Human Occupancy, ASHRAE, Atlanta, 2013.

Athienitis, Andreas K. 1997. "Investigation of Thermal Performance of a Passive Solar Building with Floor Radiant Heating." *Solar Energy* 61 (5): 337–45. doi:10.1016/S0038-092X(97)00077-7.

Bacher, Peder, and Henrik Madsen. 2011. "Identifying Suitable Models for the Heat Dynamics of Buildings." *Energy and Buildings* 43 (7): 1511–22. doi:10.1016/j.enbuild.2011.02.005.

Batista, Gilberto, Pedro Dinis Gasper, Pedro D. Silva. 2013. "Control, regulation and command system of hydronic radiant floors heating by wireless and energy harvesting sensors and actuators." *Key Engineering Materials* 543: 389–392.

Bengea, Sorin C., Anthony D. Kelman, Francesco Borrelli, Russell Taylor, and Satish Narayanan. 2014. "Implementation of Model Predictive Control for an HVAC System in a Mid-Size Commercial Building." *HVAC&R Research* 20 (1): 121–35. doi:10.1080/10789669.2013.834781.

Bernal, Willy, Madhur Behl, Truong X. Nghiem, Rahul Mangharam. 2013. "MLE+: A Tool for Integrated Design and Deployment of Energy Efficient Building Controls." *4th ACM Workshop on Embedded Sensing Systems for Energy-Efficiency in Buildings*, (BuildSys '12), Toronto, Canada.

Berthou, Thomas, Pascal Stabat, Raphael Salvazet, and Dominique Marchio. 2014. "Development and Validation of a Grey-box Model to Predict Thermal Behavior of Occupied Office Buildings." *Energy and Buildings* 74 (5): 91–100. doi:10.1016/j.enbuild.2014.01.038.

Braun, J. 2003. "Load Control Using Building Thermal Mass." *J. Sol. Energy Eng* 125(3): 292–301. doi:10.1115/1.1592184

Braun, James E. and Kyoung-Ho Lee. 2006b. "Assessment of Demand Limiting Using Building Mass in Small Commercial Buildings." *ASHRAE Transactions* 112(1).

Braun, James, and Nitin Chaturvedi. 2002. "An Inverse Grey-Box Model for Transient Building Load Prediction." *HVAC&R Research* 8 (1): 73–99. doi:10.1080/10789669.2002.10391290.

Braun, JE, KW Montgomery, and N. Chaturvedi. 2001. "Evaluating the Performance of Building Thermal Mass Control Strategies." *HVAC&R Research* 7 (4): 403–28. doi:10.1080/10789669.2001.10391283.

Cai, Jie, and James Braun. 2015. "An Inverse Hygrothermal Model for Multi-Zone Buildings." *Journal of Building Performance Simulation* 1493 (11): 1–19. doi:10.1080/19401493.2015.1108999.

Cai, Jie, Donghun Kim, Vamsi K. Putta, James E. Braun, and Jianghai Hu. 2015. "Multi-Agent Control for Centralized Air Conditioning Systems Serving Multi-Zone Buildings." *Proceedings of the American Control Conference 2015*-July: 986–93. doi:10.1109/ACC.2015.7170862.

Cai, Jie, Donghun Kim, Rita Jaramillo, James E Braun, and Jianghai Hu. 2016a. "A General Multi-Agent Control Approach for Building Energy System Optimization." *Energy & Buildings* 127. Elsevier B.V.: 337–51. doi:10.1016/j.enbuild.2016.05.040.

Cai, Jie, James E Braun, Donghun Kim, Rita Jaramillo, and Jianghai Hu. 2016b. "A Multi-Agent Control Based Demand Response Strategy for multi-zone buildings." *Proceedings of the American Control Conference 2016*-July. doi:10.1109/ACC.2016.7525271

Cai, Jie, James E Braun, Donghun Kim, and Jianghai Hu. 2016c. "General Approaches for Determining the Savings Potential of Optimal Control for Cooling in Commercial Buildings Having Both Energy and Demand Charges." *Science and Technology for the Built Environment* 22(6): 733–750, DOI: 10.1080/23744731.2016.1197716.

Cai, Jie, Donghun Kim, James E Braun, and Jianghai Hu. 2016d. "Optimizing Zone Temperature Setpoint Excitation to Minimize Training Data for Data-Driven Dynamic Building Models." submitted to *American Control Conference*.

Camponogara, Eduardo, Dong Jia, Bruce H Krogh, and Sarosh Talukdar. 2002. "Distributed Model Predictive Control" *IEEE Control Systems* 22 (1): 44–52. doi: 10.1109/37.980246.

Candanedo, Jose A. and Andreas K. Athienitis. 2011b. "Predictive control of radiant floor heating and solar-source heat pump operation in a solar house." *HVAC&R Research* 17(3).

Candanedo, Jose A., Amelie Allard, Andreas K. Athienitis. 2010. "Predictive Control of Radiant Floor Heating and Transmitted Irradiance in a Room with High Solar Gains." *ASHRAE Transactions* 117 (December).

Candanedo, Jose A., Amelie Allard, Andreas K. Athienitis. 2011a. "Solar-Assisted Radiant Floor Heating in a Net-zero Energy residential Building." *ASHRAE transactions* (Jan).

Cho, S.-H., and Zaheer-uddin, M. 1999. "An experimental study of multiple parameter switching control for radiant floor heating systems." *Energy* 24(5): 433–444.

Christofides, Panagiotis D., Riccardo Scattolini, David Munoz de la Pena, and Jinfeng Liu. 2013. "Distributed Model Predictive Control: A Tutorial Review and Future Research Directions." *Computers and Chemical Engineering* 51: 21–41. doi:10.1016/j.compchemeng.2012.05.011.

Cigler, Jiří, Samuel Prívara, Zdeněk Váňa, Eva Žáčeková, and Lukáš Ferkl. 2012. "Optimization of Predicted Mean Vote Index within Model Predictive Control Framework: Computationally Tractable Solution." *Energy and Buildings* 52: 39–49. doi:10.1016/j.enbuild.2012.05.022.

Corbin, Charles D., Gregor P. Henze, and Peter May-Ostendorp. 2012. "A Model Predictive Control Optimization Environment for Real-Time Commercial Building Application." *Journal of Building Performance Simulation* 1493 (March 2014): 1–16. doi:10.1080/19401493.2011.648343.

Davidsson, Paul, and Magnus Boman. 2005. "Distributed Monitoring and Control of Office Buildings by Embedded Agents." *Information Sciences* 171 (4): 293–307. doi:10.1016/j.ins.2004.09.007.

De Coninck, Roel, and Lieve Helsen. 2016. "Practical Implementation and Evaluation of Model Predictive Control for an Office Building in Brussels." *Energy and Buildings* 111 (1): 290–98. doi:10.1016/j.enbuild.2015.11.014.

De Coninck, Roel, Fredrik Magnusson, Johan Åkesson, and Lieve Helsen. 2015. "Toolbox for Development and Validation of Grey-Box Building Models for Forecasting and Control." *Journal of Building Performance Simulation* 1493 (July): 1–16. doi:10.1080/19401493.2015.1046933.

Del Barrio, Elena Palomo, and Gilles Guyon. 2003. "Theoretical Basis for Empirical Model Validation Using Parameters Space Analysis Tools." *Energy and Buildings* 35 (10): 985–96. doi:10.1016/S0378-7788(03)00038-0.

Del Barrio, Elena Palomo, and Gilles Guyon. 2004. "Application of Parameters Space Analysis Tools for Empirical Model Validation." *Energy and Buildings* 36 (1): 23–33. doi:10.1016/S0378-7788(03)00039-2.

Doren, Jorn F. M. Van, Sippe G. Douma, Paul M. J. Van den Hof, Jan Dirk Jansen, and Okko H. Bosgra. 2009. "Identifiability: From Qualitative Analysis to Model Structure Approximation." *Proceedings of the 15th International Federation on Automatic Control (IFAC) Symposium on System Identification*, 664–69. doi:10.3182/20090706-3-FR-2004.00110

Duan, Jianmin, and Fan Lin. 2008. "Research of Intelligent Building Control Using an Agent-Based Approach." *2008 6th IEEE International Conference on Industrial Informatics*, 991–94. doi:10.1109/INDIN.2008.4618246.

EnergyPlus. 2015. EnergyPlus engineering reference: the reference to EnergyPlus calculations. Lawrence Berkeley National Laboratory.

European Standard (UNI EN 1264-5). 2009. "Water Based Surface Embedded Heating And Cooling Systems - Part 5: Heating And Cooling Surfaces Embedded In Floors, Ceilings And Walls - Determination Of The Thermal Output"

Fabrizio, Enrico, Stefano P. Corgnati, Francesco Causone, Marco Filippi. 2012. "Numerical comparison between energy and comfort performance of radiant heating and cooling systems versus air systems." *HVAC&R Research* 18(4).

Favre, B., and Peuportier, B. 2014. "Application of dynamic programming to study load shifting in buildings." *Energy and Buildings* 82: 57–64.

Feng, Jingjuan, Frank Chuang, Francesco Borrelli, and Fred Bauman. 2015. "Model Predictive Control of Radiant Slab Systems with Evaporative Cooling Sources." *Energy and Buildings* 87 (1): 199–210. doi:10.1016/j.enbuild.2014.11.037.

Gayeski, N. T., P., R., Armstrong, L., K., Norford. 2012. "Predictive Pre-cooling of Thermo-Active Building Systems with Low- Lift Chillers." *HVAC&R Research* 18 (5): 1–16.

Gwerder, M., B. Lehmann, J. Tödtli, V. Dorer, and F. Renggli. 2008. "Control of Thermally-Activated Building Systems (TABS)." *Applied Energy* 85 (7): 565–81. doi:10.1016/j.apenergy.2007.08.001.

Gwerder, Markus, and Dimitrios Gyalistras. 2013. “Final Report : Use of Weather And Occupancy Forecasts For Optimal Building Climate Control – Part II : Demonstration (OptiControl-II).” *ETH Zürich*, no. September.

Hazyuk, Ion, Christian Ghiaus, and David Penhouet. 2012. “Optimal Temperature Control of Intermittently Heated Buildings Using Model Predictive Control: Part I – Building Modeling.” *Building and Environment* 51 (5): 379–87. doi:10.1016/j.buildenv.2011.11.009.

Henze, G. P., Felsmann, C., & Knabe, G. 2004. “Evaluation of optimal control for active and passive building thermal storage.” *International Journal of Thermal Sciences* 43(2): 173–183.

Henze, Gregor P. 2013. “Model Predictive Control for Buildings: A Quantum Leap?” *Journal of Building Performance Simulation* 6 (3): 157–58. doi:10.1080/19401493.2013.778519.

Hosni, Mohammad H., Byron W. Jones, and Hanming Xu. 1999. “Experimental Results for Heat Gain and Radiant/convective Split from Equipment in Buildings.” *ASHRAE Transactions* 105.

Hou, Xiaodong, Yingying Xiao, Jie Cai, Jianghai Hu, and James E Braun. 2016. “A Distributed Model Predictive Control Approach for Optimal Coordination of Multiple Thermal Zones in a Large Open Space.” *International high performance buildings conference*, Purdue University, West Lafayette, July 11–14.

Hu, Jianjun, and Panagiota Karava. 2014. “A State-Space Modeling Approach and Multi-Level Optimization Algorithm for Predictive Control of Multi-Zone Buildings with Mixed-Mode Cooling.” *Building and Environment* 80 (October): 259–73. doi:10.1016/j.buildenv.2014.05.003.

Jennings, N.R., and S. Bussmann. 2003. “Agent-Based Control Systems: Why Are They Suited to Engineering Complex Systems?” *IEEE Control Systems* 23 (3): 61–73. doi:10.1109/MCS.2003.1200249.

Jiménez, M.J., H. Madsen, and K.K. Andersen. 2008. “Identification of the Main Thermal Characteristics of Building Components Using MATLAB.” *Building and Environment* 43 (2): 170–80. doi:10.1016/j.buildenv.2006.10.030.

Joe, Jaewan, and Panagiota Karava. 2016. “Agent-Based System Identification for Control-Oriented Building Models.” *Journal of Building Performance Simulation*. Taylor & Francis: 1–22. doi:10.1080/19401493.2016.1212272.

Joe, Jaewan, Panagiota Karava, Xiaodong Hou, and Jianghai Hu. 2016. "Model Predictive Control of a Radiant Floor Cooling System in an Office Space" *International high performance buildings conference*, Purdue University, West Lafayette, July 11–14.

Kelly, George E, and Steven T Bushby. 2012. "Are Intelligent Agents the Key to Optimizing Building HVAC System Performance?" *HVAC&R Research* 18 (4): 750–59. doi:10.1080/10789669.2012.682693.

Kim, Kwang woo and Bjarne Olesen. 2015a. "Radiant Heating and Cooling Systems: Part 1." *ASHRAE Journal* (Feb).

Kim, Kwang woo and Bjarne Olesen. 2015b. "Radiant Heating and Cooling Systems: Part2." *ASHRAE Journal* (Mar).

Koehler, Sarah, and Francesco Borrelli. 2013. "Building Temperature Distributed Control via Explicit MPC and 'Trim and Respond' Methods." *Control Conference (ECC)*: 4334–39. http://ieeexplore.ieee.org/xpls/abs_all.jsp?arnumber=6669781.

Kramer, Rick, Jos van Schijndel, and Henk Schellen. 2013. "Inverse Modeling of Simplified Hygrothermal Building Models to Predict and Characterize Indoor Climates." *Building and Environment* 68 (10): 87–99. doi:10.1016/j.buildenv.2013.06.001.

Lacroix, Benoit, Liten Ines, and David Mercier. 2012. "Multi-Agent Control of Thermal Systems in Buildings." *Agent Technology for Energy Systems Workshop (ATES 2012)*.

Lamoudi, Mohamed Yacine, Mazen Alamir & Patrick Béguery. 2011. "Distributed constrained Model Predictive Control based on bundle method for building energy management." *Proceedings of 50th IEEE Conference on Decision and Control and European Control Conference (CDC-ECC)*: 8118–8124

Lee, Jin-Young, Myoung-Souk Yeo, Kwang-Woo Kim. 2002. "Predictive control of the radiant floor heating system in apartment buildings." *Journal of Asian Architecture and Building Engineering* 1(1): 105–112.

Lee, Kyoung-Ho and James E. Braun. 2006a. "An Experimental Evaluation of Demand Limiting Using Building Thermal Mass in Small Commercial Buildings." *ASHRAE Transactions* 112(1).

Lehmann, B., D. Gyalistras, M. Gwerder, K. Wirth, and S. Carl. 2013. "Intermediate Complexity Model for Model Predictive Control of Integrated Room Automation." *Energy and Buildings* 58 (3): 250–62. doi:10.1016/j.enbuild.2012.12.007.

Lehmann, B., V. Dorer, M. Gwerder, F. Renggli, and J. Tödtli. 2011. “Thermally Activated Building Systems (TABS): Energy Efficiency as a Function of Control Strategy, Hydronic Circuit Topology and (Cold) Generation System.” *Applied Energy* 88 (1): 180–91. doi:10.1016/j.apenergy.2010.08.010.

Li, Siwei, Jaewan Joe, Jianjun Hu, and Panagiota Karava. 2015. “System Identification and Model-Predictive Control of Office Buildings with Integrated Photovoltaic-Thermal Collectors, Radiant Floor Heating and Active Thermal Storage.” *Solar Energy* 113(March): 139–57. doi:10.1016/j.solener.2014.11.024.

Li, Xiwang, and Jin Wen. 2014. “Building Energy Consumption on-Line Forecasting Using Physics Based System Identification.” *Energy and Buildings* 82 (10): 1–12. doi:10.1016/j.enbuild.2014.07.021.

Lim, Jae-Han, Jae-Hun Jo, Yong-Yee Kim, Myoung-Souk Yeo, and Kwang-Woo Kim. 2006. “Application of the Control Methods for Radiant Floor Cooling System in Residential Buildings.” *Building and Environment* 41 (1): 60–73. doi:10.1016/j.buildenv.2005.01.019.

Ljung, L. 1999. *System Identification: Theory for the User*. Upper Saddle River: Prentice Hall.

Ma, Y, Francesco Borrelli, and Brandon Hencey. 2012. “Model Predictive Control for the Operation of Building Cooling Systems.” *IEEE Transactions on Control Systems Technology* 20(3): 796–803. doi: 10.1109/TCST.2011.2124461

Ma, Yudong, Anthony Kelman, Allan Daly, and Francesco Borelli. 2012. “Predictive Control for Energy Efficient Buildings with Thermal Storage.” IEEE Control Systems, no. February: 44–64. doi:10.1109/MCS.2011.2172532.

Ma, Yudong, Garrett Anderson, and Francesco Borrelli. 2011. “A Distributed Predictive Control Approach to Building Temperature Regulation.” American Control Conference, 2089–94. doi:10.1109/ACC.2011.5991549.

Ma, Yudong, Jadranko Matuško, and Francesco Borrelli. 2014. “Stochastic Model Predictive Control for Building HVAC Systems: Complexity and Conservatism,” *IEEE Transactions on Control Systems Technology* 23(1): 1–16. doi:10.1109/TCST.2014.2313736.

Ma, Yudong, Stefan Richer, and Francesco Borrelli. 2012. *Control and Optimization with Differential-Algebraic Constraints: DMPC for Building Temperature Regulation*. SIAM. doi:10.1137/9781611972252.ch14

Mathworks. (2015). Optimization Toolbox: User's Guide (r2015b)

Mo, ZhengChun & Ardeshir Mahdavi. 2003. “An agent-based simulation-assisted approach to bi-lateral building systems control.” *Proceedings of the International IBPSA conference*. Eindhoven, Netherlands, 887–894.

Mokhtar, Maizura, Matthew Stables, Xiongwei Liu, and Joe Howe. 2013. “Intelligent Multi-Agent System for Building Heat Distribution Control with Combined Gas Boilers and Ground Source Heat Pump.” *Energy and Buildings* 62 (7): 615–26. doi:10.1016/j.enbuild.2013.03.045.

Moroşan, Petru Daniel, Romain Bourdais, Didier Dumur, and Jean Buisson. 2010. “Distributed Model Predictive Control Based on Benders’ Decomposition Applied to Multisource Multizone Building Temperature Regulation.” *Proceedings of the IEEE Conference on Decision and Control*, 3914–19. doi:10.1109/CDC.2010.5717092.

Moroşan, Petru-Daniel, Romain Bourdais, Didier Dumur, and Jean Buisson. 2010. “Building Temperature Regulation Using a Distributed Model Predictive Control.” *Energy and Buildings* 42 (9): 1445–52. doi:10.1016/j.enbuild.2010.03.014.

Nall, D. H. 2013b. “Thermally active floors: Part2.” *ASHRAE Journal* 55(2).

Nall, D. H. 2013c. “Thermally active floors: Part3.” *ASHRAE Journal* 55(3).

Necoara, Ion, Valentin Nedelcu, and Ioan Dumitrache. 2011. “Parallel and Distributed Optimization Methods for Estimation and Control in Networks.” *Journal of Process Control* 21 (5): 756–66. doi:10.1016/j.jprocont.2010.12.010.

Nedi´c, Angelia and Asuman Ozdaglar. 2009. “Cooperative distributed multi-agent optimization.” In *Convex Optimization in Signal Processing and Communications*, edited by D.P. Palomar and Y.C. Eldar, 340–386. Cambridge University Press.

Negenborn, R.R., and J.M. Maestre. 2014. “Distributed Model Predictive Control: An Overview and Roadmap of Future Research Opportunities.” *IEEE Control Systems* 34 (August): 87–97. doi:10.1109/MCS.2014.2320397.

Nghiem, Truong X., George J. Pappas, and Rahul Mangharam. 2013. "Event-based Green scheduling of radiant systems in buildings," *Proceedings of the American Control Conference*: 455–460, June 17-19. doi:10.1109/ACC.2013.6579879

Nghiem, Truong X., Madhur Behl, George J. Pappas, and Rahul Mangharam. 2012. “Green Scheduling for Radiant Systems in Buildings.” *Proceedings of the IEEE Conference on Decision and Control*: 7577–82. doi:10.1109/CDC.2012.6426318.

Oldewurtel, Frauke, Alessandra Parisio, Colin N. Jones, Dimitrios Gyalistras, Markus Gwerder, Vanessa Stauch, Beat Lehmann, and Manfred Morari. 2012. "Use of Model Predictive Control and Weather Forecasts for Energy Efficient Building Climate Control." *Energy and Buildings* 45 (2): 15–27. doi:10.1016/j.enbuild.2011.09.022.

Olesen, Bjame W., Klaus Sommer, Bjorn Duchting. 2002. "Control of slab heating and cooling systems studied by dynamic computer simulations." *ASHRAE Transactions* 108.

Olesen, Bjarne. 2008. "Radiant Floor Cooling Systems." *ASHRAE Journal* (Sep).

Pannocchia, G. 2014. *Encyclopedia of Systems and Control:* Distributed Model Predictive Control. Verlag London: Springer. http://doi.org/10.1007/978-1-4471-5102-9

Park, Cheol-Soo, Godfried Augenbroe, Tahar Messadi, Mate Thitisawat, and Nader Sadegh. 2004. "Calibration of a Lumped Simulation Model for Double-Skin Façade Systems." *Energy and Buildings* 36 (11): 1117–30. doi:10.1016/j.enbuild.2004.04.003.

Park, Sang Hoon, Woong June Chung, Myoung Souk Yeo, and Kwang Woo Kim. 2014. "Evaluation of the Thermal Performance of a Thermally Activated Building System (TABS) according to the Thermal Load in a Residential Building." *Energy and Buildings* 73 (April): 69–82. doi:10.1016/j.enbuild.2014.01.008.

Pflaum, Peter, Mazen Alamir, & Mohamed Yacine Lamoudi. 2014. "Comparison of a primal and a dual decomposition for distributed MPC in smart districts," *Proceedings of IEEE International Conference on Smart Grid Communications*: 55–60

Prívara, Samuel, Jiří Cigler, Zdeněk Váňa, Frauke Oldewurtel, Carina Sagerschnig, and Eva Žáčeková. 2013. "Building Modeling as a Crucial Part for Building Predictive Control." *Energy and Buildings* 56 (1): 8–22. doi:10.1016/j.enbuild.2012.10.024.

Prívara, Samuel, Zdeněk Váňa, Eva Žáčeková, and Jiří Cigler. 2012. "Building Modeling: Selection of the Most Appropriate Model for Predictive Control." *Energy and Buildings* 55 (12): 341–50. doi:10.1016/j.enbuild.2012.08.040.

Putta, Vamsi, Donghun Kim, Jie Cai, Jianghai Hu, James Braun. 2014. "Distributed Model Predictive Control for Building HVAC systems - A Case Study." *International high performance buildings conference*, Purdue University, West Lafayette, July 14–17.

Reynders, G., J. Diriken, and D. Saelens. 2014. "Quality of Grey-Box Models and Identified Parameters as Function of the Accuracy of Input and Observation Signals." *Energy and Buildings* 82 (10): 263–74. doi:10.1016/j.enbuild.2014.07.025.

Rhee, Kyu Nam, Myoung Souk Yeo, and Kwang Woo Kim. 2011. "Evaluation of the Control Performance of Hydronic Radiant Heating Systems Based on the Emulation Using Hardware-in-the-Loop Simulation." *Building and Environment* 46 (10): 2012–22. doi:10.1016/j.buildenv.2011.04.012.

Rhee, Kyu-Nam, Kwang Woo Kim, T. Zakula, P.R. Armstrong, and L. Norford. 2015. "A 50 Year Review of Basic and Applied Research in Radiant Heating and Cooling Systems for the Built Environment." *Building and Environment* 91. Elsevier Ltd: 640–50. doi:10.1016/j.enbuild.2014.10.054.

Royer, Sullivan, Stéphane Thil, Thierry Talbert, and Monique Polit. 2014. "A Procedure for Modeling Buildings and Their Thermal Zones Using Co-Simulation and System Identification." *Energy and Buildings* 78 (8): 231–37. doi:10.1016/j.enbuild.2014.04.013.

Samar, S, Stephen Boyd, and Dimitry Gorinevsky. 2007. "Distributed Estimation via Dual Decomposition." *Proc. European Control Conference*, 1511–16. https://www.stanford.edu/~boyd/papers/pdf/distr_estim_ecc.pdf.

Schmelas, Martin, Thomas Feldmann, and Elmar Bollin. 2015. "Adaptive Predictive Control of Thermo-Active Building Systems (TABS) Based on a Multiple Regression Algorithm." *Energy and Buildings* 103. Elsevier B.V.: 14–28. doi:10.1016/j.enbuild.2015.06.012.

Seo, Jung-Min, Doosam Song, and Kwang Ho Lee. 2014. "Possibility of Coupling Outdoor Air Cooling and Radiant Floor Cooling under Hot and Humid Climate Conditions." *Energy and Buildings* 81 (October): 219–26. doi:10.1016/j.enbuild.2014.06.023.

Sharples, Sue, Vic Callaghan, and Graham Clarke. 1999. "A Multi-Agent Architecture For Intelligent Building Sensing and Control A Multi-Agent Architecture For Intelligent Building Sensing and Control." *International Sensor Review Journal*, no. May: 1–8. doi:10.1108/02602289910266278.

Shumway, Robert H, and David S Stoffer. 2011. *Time Series Analysis and Its Applications With R Examples*. *Book*. doi:10.1007/978-1-4419-7865-3.

Simoes, M Godoy, and Saurav Bhattarai. 2011. "Multi Agent-based Energy Management Control for Commercial Buildings." *2011 IEEE Industry Applications Society Annual Meeting*, 1–6. doi:10.1109/IAS.2011.6074360.

Široký, Jan, Frauke Oldewurtel, Jiří Cigler, and Samuel Prívara. 2011. "Experimental Analysis of Model Predictive Control for an Energy Efficient Building Heating System." *Applied Energy* 88 (9): 3079–87. doi:10.1016/j.apenergy.2011.03.009.

Song, Doosam, Taeyeon Kim, Suwon Song, Suckho Hwang, and Seung-Bok Leigh. 2008. "Performance Evaluation of a Radiant Floor Cooling System Integrated with Dehumidified Ventilation." *Applied Thermal Engineering* 28 (11–12): 1299–1311. doi:10.1016/j.applthermaleng.2007.10.020.

Sourbron, Maarten, Clara Verhelst, and Lieve Helsen. 2013. "Building Models for Model Predictive Control of Office Buildings with Concrete Core Activation." *Journal of Building Performance Simulation* 6 (3): 175–98. doi:10.1080/19401493.2012.680497.

Sun, Biao, Peter B. Luh, Qing Shan Jia, Ziyan Jiang, Fulin Wang, and Chen Song. 2010. "An Integrated Control of Shading Blinds, Natural Ventilation, and HVAC Systems for Energy Saving and Human Comfort." *2010 IEEE International Conference on Automation Science and Engineering, CASE 2010*, 7–14. doi:10.1109/COASE.2010.5584637.

Treado, S. J. 2010. "An Agent-based Methodology for Optimizing Building HVAC System Performance." ASHRAE 2010 Annual Conference, 124–134.

Treado, Stephen, and Payam Delgoshaei. 2010. "Agent-Based Approaches for Adaptive Building HVAC System Control." *International high performance buildings conference*, Purdue University, West Lafayette, July 12–15.

Tridium Inc. Niagara AX Software. http://www.tridium.com/.

TRNSYS 17, 2010, Solar Energy Laboratory, University of Wisconsin-Madison

Turner, W.J.N., I.S. Walker, and J. Roux. 2015. "Peak Load Reductions: Electric Load Shifting with Mechanical Pre-Cooling of Residential Buildings with Low Thermal Mass." *Energy* 82 (March): 1057–67. doi:10.1016/j.energy.2015.02.011.

Váňa, Zdeněk, Jiří Cigler, Jan Široký, Eva Žáčeková, and Lukáš Ferkl. 2014. "Model-Based Energy Efficient Control Applied to an Office Building." *Journal of Process Control* 24 (6): 790–97. doi:10.1016/j.jprocont.2014.01.016.

Wang, Yan, Xi Meng, Lili Zhang, and Yulan Liu, Enshen. 2013. *Proceeding of the 8th International Symposium on Heating, Ventilation, and Air Condigioning: Chapter 51 Angle Factor Calculation for the Thermal Radiation Environment of the Human Body*. Springer. doi: 10.1007/978-3-642-39584-0.

Wang, Zhu, Rui Yang, and Lingfeng Wang. 2010. "Multi-Agent Control System with Intelligent Optimization for Smart and Energy-Efficient Buildings." *IECON Proceedings (Industrial Electronics Conference)*, 1144–49. doi:10.1109/IECON.2010.5675530.

West, Samuel R., John K. Ward, and Josh Wall. 2014. "Trial Results from a Model Predictive Control and Optimisation System for Commercial Building HVAC." *Energy and Buildings* 72 (4): 271–79. doi:10.1016/j.enbuild.2013.12.037.

Wilkins, Christopher K., and Mohammad H. Hosni. 2011. "Plug Load Design Factors." *ASHRAE Journal* 53 (5): 30–34.

Yang, Rui, and Lingfeng Wang. 2013. "Multi-Zone Building Energy Management Using Intelligent Control and Optimization." *Sustainable Cities and Society* 6 (1): 16–21. doi:10.1016/j.scs.2012.07.001.

Žáčeková, Eva, Zdeněk Váňa, and Jiří Cigler. 2014. "Towards the Real-Life Implementation of MPC for an Office Building: Identification Issues." *Applied Energy* 135 (12): 53–62. doi:10.1016/j.apenergy.2014.08.004.

Zhao, Peng, Siddharth Suryanarayanan, and Marcelo Godoy Simões. 2013. "An Energy Management System for Building Structures Using a Multi-Agent Decision-Making Control Methodology." *IEEE Transactions on Industry Applications* 49 (1): 1–9. doi: 10.1109/IAS.2010.5615412.

VITA

Ph.D., Civil (Architectural) Engineering, Purdue University Aug. 2013 ~ Aug. 2018
Thesis: Agent-based approach for system identification and optimal control of high performance buildings

M.S., Architectural Engineering, University of Seoul Mar. 2010 ~ Feb. 2012
Thesis: Load characteristics and optimization of a building integrated with multi-story double skin facades

B. S., Architectural Engineering, University of Seoul Mar. 2003 ~ Feb. 2010
Thesis: A heating energy savings proposal for the university dormitory building

PUBLICATIONS

J. Joe and P. Karava, "Optimizing the energy performance of a radiant floor system with model predictive control - Implementation in an office building and comparison with baseline control and air delivery system", In preparation.

J. Joe, P. Karava, X. Hou, Y. Xiao, and J. Hu, "A distributed approach for model-predictive control of high performance buildings with local radiant comfort delivery", *Energy and Buildings*, under revision.

J. Joe and P. Karava, "Agent-based *system* identification for control-oriented building models", *Journal of Building Performance Simulation* 10(2), 183–204, 2016.

S. Li, **J. Joe**, J. Hu, and P. Karava, "System identification and model-predictive control of office buildings with integrated photovoltaic-thermal collectors, radiant floor heating and active thermal storage", *Solar Energy* 113, 139–157, 2015.

J. Joe, W. Choi, Y. Kwak, J-H. Huh, "Optimal design of multi-story double skin facade", *Energy and Buildings* 76, 143–150, 2014.

J. Joe, W. Choi, H. Kwon, J-H. Huh, "Load characteristics and operation strategies of building integrated with multi-story double skin facade", *Energy and Buildings* 60, 185–198, 2013.

W. Choi, **J. Joe**, Y. Kwak, J-H. Huh, "Operation and control strategies for multi-storey double skin facades during the heating season", *Energy and Buildings* 49, 454–465, 2012.